A Research Regarding Development and Application of Tactile Sensing for Robots

ロボットのための触覚センシングの開発とその応用に関する研究

February 2010

Major in Pure and Applied Physics

Graduate School of Science and Engineering

Waseda University

Kitti Suwanratchatamanee

A Research Regarding Development and Application of Tactile Sensing for Robots

ロボットのための触覚センシングの開発とその応用に関する研究

キティ・スワナラチャタマニイ

DEDICATION

My Ph.D. researches and achievements including this dissertation, publications and awards are dedicated to all of my family members especially to my beloved grandmother Mrs. Tei Suihuai who has been taking care of me since I was born and directed my understanding of honesty and earnest comportments, to my father Mr. Bandhit Suwanrajatamanee and mother Mrs. Malee Suwanrajatamanee for their abundant financial support and guidance for my understanding of the sense of family responsibility, to my uncle Mr. Boonchai Suwanratchatamanee who directed my understanding of the excellent engineer performances and engineering skillfulness, to my aunt Ms. Wanna Suwanratchatamanee who has been taking care of me and help me to be in touch with other family members during my study aboard, Lastly to my sweetie Ms. Sirima Treenate who always encouraged me and understand all of my situations.

Tokyo, Japan
February 2010
Kitti Suwanratchatamanee

ii

ACKNOWLEDGMENTS

iii

TABLE OF CONTENTS

LIST OF FIGURES

- CHAPTER III -

xiv

LIST OF TABLES

CHAPTER I

1. INTRODUCTION

Tactile sensing is a detecting procedure to distinguish the actual properties through the contacted objects physically. As a human, we often use our hands to assess the object's properties such as size, shape and texture especially in the no vision situations such as in the dark environment. We also sense and interpret tactile stimuli from our environment and perform tasks with our hands in a nearly an instinctual manner. Tactile and touch sensors are sensing devices for measuring the parameters of contacted among sensor and touched object. This interaction can obtained information that restricted to a defined area which is contrasts with force/torque sensor to measure the entire forces being applied on a contacted object. There are three definitions commonly used for this kind of sensor; the first definition is "*Touch sensing*" which refers to the detecting procedure to distinguish the existence of the touched object by measuring the contacted reaction force at the specified point. Hence the output of touch sensor can be converted into binary information, called touched as logic '1', and non-touch as logic '0'. The second definition is "*Tactile sensing*" which refers to the detecting procedure to distinguish the actual properties of the touched object by measuring the scattering reaction forces at predefined physical area. Tactile sensor is the sensing array can be deliberated as a coordinated set of numerous touch sensors. Hence the output of tactile sensor can be converted into many digital bits which can be bytes or words, depend on the sensing resolution as spatial information of touched object. The third definitions is "*Slip sensing*" which refers to the detecting procedure to distinguish the touching movement of the touched object interrelated to the sensing device. The slip sensor can be achieved by interpreting of sensing data from touch and tactile sensors or particularly designed method.

In order to recognize the tactile image completely, we can apply to use tactile sensor for detecting the different ranges of active points from the measurement of an existence or non-existence area of touched object. Generally, tactile sensor is the sensing

array of numerous touch sensitive spots. Those spots able to detecting one or more than one properties of touched object depend on the capable of selected sensing elements. By utilizing the large amount of tactile information that detected from the touch sensitive spots can help us to understand the object's gripping statuses of the robotic hand such as, textures, slips, and touching impacts. In addition, we can categorize the statuses to manipulate the robot motions by using the contacted position signatures subsequent interpretation of the different contacting forces. Currently, many kinds of technology have been involved in this study topic. There are several physical philosophies had been apply for developing tactile sensors. In addition, the physical properties of the touched object is very important. It is the key information that will allow developers to indicate the method to produce and use of tactile sensor for suitable gripping material. About touched objects. Hence, the touched objects were discussed in this manuscript are rigid form which can be used with our developed tactile sensors.

1.1. Research Background

Recently, varieties of sensors have been reported for robot, such as vision type sensors [1]-[2] and tactile type sensors. While computer vision is often employed to recognize the object shape with the position and orientation, tactile sensing is an essential ability for a robot to handle an object [3]. The tactile sensor attached on the robot hand can sense the object surface even when the robot vision cannot get the occluded surface image. In bilateral tele-operation, information is transmitted not only from master to slave but also from slave to master. Therefore, the operator on the master side can feel tactile sensation from the slave side as well [4]. A variety of tactile sensing systems have been proposed not only for robots, but also for human-machine interfaces and human-system interactions [5]-[8], force-feedback, and pattern recognition. The tactile sensor equipped on the fingertip gives a signal to maintain a stable grasp [9]. In real situations, the friction between the object and the finger should be measured for grasping an object [10]. Although the manipulation is one of the most interesting tasks, the local shape recognition is another valuable tactile sensing application. The object surface orientation is important information when the robot contacts the object [11]. The object edge sensing

2

and tracking are also important to recognize the shape without a vision system [12]. Concerning object tracking for industrial welding robot, there are a variety of techniques. Some researchers have used visual system (CCD camera) [13]-[15], while others focused on range sensing methodology of echo pulse amplitude and time of flight [16]-[17]. In order to acquire more information on an object, some researches combine a tactile sensor with an actively controlled arm. Some of them aimed to identify surface patterns [18], while others focused on recognizing the roughness and softness of objects [19]. To track humans and to avoid obstacles, some researchers have reported the robot equipped with 16 tactile and 16 ultrasonic sensors with 360∘ coverage [20]. There are a variety of techniques and sensing devices utilized as a part of tactile sensing. Previous works have used traditional strain gauges, electro-magnetic device sensors, force sensitive resistors, capacitive tactile array, optical device, piezoelectric resonance and the shape memory alloy (SMA) device as micro-coil actuators used for 2-D and 3-D tactile display [21]-[24]. The use of 3D or 6D force sensors located within the body can perform the same task. They are robust and have good performance over a period of time. They are widely used in robotics [25]-[27]. It may also be easy to use these types of sensors. However, this research aims to study the application range by using the simplest system not only about the usability but also about the principle.

According to [21], tactile sensor is a sensing device or system which can measure a given property of contacted object or the contact between sensor and object. The tactile sensor units with two and three elements of low cost force sensitive resistors have been reported with preliminary experimental results by the author [28]-[31]. The development of proposed sensor unit is one of the simple implementations structured with three sensing elements (FSRs). The proposed technique is to use such devices with a layout specialized for object edge tracing and object surface sensing. There are some previous works using the same sensing device. For a control task, the dynamic behavior has to be evaluated. However, there are a few works utilizing this thin film sensor. A comparison of the respective performances of commercial products has been reported [32]-[33].

This dissertation presents the tactile sensor system for robots and various active tactile sensing techniques. The developed tactile sensing system is implemented on the

industrial robot hand and humanoid robot feet are able to detect the distribution of planer surfaces by using three force sensitive resistors arranged triangularly. To confirm the suitability of the proposed system for practical use in robot applications, I have introduced the various applications. First application is to use the proposed sensor implemented on the industrial robot to recognize object information such as, measuring an object surface angle and object shape. Second application is a hand pose control of industrial robot to keep the direction of movement normal to the 3-D plane object, which is often required to push an object for positioning. This technique can be used for a cooperative task between human and robot to move an object together. Third application is a hand poses and motion controls of industrial robot for recognizing and tracing an active object edge. As a typical example, a simulated welding torch for industrial robot has been developed. This unit has two functions; first function is to detect the object information such as welding points before doing the welding process. Second function is to simulate the welding task. In these applications, the user does not need to provide information about object shape or orientation in advance. For the last possible application, I attempted to apply this sensing technique into the humanoid robot. The proposed sensors are implemented on the back of two robotic feet. Each foot contains three thin sheets of force sensitive resistor which are arranged triangularly. As the possible application of humanoid robot, I attempted to let the robot autonomously maintain the balance with two legs and one leg in various environments. Additionally, I attempted to let the robot walk on the different ground slopes. Finally, I also attempted to test the contact states interacting between human and robot. In order to do that, I let the robot avoid falling down due to the external force exerted by the unpredicted pushing action during human-robot interaction. In these applications, the information about the contacted ground floor or robot orientation is not required in advance.

1.2. Research Objectives

The research objective is to realize an effective controller for robot to handling the 3D object. An additional final aim is to produce an artifact that is a kind of artificial creature, which enables to cooperative works between human and machine (robot) in a

4

natural and intuitive manner. Throughout these works, I aim to realize an autonomous robot and a harmonized Human-Machine and Machine-Environment. Concerning about possible applications of the proposed system, I aim to realize the proposed method in to the three main potential applications as follow;

First, I aim to realize my method to eliminate the manual teaching procedures for improving the safety and efficiency of industrial task. Recently at the human work space, it is often required that human to be close to the industrial robot for teaching the robot about the object information such as the welding positions before doing the welding task. One of research goal aims to employ the proposed sensing system as a replacement of manual teaching. In order to achieve this aim, I would like to develop a novel welding torch for industrial robot. This novel torch can employed for welding task and it can also be employed for recognizing and tracing an object's edge in order to obtain the welding points. The advantage of utilizing the proposed system is that a skilled person is not require to stay at the work-site during the teaching all the time, s/he can do other jobs and hence improving the man power efficiency in the industry areas.

Second aim is to focus on a cooperative work between human and robot in a natural and intuitive manner. The idea of cooperative task between human and robot is to move the large object together, during the moving task, human might not be able to maintain the object orientation such as the object angle and object level from the floor due to the object weight. Thus robot should hold the object in difference levels and angles to support human. In order to enable the robot for this task, I would like to develop a novel robotic hand utilizing the proposed tactile sensing technique. The proposed tactile sensor is implemented on the robotic hand that can estimate the contact angle between the sensor and an object to be touched. Then the robot will move its hand for support such as holding an object in difference angles and levels.

Third aim is to focus on the study and development of an autonomous biped walking robot. I would like to introduce a novel method of walking pattern generation by using the proposed tactile sensing system for humanoid robot. As a research goal, the robot should be able to walk autonomously in various environments without the complex kinematics calculations. Accordingly, I would like to apply my technique to make the

recently biped walking system simpler by utilizing a tactile feedback sensing method instead the complex calculations. My idea is to use such devices with a specialized layout implement into the back of robot feet for active planar ground surface recognition. By utilizing the feedback information, the robot controller can recognize the robot foots conditions. Then is able to control the robot foot poses and motions to make the robot foots normal to the ground surface. Thus, it can be assisting the humanoid robot to be balance on various environments. After, the humanoid robot is able to balance with tactile sensing method. Next, I would like to apply this system to enable walking on different environments such as the difference slopes, floors, stairs and rough surfaces to support the actual human daily tasks.

1.3. Dissertation Outline

This dissertation is organized into seven chapters. This chapter provides an introduction to the background and objectives of this research regarding to the development of tactile sensing for robots.

Chapter 2 introduces a development of tactile sensor systems. This chapter begins with the key developing idea of the proposed sensor unit. The information about prepared sensing devices of the proposed sensor unit is presented in the next section. Follow by the sensor measuring method. The sensor signals are digitized using resistance measuring method by utilizing the RC time constant technique described in this section. In the next two sections introduce the proposed sensing system for industrial robot and humanoid robot respectively. These two sections provide the details of the main components of this system including, robots, hardware, software and interface. This chapter also provides the inverse kinematics calculation of proposed robot manipulator system, preliminary experiments including sensor linearity test and filtering effect test.

Chapter 3 introduces the tactile sensing techniques. First section introduces the tactile sensing techniques of sensor hand for industrial robot arm. This section provides two sensing methods namely object surface normal sensing and of object edge sensing. Second section introduces the tactile sensing techniques of sensor feet for humanoid robot. This section also provides two sensing methods namely ground slopes sensing and balance sensing.

6

Chapter 4 introduces the possible applications of proposed sensing system into the industrial purpose. First section introduces the object recognizing applications. This section provides three possible applications such as, surface angle measurement, object shape measurement and surface normal following. An approach for welding application using the proposed method is presented in the next section such as, recognizing, finding and tracking of an object edge. This experiment aimed to obtain object information by tracing an object edge continuously. Welding is one potential application of hand pose control for finding and tracing an object's edge. This technique can be used instead of manual teaching by a person, which is currently often necessary to obtain object information for welding points before carrying out the welding process.

Chapter 5 introduces the possible applications of proposed sensing system for humanoid robot. First section introduces the ground slopes recognizing application. In this section I conducted some experiments to confirm the ability of the proposed tactile sensing system for humanoid robot to move its foot in 3-D. I mainly examined four cases such as, downward, upward, rightward and leftward slopes. Second section introduces the balancing applications by utilizing the proposed sensor feet. The humanoid robot kinematics for balancing controls is also introduced. In this application, I conducted the experiments on two legs and one leg balancing control of the humanoid robot on the various environments such as different ground slopes, internal and external disturbances. The last section introduces some experiments to confirm the ability of the proposed tactile sensing system for humanoid robot. I attempted to realize effective walking tasks of the humanoid robot on the various slopes.

Chapter 6 introduces the possible applications of proposed sensing system for human-robot interacting applications. The cooperating applications are introduced in the first section. In this section, I conducted the two main experiments to confirm the ability of proposed tactile sensing system. The first experiment is to confirm the effectiveness of the robot hand pose action. The second experiment is to show some examples of human-robot cooperation to move various kinds of object together in 3-D. The next section introduces the effective human and robot interaction, especially in case of contact states interaction between human and robot to avoid the robot damages which cause the falling

down due to the unpredicted external force from the human. The first experiment is to confirm the ability of the robot to maintain balance with their sensing feet against the human pushing force. In the second experiment, as the robot could not maintain the two leg balance if the pushing force is too large, the robot should move its leg on an opposite side to support its body against the various pushing force direction even human pushing harder as step motions.

Chapter 7 summarizes the result of this research and suggests future extensions of this researching work.

CHAPTER II

2. DEVELOPMENT OF TACTILE SENSOR SYSTEMS

2.1. Key Developing Idea

(A)　　　　　　　　(B)　　　　　　　　(C)
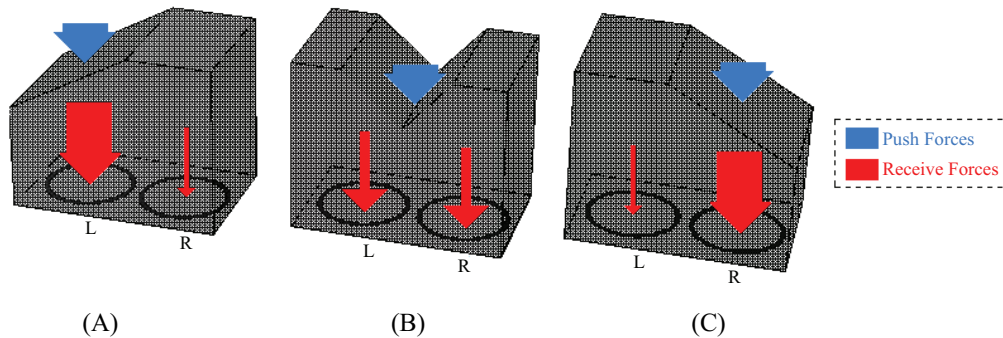
Figure 2-1. Receiving forces effect on different pushing points on two sensing elements

The key idea of tactile sensing device originated from the nature of two force sensing elements. Figure 2-1 shows the test example of two pieces of the force sensitive resistor covered with soft material on top. Note that this sensor type has the resistance behavior inversely proportional to the applied force on the sensing area of the element sheet. As can be seen from this figure, two sensing element sheets (L and R) are located under the soft material. The received force is affected on the different pushing spots above two sensing elements. For example, when applied the pushing force on the left side as shown in Figure 2-1(A), the received force on sensor L is larger than the sensor R. In this case the resistance of sensor L decreased and it should become smaller than the resistance of sensor R. Following, when applied the pushing force on the center of two sensing elements as shown in Figure 2-1(B), the received forces on both sensors are equal. In this case the resistances of both sensing elements should decrease to the same values. On the other hand, when applied the pushing force on the right side as shown in Figure 2-1(C), the received force on sensor R is larger than the sensor L. In this case, the resistance of sensor R decreased and it becomes smaller than the resistance of sensor L. Accordingly, the gradient of the contacted object can be obtained from the differences values between these two sensing elements as example.

2.2. Sensing Element

Figure 2-2. Sensing element pressure sensor

The prepared sensing devices are "*Flexi-Force*" which is a sort of force sensitive resistor (FSR.) produced by Tekscan, Inc [34] as shown in Figure 2-2. According to the information provided by Tekscan Inc., this sensing device is made of 0.127mm polyester film thickness, which measuring force between two surfaces. The sensing outputs are very linearity, small drift and low hysteresis compared to the other available thin-film typed sensors. The single element of Flexi-force sensor performs as a resistor which can be used in electrical circuit generally. The sensing output of Flexi-force is the resistance which is proportional to applied load on the active sensing area. The active sensing area is 9.53 mm diameter which can be seen as the round tab at the end of the film. The output resistance is extremely high when no-loaded applying on the sensing element sheet. On the other hand, the output resistance will be decreases when applied load into the sensor. Flexi-force has three connecting pins however the middle pin is not used. The outer two pins act as the resistor in an electrical circuit, which can be read the resistance values by connecting an ohmmeter on both pins. Flexi-Force has three models. First model is A201-1 is capable of sensing forces up to 4.4 N (0.45kg). Second model is A201-25 is capable of sensing forces up to 110 N (11.3kg). Third model is A201-100 is capable of sensing forces up to 440 N (45.4kg). In order to acquire the fastest response, the minimum sensing forces model A201-1 was chosen as the sensing elements to develop the prototype tactile sensor. Although, this sensor model has a small capable of sensing forces just 4.4 N. In order to increase the capable of sensing values, we covered those sensing elements with soft material (Sponge, 15 mm thickness and 0.496N/mm^2 Young's modulus). Hence, the prototype sensor is capable of sensing forces stretched up to 25.4 N (25.9kg) as described in section 2.6 (Preliminary Experiment).

10

2.3. Sensor Measuring Method
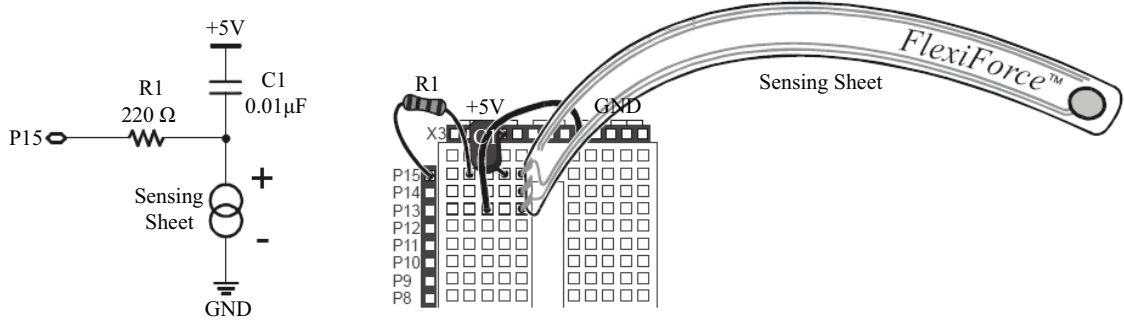
Figure 2-3. Sensor measuring circuit

The sensor signals are digitized by employing resistance measuring method using RC time constant technique. The measurements are carried out in real time with sensor interfacing unit. The resistance value is measured by using the charge and discharge of RC circuit as shown in Figure 2-3. After charging the capacitor, the discharge will start through the force sensitive resistor. The microprocessor measures the discharge time using the software clock counter. In order to measure the variable resistance of this sensing element, I utilize the RC time constant method. The step input is applied to the circuit and the discharge time is measured. The microcontroller checks the voltage of the capacitor with 1ms interval. To measure the discharge time of the capacitor, I estimate the time when the voltage of capacitor is less than the logic threshold voltage. The variable resistance of sensing element R can be obtained as:

$$R = \frac{t}{C \times \ln\left(\dfrac{V_{Supply}}{V_{I/O}}\right)} \tag{2-1}$$

where V_{Supply} and $V_{I/O}$ represent the supply voltage and the logic threshold voltage, respectively. C represents the capacitance of capacitor. t represents the discharge time. In this method V_{Supply}, $V_{I/O}$ and C were set to 5V, 1.4V and 0.01μF, respectively.

The relation among forces, the resistance and time in equation (2-1) is non-linear. Although such a behavior makes the electronics complex and affects the computation

11

time, modern microcontrollers today offer the computation speed high enough to solve such a problem. Moreover, it also offers the RC-time computing functions. Thus, the system can simply connect the RC circuits to the microcontroller. As the research aim is to introduce a simple system, it is considered that FSRs are better than other available sensing devices. The selected FSRs devices are the thin sheet type sensor, which has suitable dimension and are flexible to be structured in a sensing module such as the proposed sensing unit. In addition, the selected FSRs are cost effective sensing elements.
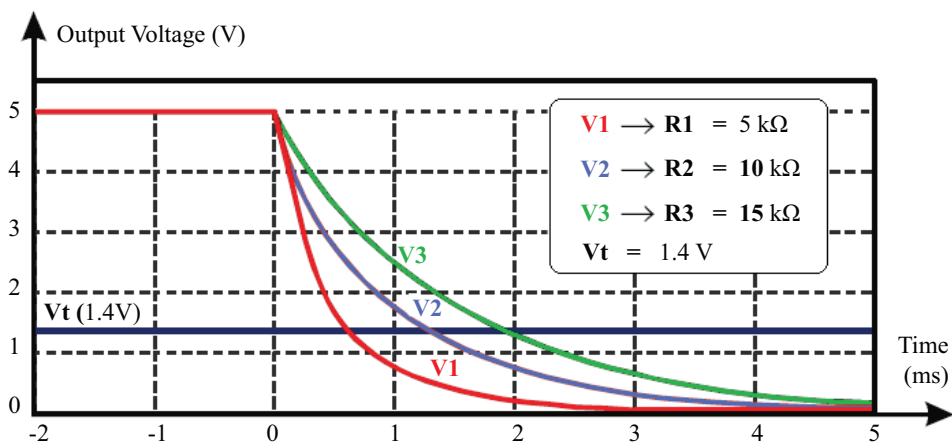
Figure 2-4. RC circuit responses (Resistance changes)

Figure 2-4 shows the RC circuit responses. The graph in this figure has shows the decays of RC circuit when the resistance values in the circuit are changed to 5kΩ, 10kΩ and 15kΩ, respectively. It takes a different amount of time to decay from 5V to 1.4 V. As the maximum discharge time for each element is less than 3 ms, the cycle time of the RC time measurement is short enough for the real time control in each moving step of robot manipulator and humanoid robot. In addition, the linearity is not essential for the proposed applications. Because, the research aim is not to use the proposed sensor for measuring the exact load forces but to use the relationship between three sensor outputs for sensing data analysis to define contacted object information for robot movement control. I can also use the direct A/D converter inside the CPU of the robot controller unit instead of the RC time method; however, in order to do that, the robot controller unit should include the tactile analyzing function of the sensor interfacing unit.

12

2.4. Sensing System for Industrial Robot
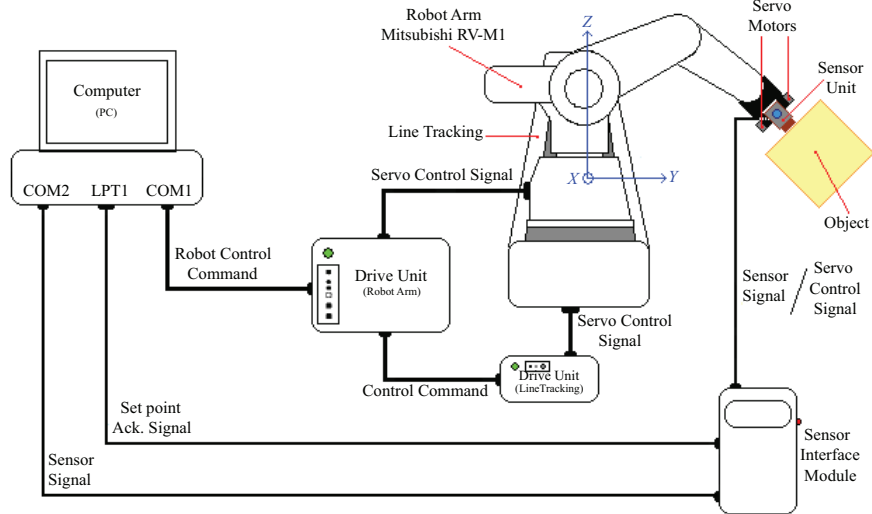
Figure 2-5. Diagram of tactile sensing system for robot arm
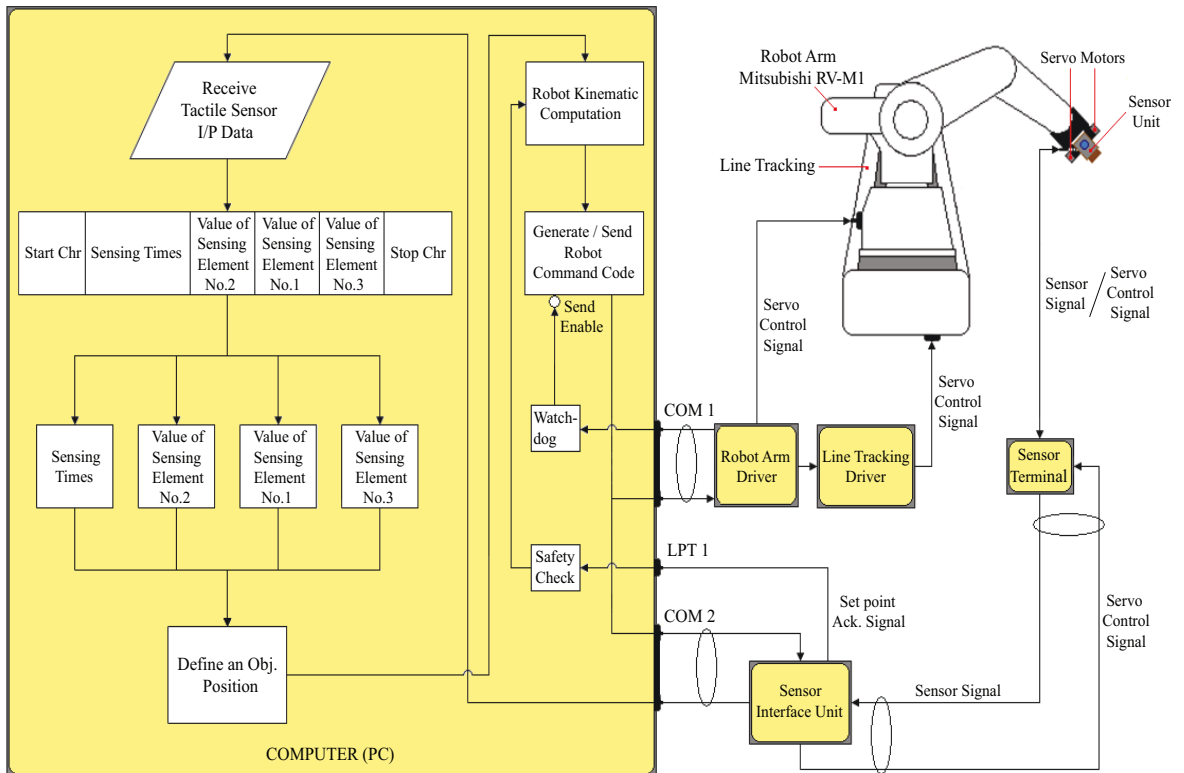
Figure 2-6. Architecture and data flow chart of the tactile sensing system for robot arm
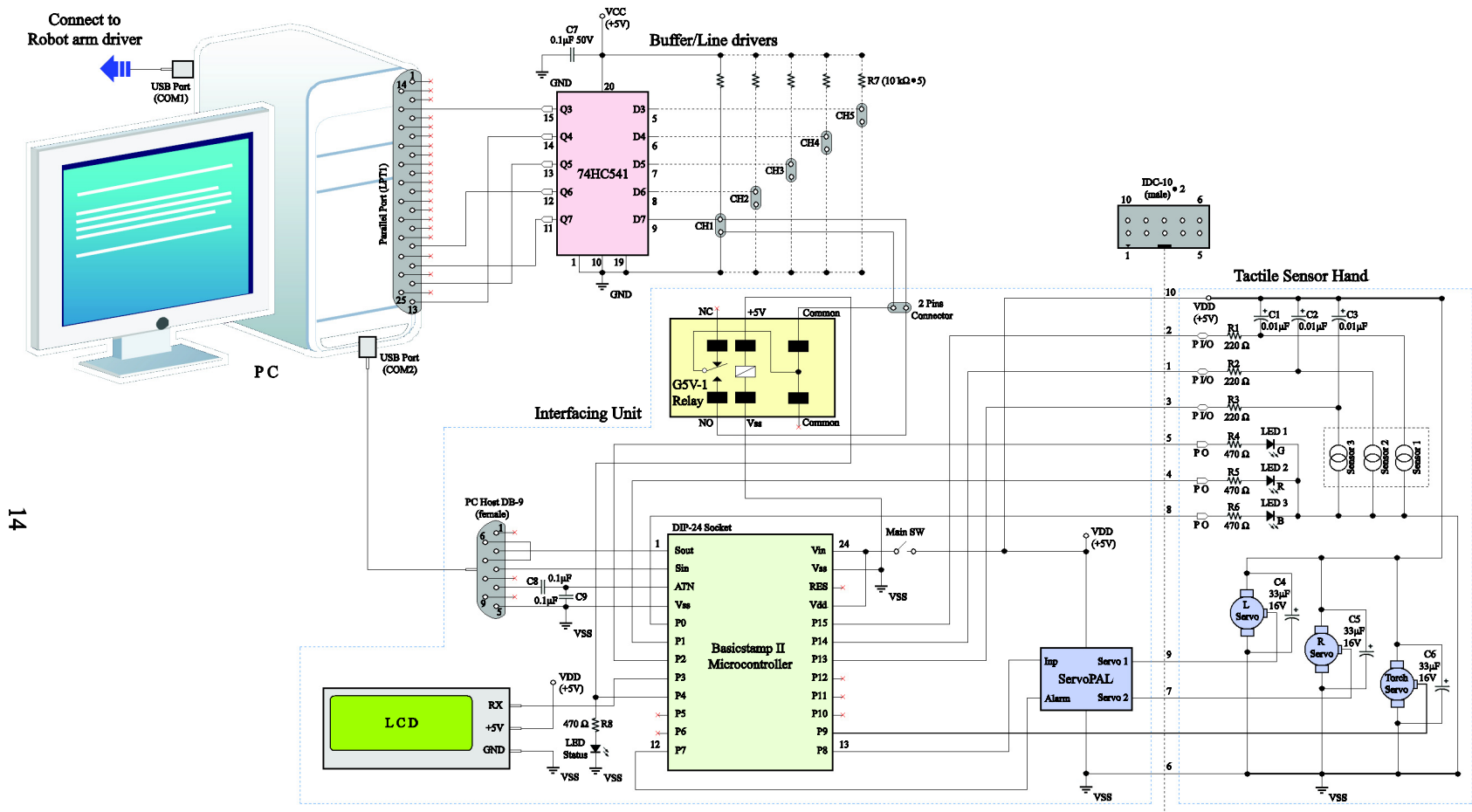
Figure 2-7. Electronic circuit diagram of tactile sensing system for robot arm

Tactile sensing system diagram for robot arm is shown in Figure 2-5. This figure shows the hardware units installation. In order to complete my research aims, I also created software appropriate for this system and installed it into the personal computer (PC). Figure 2-6 shows the software architecture and data flow chart of the tactile sensing system. This architecture consists of three programs which are described in section 2.4.2(PC and Developed programs). I also designed electronic circuits for each hardware unit. The electronic circuit diagram of proposed tactile sensing system for robot arm is shown in Figure 2-7. The system consists of robot arm system (robot arm and line tracking unit), Personal computer (PC), tactile sensor unit and Sensor interfacing module. All the devices are designed to perform the tactile system to realize 3-D object recognitions. The sensing robot can interact with the touched object through a developed tactile sensor unit. The main parts of this system are described as following sections.

2.4.1. Robot arm
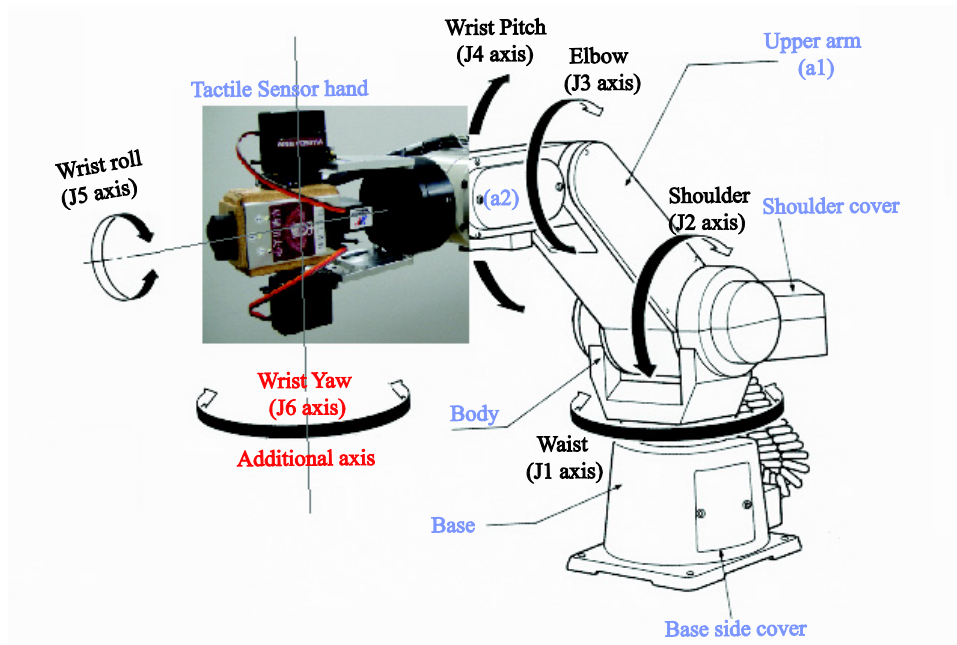
Figure 2-8. Joints and parts of robot arm

This research utilizes Mitsubishi "*Move-Master*" robot arm system for industrial and human interaction tasks. This robot arm system originally has five degrees of freedom (DOF). The robot's end-effector is equipped with the developed tactile sensor

hand. In order to perform the sensing task full range of 3-D motions. I decided to attach two servo motors on the sensor unit as shown in Figure 2-8. These two servo motors are used as an additional DOF in the robot arm. Thus after improvement, in total the robot arm has a total of 6 DOFs, allowing the full range of 3-D sensing area. Note that this is an especially improvement of robot arm hardware designed for this research.
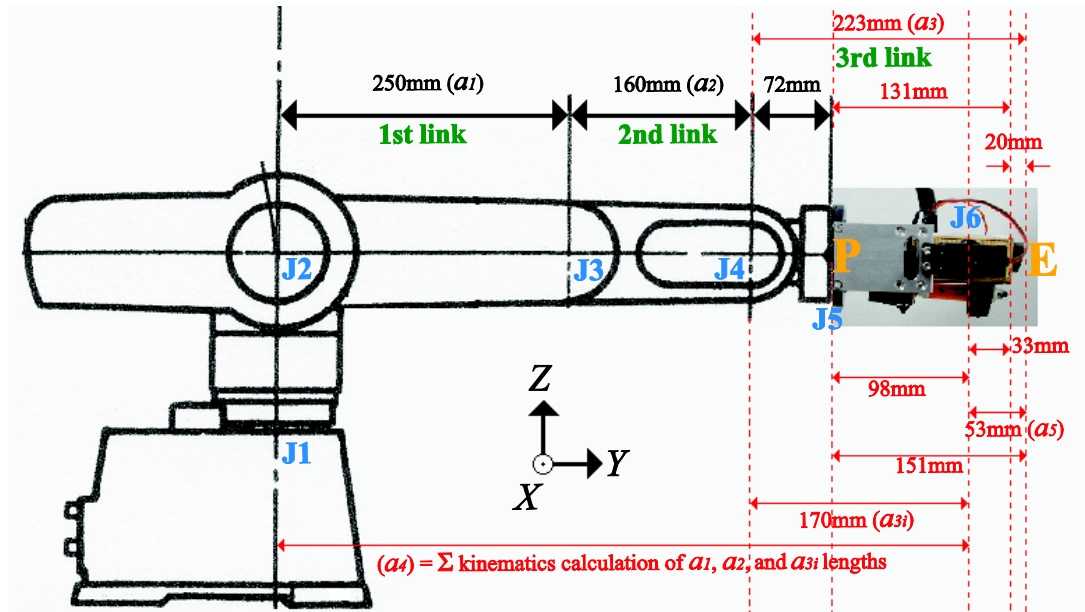
Figure 2-9. External dimensions of robot arm

Figure 2-9 shows the external dimensions of robot arm. The robot arm has a total of six moving joints J_1 to J_6 respectively. These 6 DOFs are allowing the full range of sensing area in 3-D. The main dimensions of an original robot arm are the length of first link, a_1 which is measure from J_2 to J_3 and the length of second link, a_2 which is measure from J_3 to J_4 as 250mm and 160mm respectively. The dimensions after installation of the tactile sensing hand are also provided in this figure. These dimensions are the length of third link, a_3 which is measure from J_4 to the sensing hand's end-effector as 223mm. The this third link is combined with two small links, a_{3i} which is measure from J_4 to J_6 and a_5 which is measure from J_6 to the sensing hand's end-effector, E as 170mm and 53mm respectively. In order to solve an inverse kinematics, the length in Y axis at J_6, a_4 is concerned. The length of a_4 is computed by the summation of kinematics calculation of a_1, a_2, and a_{3i} lengths described in section 2.4.2.3(Inverse kinematics calculating program).

16
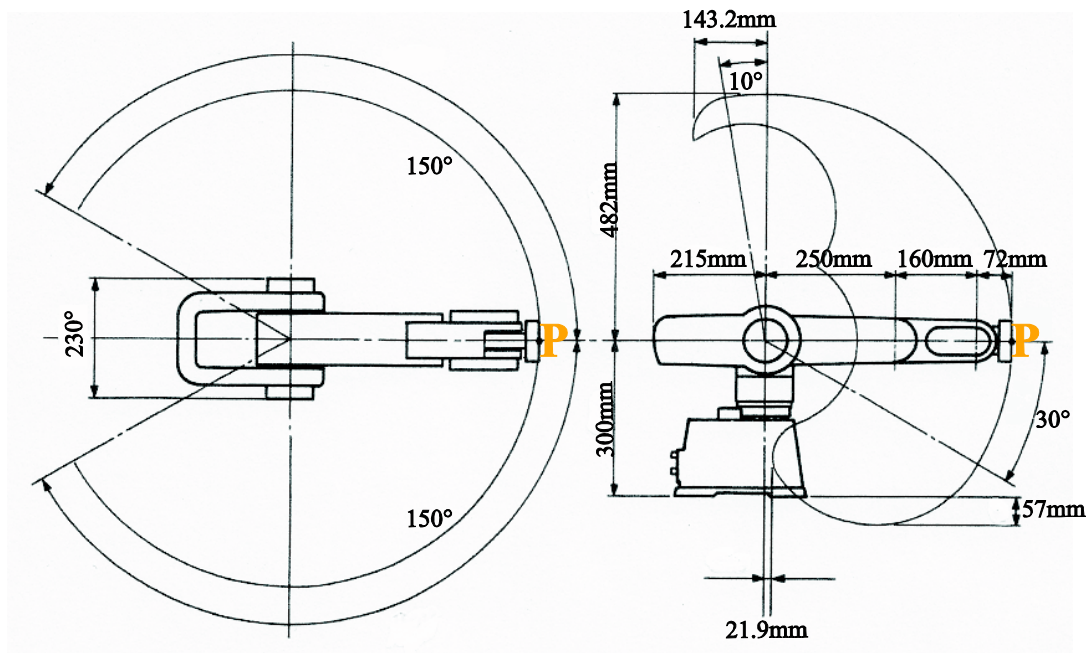
Figure 2-10. Operation space of robot arm (without tactile sensor hand)

The operational space of robot arm is shown in Figure 2-10. The operational space indicated in this figure only assumes that when the tactile sensor hand is not installed to the robot the maximum operation in Y direction is 482mm (Trace of point, P). According to the figure 2-9 after installation the maximum operation in Y direction should extended from 482mm (P) to 633mm (End-effector, E) with an additional DOF. Moreover, in order to allow the robot perform an effective welding task, the robot is also set on a line tracking system as shown in Figure 2-5. This line tracking is a Mitsubishi "LU08-M1" which is allows 800mm for moving the robot arm along the X-axis. Thus the whole robotic system has a total of 7 DOFs, allowing it a full range of 3-D sensing area and moving in X-axis.

2.4.2. PC and Developed programs

In order to control the robot arm system and communicate with the sensing module, I created the software appropriate for the proposed sensing system and installed them into PC. The PC block shown in Figure 2-6 describes the functions and data flow of developed three programs. Each program is created for special purpose. The details of each program are described as the following details;

17

2.4.2.1. Sensor interfacing program
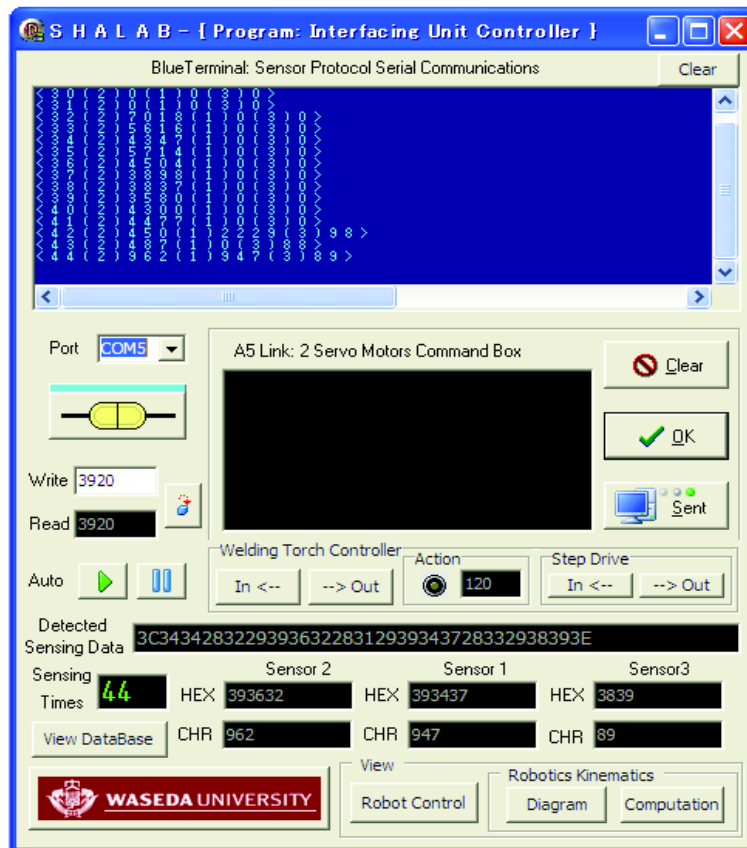
Figure 2-11. Sensor interfacing program

First developed program is the sensor interfacing program. Figure 2-11 shows an image of the sensor interfacing program. This program mainly handles the receiving and sending functions of data between the PC and the interfacing unit via the serial line communications (Serial port: COM2).

For the receiving process, after send the sensing request command to the interfacing unit, the program receives sensing feedback data from the sensor interfacing unit in a network layer as a data packet utilizing the Time Division Multiplexing (TDM) method. The information utilizes ASCII code system for coding and decoding. The data packet is a stream of Hex code in the communication line. Sample of receiving data is shown in Figure 2-11 on the monitor labeled "*Detected Sensing Data*". In this monitor shows a numerical data packet as "3C34342832229393632283129393437283329938393E".

This stream of data is the Hex code which is can be converted from ASCII code into character code as "<44(2)962(1)947(3)89>". At this state, the packet was decoded for easier visualization. This character code is beginning with start character "<", sensing times "44", read value of sensing element 2 as "962", read value of sensing element 1 as "947", read value of sensing element 3 as "89" and stop character ">" respectively. Note that the unit of three sensing values is in μ second. Finally the data packet is decoded into useful information as the sensing times and three sensing values as shown in separate blocks as shown in figure 2-11. Additionally, this program also receiving an acknowledge signal via the data bus parallel port (LPT1). This signal is used for two reasons; one is to let the system or user recognizes that the sensing data has reach the set point value, which can be used to stop for emergency case or to interrupt the system to observe some particular investigation. Second is to let the system or user recognizes that the simulated torch is in moving or non-moving status. For example, the yellow LED on the block labeled "*Action*" is flashing when the simulated torch is in the moving status.

For the sending process, the program mainly handles the sending of sensing request command to the interfacing unit. Additionally, this program also contains the control function to control three additional servos including two servo motors for an additional DOF of robot arm and a servo for a simulated welding torch which is describe more details on section 2.4.3(Tactile sensor hand). Two types of controlling commands are generated from this program for sending to the tactile sensing hand. One is the command for controlling the sensing hand to do the sensing task with additional DOF controlled. Another command is for controlling the sensing hand to do only sensing task.

2.4.2.2. Robot manipulator controlling program

The second developed program is the robot manipulator controlling program. This program mainly handles the communication tasks to send the robot controlling command to the driver unit via a serial line (COM1) as a data link layer (frames). The controlling command is depend on the task given by users. Figure 2-12 shows an image of the robot manipulator controlling program. The green terminal in this figure shows the position of the robot arm after the robot executed the previous command. The example of a robot

19
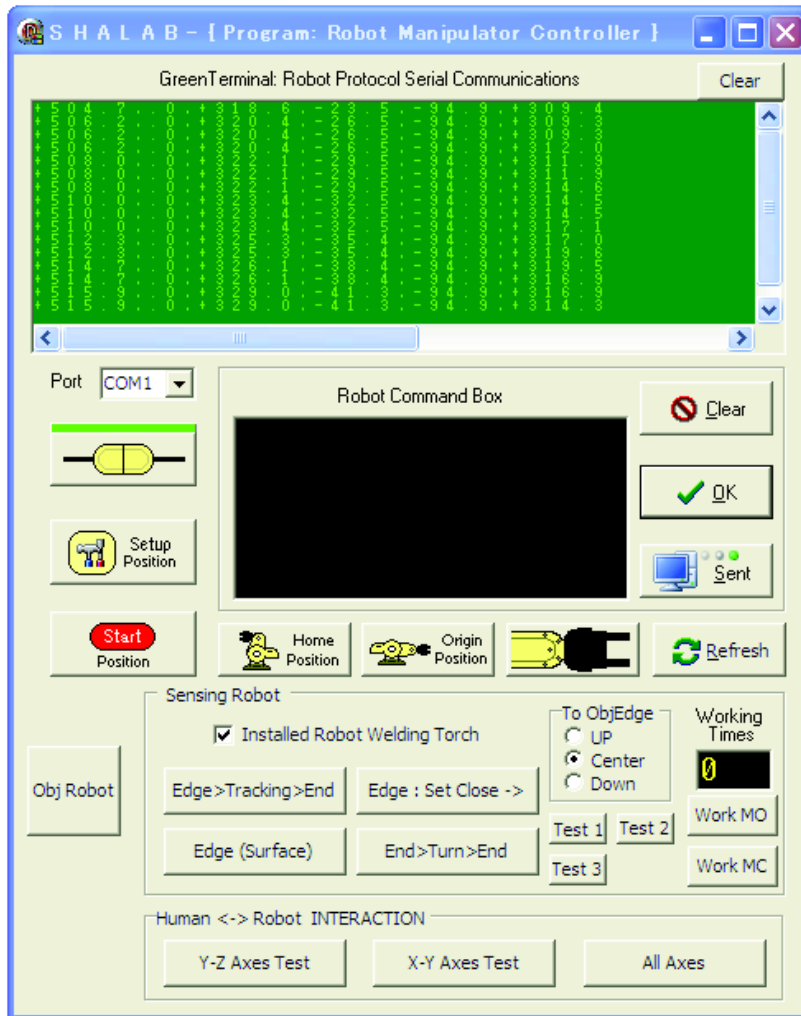
Figure 2-12. Robot manipulator controlling program

protocol in the serial line is "+515.9, .0, +329.0, −41.3, −94.9, +314.3". It means that the position of joint 1 is +515.9, the position of joint 2 is 0, the position of joint 3 is +329.0, the position of joint 4 is −41.3, the position of joint 5 is −94.9 and the position of line tracking is +314.3. Note that the unit of these values is in mm. This program is working together with inverse kinematics calculating program by providing the parameters such as the *X*, *Y*, *Z* coordinates and the sensing hand's orientation angle to the inverse kinematics calculating program for generating the robot command code. After the robot manipulator controlling program receive the robot command code, then this code will send to move the five DOF of the robot arm and the line tracking for particular working tasks is simply

by click the "*send*" button. When the robot is set in automatic mode, the send function is automatically sent by utilizing the developed watch dog function.

This program also contains some fundamental control buttons (hot keys). For example, "*home position*" button, which is use when the user wish to set the robot to the home position, "*origin position*" button, used when the user wish to set the robot to the origin position, "*setup position*" button, used to control the robot to move to the suitable position for the user to install the developed tactile sensing hand on the robot's end-effector. In cases when the robot has no response, the "*Error lamp*" on the driver unit will lit up. In this situation, the robot will keep the position for safety due to the driver unit cannot receive the new command. It will available to receive the new command after does the refresh function. The "*refresh*" button is required for the user to reset the robot to unexecute the particular bad command. For instance, it is used when the command set the moving position out of the operation space of robotic arm as shown in figure 2-10. This reset function can be automatically reset by utilizing the developed time out function.

In order to make the robot capable of sensing an environment during the motion, the continuous motion control is required. Note that the original robot system was developed in 1980 period and only point to point motion can be controlled. To solve this problem, I developed the continuous moving function into this program. The software of the robot arm system is specially improved of robot arm software designed for this research. The continuous motion control is achieved by dividing the total moving length of starting point to ending point into diminutive moving step. I set the normal speed of moving step within 30ms interval. However, for faster speed motion user can increase the moving step. In order to do the continuous motion control, I developed a watchdog timer function for automatic hand shaking between the PC and Robot into this program. This is because the driver unit cannot receive the new command during execution of the previous command. It will available to receive the next command after does the last motion. The watchdog function handles the enabled or disabled function to send the robot commands to the driver unit in the suitable time. In other word, this function is use for distinguishing the robot status, such as busy status (executing, moving status), and idle status (executed or finished a motion).

2.4.2.3. Inverse kinematics calculating program

Third developed program is the inverse kinematics calculating program. This program handles a function to generate the command code for controlling an arm robot with inverse kinematics method. In this section, I given the inverse kinematics calculation of the proposed system, followed by the developed program's information.

A) Inverse kinematics calculation
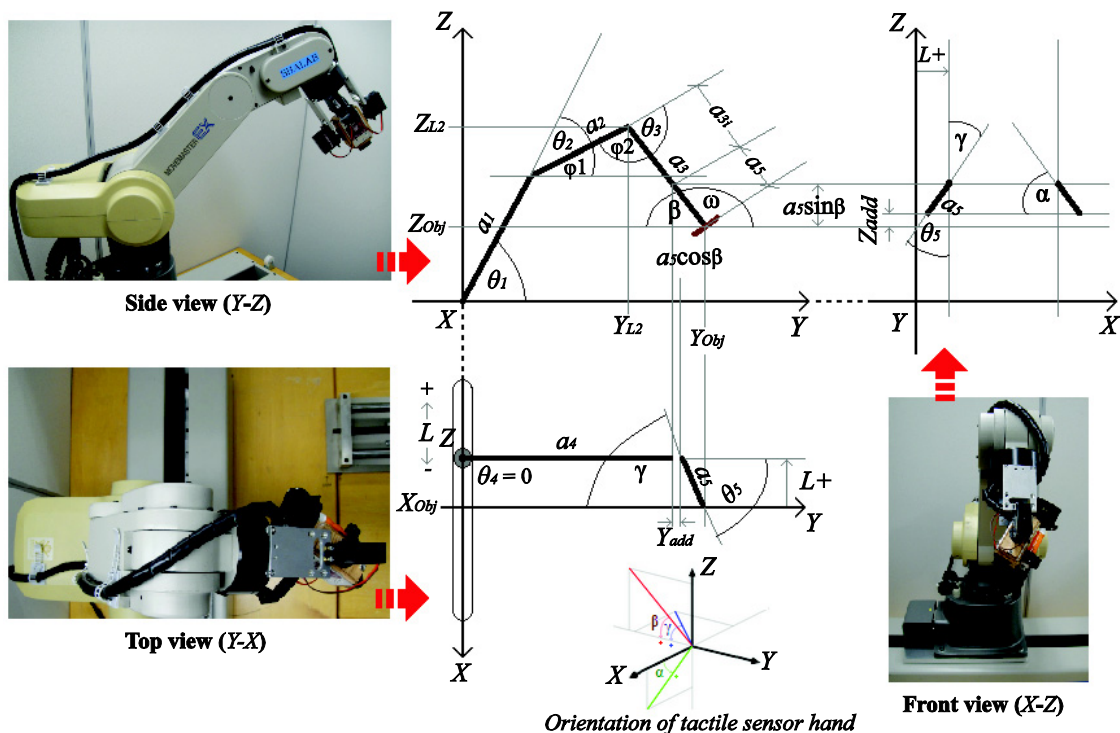
Figure 2-13. The relation between the actual robot arm and the robot model in 3-D for solving the inverse kinematics of 7 DOFs link system

In order to solve an inverse kinematics calculation of the proposed tactile sensing system, I sketched the model of robot arm system as shown in Figure 2-13. This figure shows the relation between the actual robot arm system and the model of robot arm system in 3-D for solving all of the joint angles and links. Inverse kinematics is the determination of all possible and feasible sets of joint variables, which would achieve the specified positions and orientations of the robot arm's end-effector with respect to the base frame. In practice, a robot manipulator control requires knowledge of the end-

22

effector location and orientation for instantaneous location of each joint as well as knowledge of the joint displacements to place the end-effector in a new location. This inverse kinematics target is the end-effector position, (X_{obj}, Y_{obj}, Z_{obj}) and the orientation, (β, γ, α). Note that β is the angle around X axis; γ is the angle around Y axis and α is the angle around Z axis as shown in Figure 2-13. Many industrial application such as welding and certain types of assembly operations require that a specific path to be followed by the end-effector. Thus, necessary to determine the corresponding motion of each joint, which will produce the desired tip motion. This is typical case of inverse kinematic application.

The robot arm in this system has a total of six moving joints J_1 to J_6 respectively. These 6 DOFs are allowing the full range of sensing area in 3-D. The main external dimensions of an original robot arm are the length of first link, a_1 which is measure from J_2 to J_3 and the length of second link, a_2 which is measure from J_3 to J_4. The dimensions after installation of the tactile sensing hand are also provided in this figure. These dimensions are the length of third link, a_3 which is measure from J_4 to the sensing hand's end-effector. The third link is combined with two small links, a_{3i} which is measure from J_4 to J_6 and a_5 which is measure from J_6 to the sensing hand's end-effector. In order to solve an inverse kinematics, the length in Y axis at J_6, a_4 is concerned. This length is computed by the kinematics method from a_1, a_2, and a_{3i} lengths. The relation between a_4 length and a_1, a_2, and a_{3i} lengths can be seen as the top view and side view of Figure 2-13. The a_4 length is the summation of the projection of the a_1, a_2, and a_{3i} lengths in Y axis. In order to achieve the specified positions and orientations of the robot arm's end-effector, all possible and feasible sets of joint variables should be determination. These joint variables are θ_1: the angle from Y-Axis to a_1, θ_2: the angle between a_1 and a_2, θ_3: the angle between a_2 and a_3, θ_4: the angle from Y-Axis to a_4, θ_5: the angle from Y-Axis to a_5 which is equal to the angle from Z-Axis to a_5.

The inverse kinematics solution is divided into seven calculation procedures for programming purpose. The first step is to obtain $\cos\theta_2$, Second step is to obtain θ_2, Third step is to obtain θ_1, Forth step is to obtain θ_3, Fifth step is to obtain θ_5, Sixth step is to obtain the additional length to move the 6 DOFs robot arm in Y direction and Z direction and the final step is to obtain the additional length to move the line tracking in X direction.
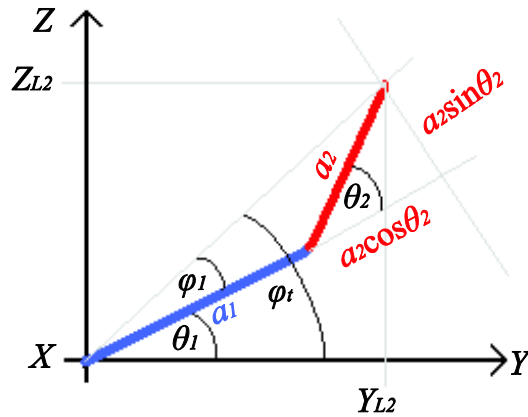
Figure 2-14. Solving the joint angles of two link planar arm (a_1 and a_2)

The kinematics solution is obtained by firstly solving the joint angles of two link planar arm (a_1 and a_2), as shown in Figure 2-14. Simply two links a_1 and a_2 planar arm were considered without other links in this figure. Given the joint angles θ_1 and θ_2, the end-effector of the first two links coordinates Z, Z_{L2} and coordinate Y, Y_{L2} can determine by utilizing forward kinematics technique. However, in order to command the robot the move at specific location as (Z_{L2}, Y_{L2}), the inverse method is required. In this case the answers are the joint variables θ_1 and θ_2 in term of the Z and Y coordinates of (Z_{L2}, Y_{L2}). This is the problem of inverse kinematics that taking into account in this section. Regarding to the Figure 2-14, the end-effector coordinates (Z_{L2}, Y_{2L}) of the first two links of robot arm are expressed in this coordinate frame according to equation (2-2) and (2-3);

$$Y_{L2} = a_1 \cos\theta_1 + a_2 \cos(\theta_1 + \theta_2) \tag{2-2}$$

$$Z_{L2} = a_1 \sin\theta_1 + a_2 \sin(\theta_1 + \theta_2) \tag{2-3}$$

Consider the diagram of Figure 2-14. Using the *Law of cosines* to obtain the θ_2:

$$(Y_{L2})^2 + (Z_{L2})^2 =$$
$$= \left[a_1^2 \cos^2\theta_1 + 2a_1a_2 \cos\theta_1 \cos(\theta_1 + \theta_2) + a_2^2 \cos^2(\theta_1 + \theta_2) \right]$$
$$+ \left[a_1^2 \sin^2\theta_1 + 2a_1a_2 \sin\theta_1 \sin(\theta_1 + \theta_2) + a_2^2 \sin^2(\theta_1 + \theta_2) \right]$$

24

$$(Y_{L2})^2 + (Z_{L2})^2 =$$

$$= a_1^{\,2} \cos^2 \theta_1 + a_1^{\,2} \sin^2 \theta_1 + a_2^{\,2} \cos^2 (\theta_1 + \theta_2) + a_2^{\,2} \sin^2 (\theta_1 + \theta_2)$$

$$+ 2a_1 a_2 \left[\cos\theta_1 \cos(\theta_1 + \theta_2) + \sin\theta_1 \sin(\theta_1 + \theta_2) \right]$$

$$= a_1^{\,2} + a_2^{\,2} + 2a_1 a_2 \left[\cos\theta_1 \cos(\theta_1 + \theta_2) + \sin\theta_1 \sin(\theta_1 + \theta_2) \right]$$

$$\frac{(Y_{L2})^2 + (Z_{L2})^2 - a_1^{\,2} - a_2^{\,2}}{2a_1 a_2} =$$

$$= \cos\theta_1 \cos(\theta_1 + \theta_2) + \sin\theta_1 \sin(\theta_1 + \theta_2)$$

$$= \cos\theta_1 (\cos\theta_1 \cos\theta_2 - \sin\theta_1 \sin\theta_2) + \sin\theta_1 (\sin\theta_1 \cos\theta_2 + \cos\theta_1 \sin\theta_2)$$

$$= \left[\cos^2 \theta_1 \cos\theta_2 - \cos\theta_1 \sin\theta_1 \sin\theta_2 \right] + \left[\sin^2 \theta_1 \cos\theta_2 + \sin\theta_1 \cos\theta_1 \sin\theta_2 \right]$$

$$= \cos^2 \theta_1 \cos\theta_2 + \sin^2 \theta_1 \cos\theta_2$$

$$= \cos\theta_2 \left[\cos^2 \theta_1 + \sin^2 \theta_1 \right]$$

$$= \cos\theta_2$$

$$\therefore \cos\theta_2 = \frac{(Y_{L2})^2 + (Z_{L2})^2 - a_1^{\,2} - a_2^{\,2}}{2a_1 a_2}$$

As →

$$1 = \sin^2 \theta_2 + \cos^2 \theta_2$$

$$1 - \cos^2 \theta_2 = \sin^2 \theta_2$$

$$\pm \sqrt{1 - \cos^2 \theta_2} = \sin\theta_2$$

$$\theta_2 = \tan^{-1} \frac{\sin\theta_2}{\cos\theta_2} = \tan^{-1} \frac{\pm \sqrt{1 - \cos^2 \theta_2}}{\cos\theta_2}$$

$$\therefore \theta_2 = \tan^{-1} \frac{\pm \sqrt{1 - \left[\dfrac{(Y_{L2})^2 + (Z_{L2})^2 - a_1^{\,2} - a_2^{\,2}}{2a_1 a_2} \right]^2}}{\dfrac{(Y_{L2})^2 + (Z_{L2})^2 - a_1^{\,2} - a_2^{\,2}}{2a_1 a_2}} \qquad (2\text{-}4)$$

At this step, θ_2 can determine base on $cos\theta_2$ in equation (2-4). Next step, I would like to obtain the θ_1 by utilizing variable θ_2. Consider the diagram of Figure 2-14 can be obtained:

$$\varphi_T = \theta_1 + \varphi_1$$

$$\theta_1 = \varphi_T - \varphi_1 = \tan^{-1} \varphi_T - \tan^{-1} \varphi_1$$

$$\therefore \theta_1 = \tan^{-1}\left(\frac{Z_{L2}}{Y_{L2}}\right) - \tan^{-1}\left(\frac{a_2 \sin\theta_2}{a1 + a2\cos\theta_2}\right) \tag{2-5}$$

Note that the angle θ_1 depends on which solution is chosen for θ_2. At this step, θ_1 can determine base on θ_2 as equation (2-5). Next step, I would like to obtain the θ_3 by utilizing variable both θ_1 and θ_2. Consider the diagram of Figure 2-13:

$$\theta_3 = \beta - \theta_1 - \theta_2 \tag{2-6}$$

At this step, θ_3 can be determined based on θ_1 and θ_2 by using equation (2-6).

Next step is to obtain the θ_5. Consider the diagram of Figure 2-13 found as:

$$\theta_5 = \gamma \tag{2-7}$$

At this step, θ_5 can be determined as γ as equation (2-7).

Next step is to obtain the additional length to move the 6 DOFs robot arm in Y direction. Considering the diagram of Figure 2-13 I found that:

$$a_4 = Y_{L2} + (a_{3i}\cos\beta) \tag{2-8}$$

$$a_5 = a_5\cos\gamma\cos\beta \tag{2-9}$$

$$Y_{add} = Y_{obj} - a_4 - a_5 \tag{2-10}$$

Y_{add} can be rewritten by using equation (2-8) and (2-9) into equation (2-10) as follow:

$$\therefore Y_{add} = Y_{obj} - Y_{L2} + (a_{3i}\cos\beta) - a_5\cos\gamma\cos\beta \tag{2-11}$$

Next step is to obtain the additional length to move the 6 DOFs robot arm in Z direction, Z_{add}. Consider the diagram of Figure 2-13 found as;

The total position in Z coordinates, $\quad\quad Z_{length} = Z_{L2} - Z_{obj}$ $\quad\quad\quad$ (2-12)

The position of a_{3i} link in Z coordinates, $\quad Z_{a3i} = a_{3i}\sin\beta$ $\quad\quad\quad$ (2-13)

The position of a_5 link in Y-Z plane, $\quad\quad Z_{a5(YZ)} = a_5\cos\gamma\sin\beta$ $\quad\quad$ (2-14)

The position of a_5 link in Z-X plane, $\quad\quad Z_{a5(ZX)} = a_5\sin\gamma\sin\alpha$ $\quad\quad$ (2-15)

26

The additional length to move the 6 DOFs robot arm in Z direction can be obtained as:

$$Z_{add} = Z_{length} + Z_{a3i} + Z_{a5(YZ)} + Z_{a5(ZX)} \quad (2\text{-}16)$$

Then add the terms Z_{length} from equation (2-12), Z_{a3i} from equation (2-13), $Z_{a5(YZ)}$ from equation (2-14) and $Z_{a5(ZX)}$ from equation (2-15) into equation (2-16) as:

$$\therefore Z_{add} = \left(Z_{L2} - Z_{obj}\right) + \left(a_{3i}\sin\beta\right) + \left(a_5\cos\gamma\sin\beta\right) + \left(a_5\sin\gamma\sin\alpha\right) \quad (2\text{-}17)$$

The final step is to obtain the additional length to move the line tracking in X direction, L. Consider the Figure 2-13, the position of a5 link in X-Y and Z-X planes can be obtained as:

$$Z_{a5(XY-ZX)} = \left(a_5\sin\gamma\cos\alpha\right) + X_{obj} \quad (2\text{-}18)$$

$$L = -Z_{a5(XY-ZX)} \quad (2\text{-}19)$$

Adding terms $Z_{a5\,(XY-ZX)}$ from equation (2-18) into equation (2-19)

$$\therefore L = -\left(a_5\sin\gamma\cos\alpha\right) + X_{obj} \quad (2\text{-}20)$$

The value of L is inversed due to the reverse direction of the line tracking to the reference coordinate frame set by the factory. Note that the dimensions of robot can be obtained as Figure 2-9 such as $a_1 = 250$mm, $a_2 = 160$mm, $a_3 = 223$mm, $a_{3i} = 170$mm and $a_5 = 53$mm. The inverse kinematics of the proposed system has been solved. All the equations are used for creating the inverse kinematics calculating program as described in next section.

B) Developed program

This program handles the function to generate the robot controlling command code by using inverse kinematics computations given in the previous section. Figure 2-14 shows an image of this program. The example of the inverse kinematics target are the end-effector position is ($X_{obj} = 0$mm, $Y_{obj} = 545$mm, $Z_{obj} = 0$mm) and the orientation of tactile sensor hand as ($\beta = -45°$, $\gamma = -18°$, $\alpha = 0°$) as shown in figure 2-14. Note that, the orientation of tactile sensor hand in this case β is the angle around X axis; γ is the angle around Y axis and α is the angle around Z axis. This program received the target

27
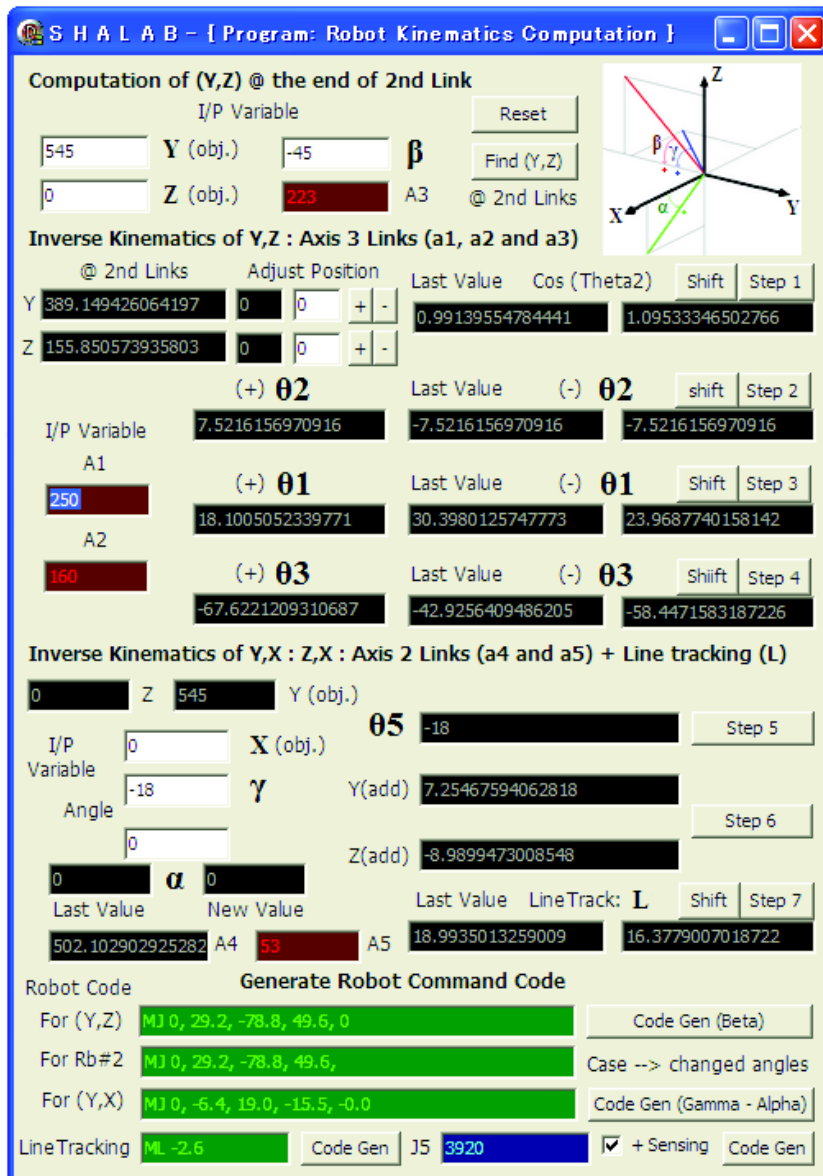
Figure 2-15. Inverse kinematics calculating program

parameters from the robot manipulator controlling program. Then the program does the inverse kinematics calculation to obtain of all possible and feasible sets of joint variables, which would achieve the specified positions and orientations of the robot arm's end-effector with respect to the base frame. Finally, the program will generate the robot command code. The green terminal labeled "Robot Code" in this figure also shows the robot code for controlling the line tracking (*L*) and the robot arm in (*Y-Z*), (*Y-X*) planes.

28

As results, this program generates four robot codes to move the robot in (Y-Z) plane and (Y-X) plane, the line tracking in X direction and the additional DOF servo motor joints. First motion is to move the robot in (Y-Z) plane using the command "MJ 0, 29.2, −78.8, 49.6, 0". It means that the target angle of the joint 2 is 29.2 degree, joint 3 is −78.8 degree, joint 4 is 49.6 degree and keep the position of joints 1 and 5 still. Second motion is to move the robot in (Y-X) plane using the command "MJ 0, −6.4, 19, −15.5, 0", which means move the joint 2 is −6.4 degree, move the joint 3 as 19 degree, move the joint 4 as −15.5 degree and keep the position of joints 1 and 5. Third motion is to move the line tracking in X direction using command "ML −2.6". It means that the line tracking with 2.6mm in −X direction. The last motion is to move the additional DOF servos joint using command "3920" which means move this joint with −18 degree (γ).

2.4.3. Tactile sensor hand

The proposed tactile sensor hand is attached to the end-effector of robot arm. In this research, three prototypes of tactile sensor hands were developed.
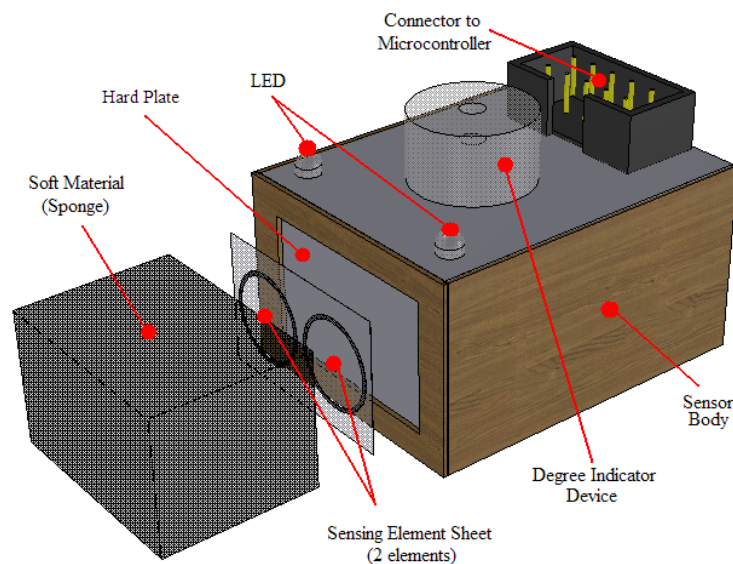
Figure 2-16. Tactile Sensor hand with 2 sensing elements

In order to confirm the principle of tactile sensing (key idea), the first prototype is the unit with two sensing elements. The gradient of the contacted object can be obtained

29

from the differences values between two sensing elements. Figure 2-16 illustrates the first prototype of tactile sensor unit. This unit has two sensing points for sensing the object information in one plane. It is simple to develop and easy to apply for sensing an object in one plane.
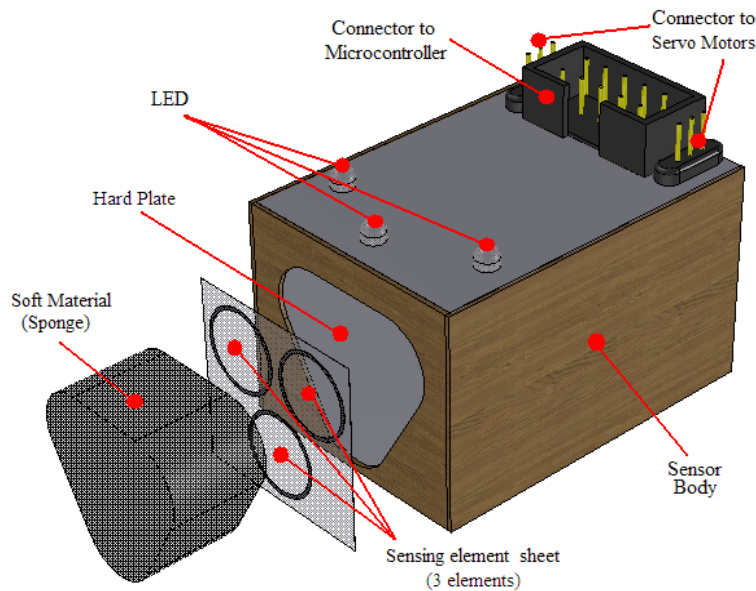
Figure 2-17. Tactile Sensor hand with 3 sensing elements

To enable the sensing unit to obtain object information in 3-D, the second prototype of tactile sensor unit was developed. This unit has three sensing elements, which is increased the sensing points to obtain an object information in two planes (3-D). Figure 2-17 illustrates the second prototype of tactile sensor unit. To simplify the functional check, these two sensing devices have LED indicators to show the sensor which received the strongest force.

As the proposed tactile sensor unit works together with the robotic arm and can scan the space, the sensor unit does not need to have a lot of sensing elements. The minimum number of sensing points required for detecting the local shape and surface orientation is three. The global shape measurement can be done by moving the arm along the surface of the object. There are some special cases in which flat surfaces and edges cannot be distinguished with just three sensing points. However, in most practical applications, I can avoid such cases by setting the relation between the sensor unit and the

object adequately. The global shape measurement can be done by moving the robot arm along the surface of the object. The developed sensor hand uses three force-sensitive resistors, which is described on the section 2.2(Sensing Element).
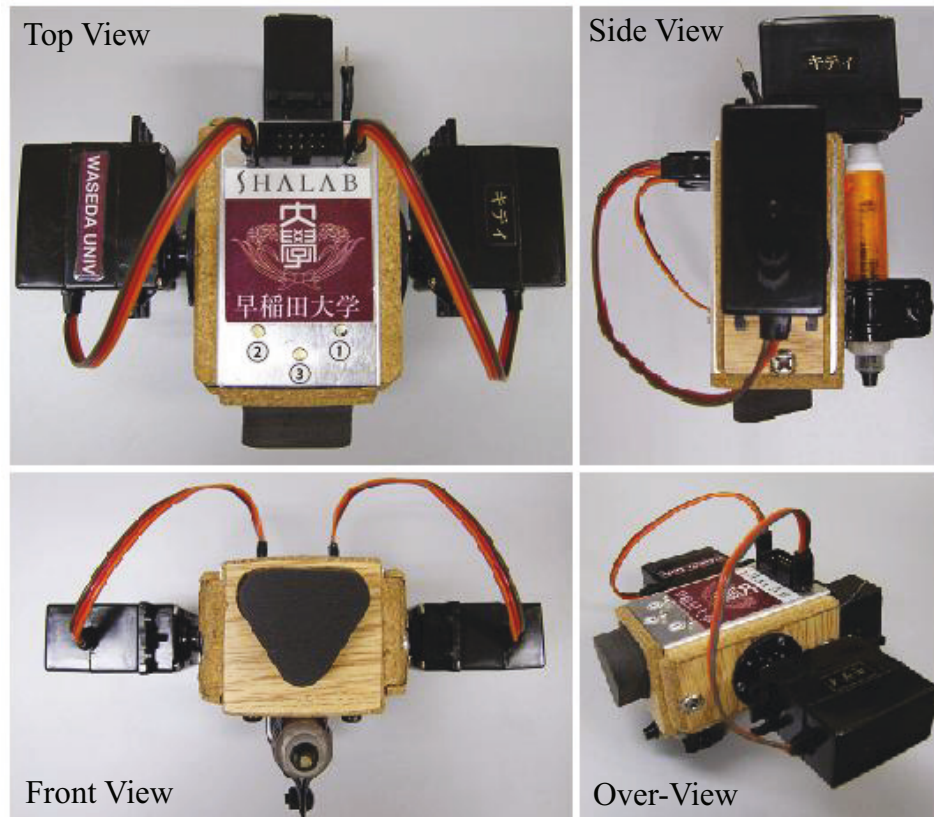
Figure 2-18. Various views of prototype tactile sensor hand for welding arm robot

To perform the object sensing and control in 3-D with simulated welding torch, the third version of tactile sensor hand was developed. Some photos of an actual prototype tactile sensor hand with simulating torch from various viewpoints are shown in Figure 2-18. Figure 2-19 demonstrates the design concept of prototype tactile sensor hand for industrial arm robot. The developed tactile sensor hand consists of two automatic swapping functions. One is a simulated welding torch function with moving mechanisms. I utilize the worm gear with servo drive for the moving mechanisms. The other is tactile sensing for object edge detection. The three sensing elements are fixed to make triangular position and located in 120 degree interval for each element.

Connector for
Microcontroller

Connectors for
Servo motor

LED indicators

17 mm

Sensor Body

35 mm

Servo motor

Worm gear
Mechanism

Simulated
welding torch

Hard Plate

Sensing element sheet
(3 elements)

Soft Material
(Sponge)

X

120°

60°   60°

9.53 mm

2   1

Z

Sensing
element
No.2

3

Sensing
element
No.1

Sensing
element
No.3

26 mm

The Locations of Sensing elements
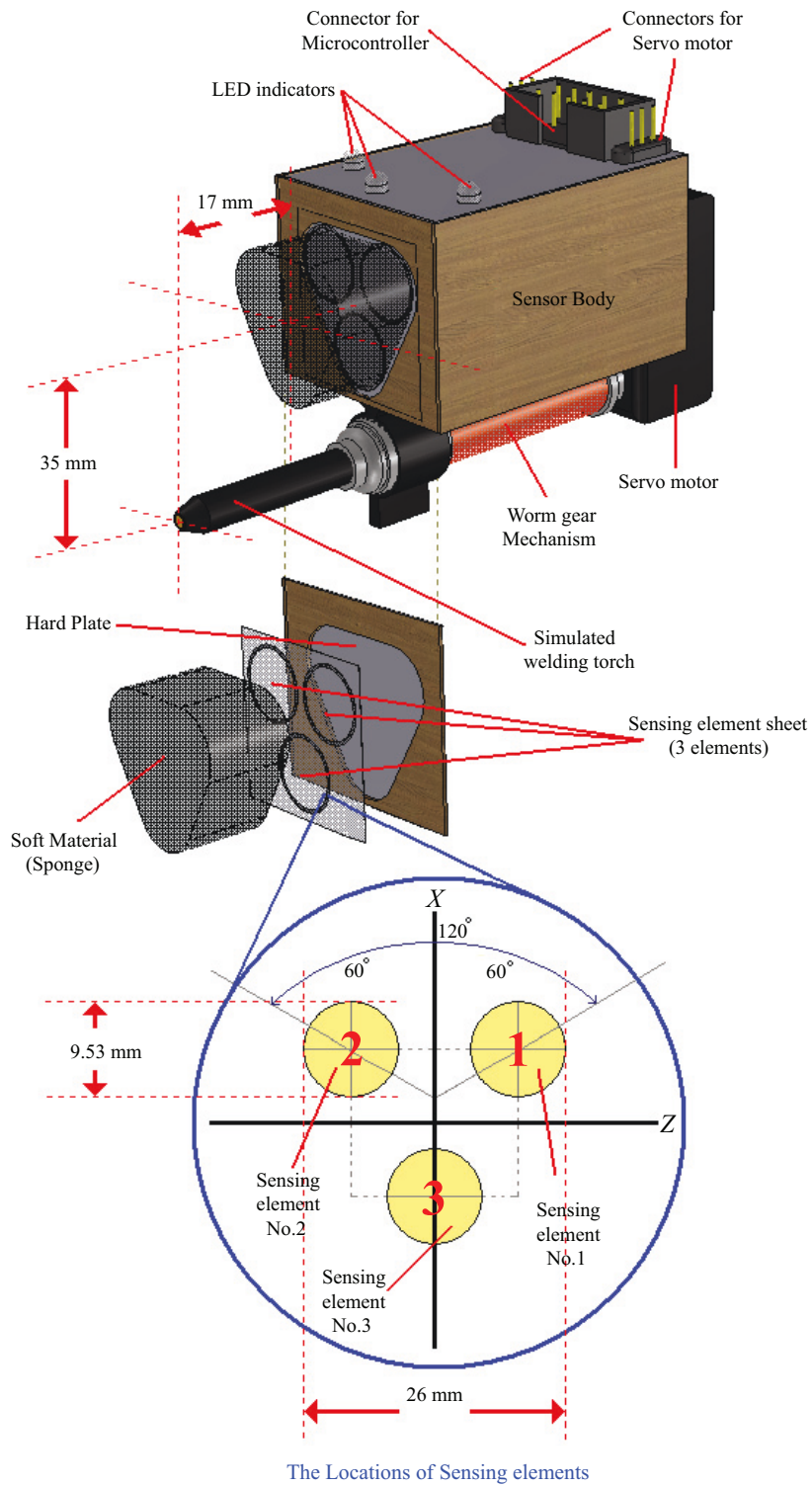
Figure 2-19. Design concept of prototype tactile sensor hand for welding arm robot

32
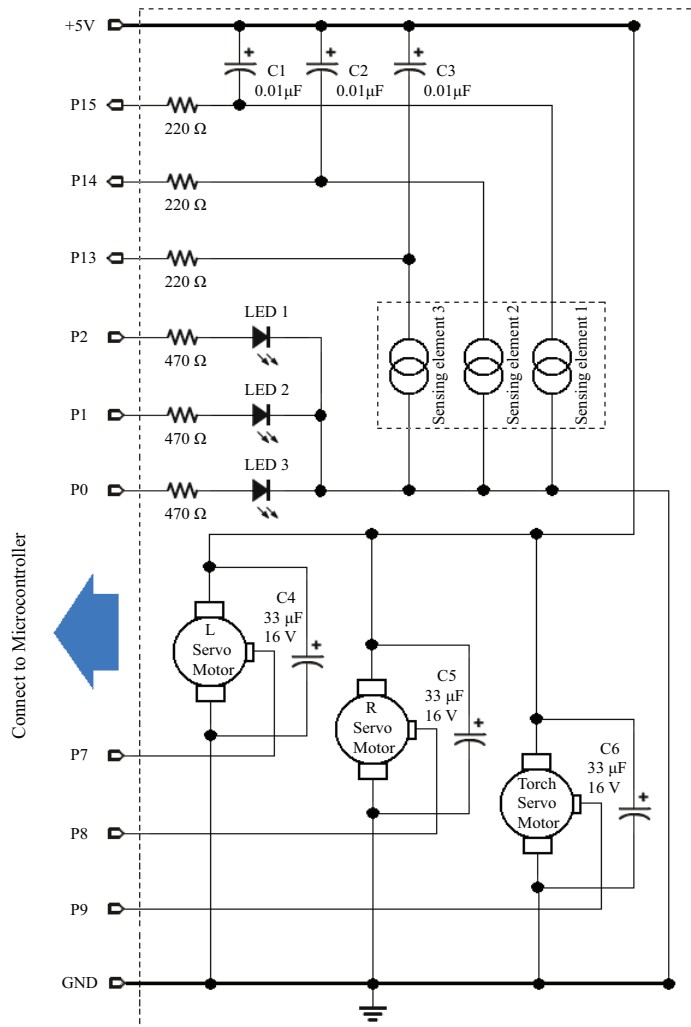
Figure 2-20. Electronic circuit diagram of the tactile sensor hand for welding arm robot

The resistances are measured by using the charge and discharge of an RC circuit as shown in Figure 2-20. These sensing elements were covered with a sponge rubber plate (soft material) which thickness can be changed depending on the object. Based on the preliminary experiments for selecting materials, which is described on section 2.6, I employed a sponge whose thickness is 15 mm and Young's modulus is 0.496N/mm^2 for the following experiments. The other side of the device is covered with a hard plate and fixed on the sensing hand module installed on the robot arm's end-effector. To simplify the functional check, the circuit of the sensing devices has LED indicators to show the sensor which received the strongest force.

33

2.4.4. Interfacing unit
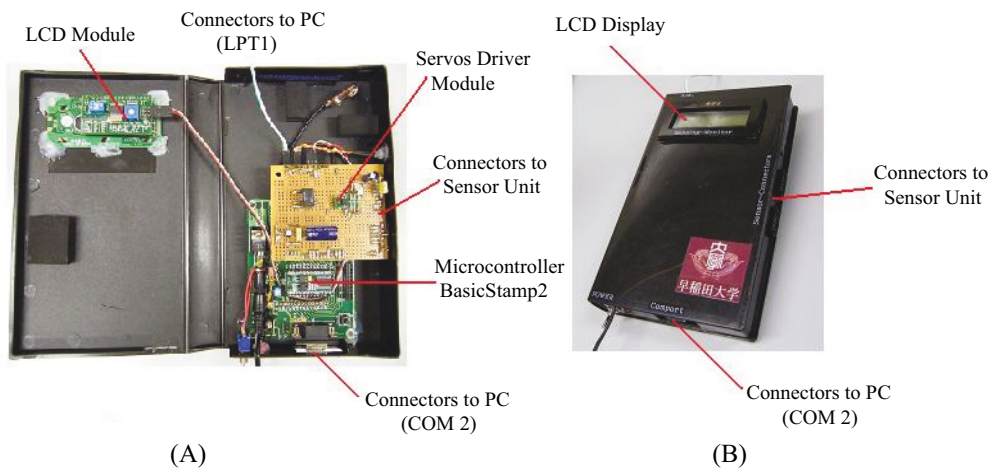
Figure 2-21. Prototype of tactile sensor interfacing unit for robot arm

To perform a real time sensing to control the robot arm system, I developed a suitable interfacing system to connect computer (PC), tactile sensing hand and robot arm system. This system carry out the processing task with a *BasicStamp2* microcontroller, produced by *Parallax* Inc., USA with peripheral circuits such as supply circuit, servo motor driver circuits, interfacing/communication circuits and display driver circuits.

The prototype of interfacing module is shown in Figure 2-21. Figure 2-21(A) shows electronics board inside the module. Figure 2-21(B) shows the overall view of the module. The sensing interface module handles the communicating function via serial port (COM2) and Parallel port (LPT) through the PC.

The interface module mainly handles the reading value of the RC-time constant from the RC circuits inside the tactile sensing hand. After obtain the RC-time constant value of each sensing elements the microcontroller will generate the data packet and send them to the PC via serial port. The data has been described in the section 2.4.2.1(Sensor interfacing program) In addition, to simplify display the tactile sensing data at the work site, this interface module also contains the LCD display as shown in Figure 2-20(B). This function is useful when the users are working close to the module.   Moreover, this interfacing module also contains the servo driver to control an additional DOF of robot arm and a servo motor for an attached simulate welding torch. The module also capable to provide the acknowledgement signals to the PC via parallel port (LPT1). Generally,

parallel port is mainly meant for connecting the printer to PC. However, this port can be programmed for many more applications beyond. Usage of the PC's parallel port, this port contains a set of signal lines that CPU procedures to send or receive data with other connecting components outside. In signaling, open signals are "1" and closed signals are "0". This port act to sends 8 bits and receives 5 bits at a time.

	CH1	CH2	CH3	CH4	CH5				
Acknowledgement	$\overline{S7}$	$S6$	$S5$	$S4$	$S3$	$S2$	$S1$	$S0$	DEC
Normal	0	1	1	1	1	0	0	0	128
Torch is moving	1	1	1	1	1	0	0	0	248
available	0	0	1	1	1	0	0	0	56
available	0	1	0	1	1	0	0	0	88
available	0	1	1	0	1	0	0	0	104
available	0	1	1	1	0	0	0	0	112

Table 2-1. Coding of parallel port information to obtain the tactile system status

In order to create the rapid acknowledgement signals to let the system or user can distinguishes the system's safety situation promptly. I decided to employ the input status register $(\overline{S7}, S6, S5, S4, S3)$ of PC parallel port (LPT1: 379H) as the acknowledgement port due its faster communication compared with serial ports. This signals is use to let the system can distinguish the simulated torch is on the driving process or stop. Also it can be used for alarm signal when the sensing value reaches at the set point. This function is useful for detecting some specific value in particularly task such as, an emergency stop, an interrupt to observe some special investigation, etc. The electronic circuit diagram of this parallel interface is shown in Figure 2-7. The total reserve acknowledges signals are six cases can be determined by using in the proposed system. However, at the moment the only one signal, CH1 is use for determined the status of moving simulated welding torch is moving or not moving. For example, when the PC read the status register as 128 DEC value is mean the torch is in the normal status, while the 248 DEC value is mean the torch on moving process (Torch activated). The user can add more cases to be check in this system by add the contact relay or digital switch into the circuits. This system has available 4 channels as CH2 to CH5 can be used to recognize more in the other cases.

2.5. Sensing System for Humanoid Robot
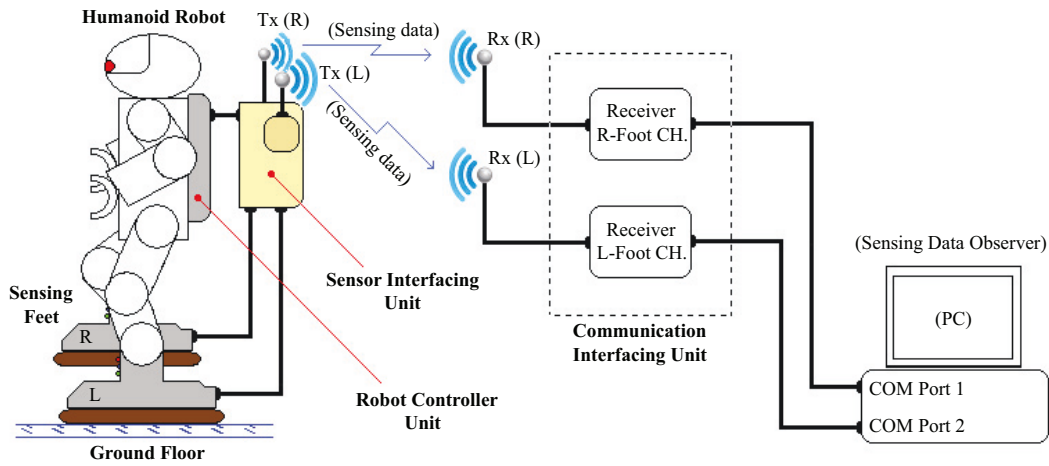
Figure 2-22. Diagram of tactile sensing system for humanoid robot
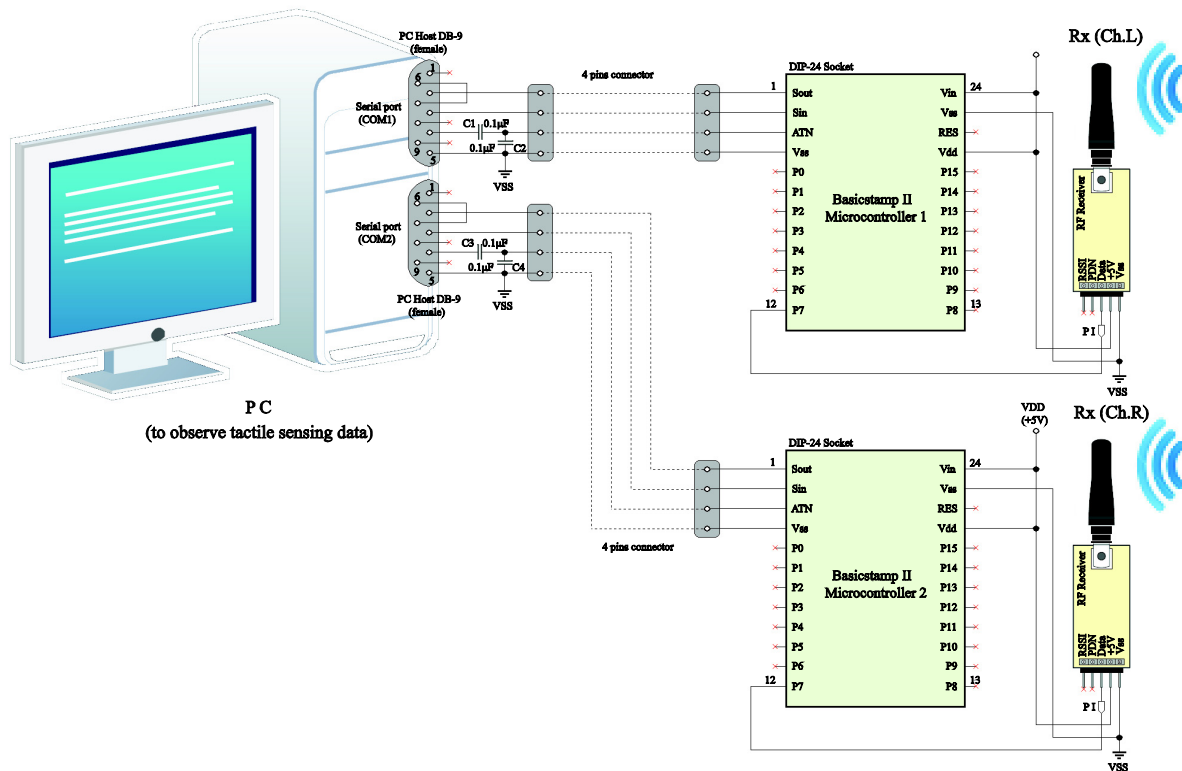
Figure 2-23. Electronic circuit diagram of wireless sensing data observer system

36
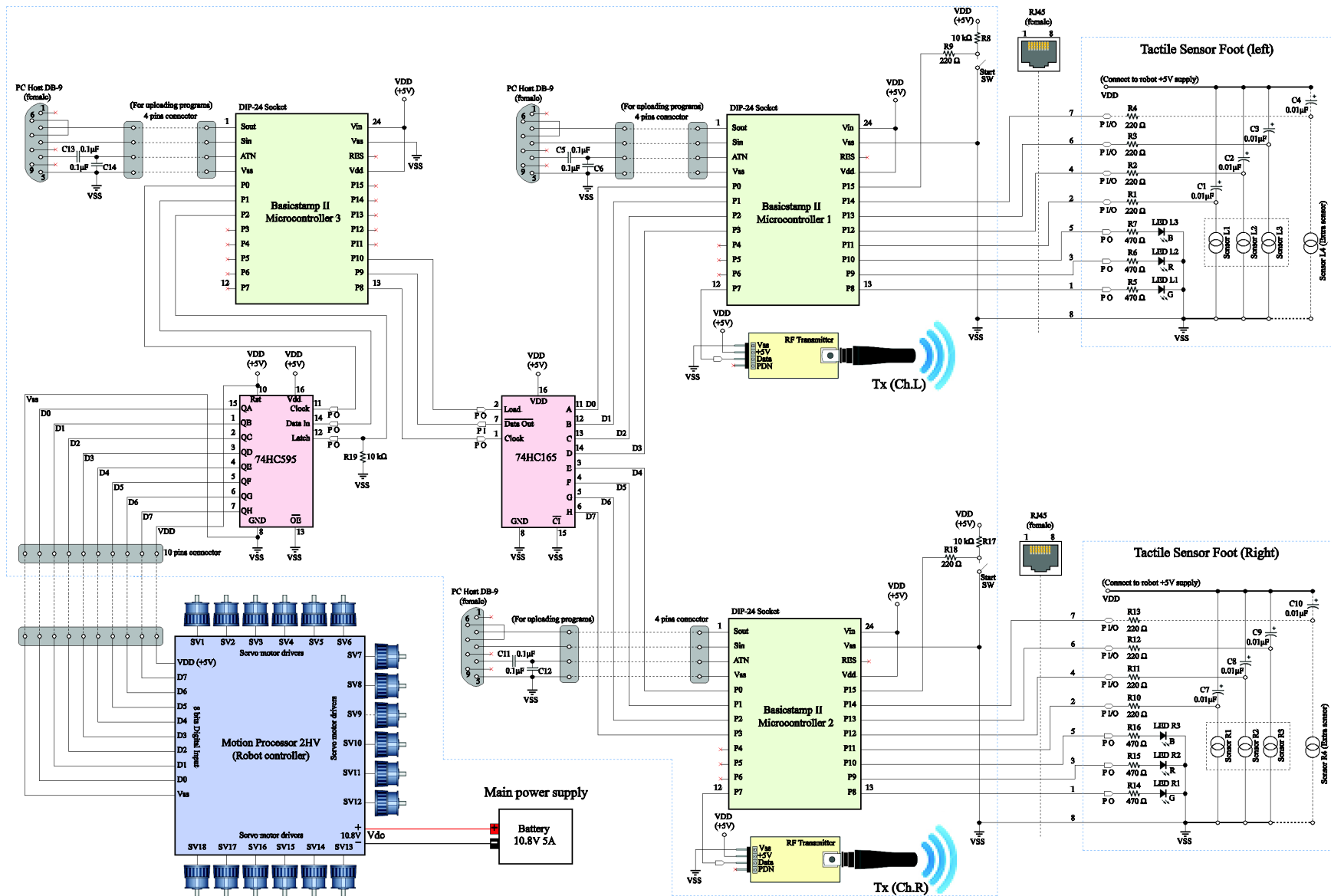
Figure 2-24. Electronic circuit diagram of tactile sensing system for an autonomous humanoid robot

37

The tactile sensing system diagram for humanoid robot is shown in Figure 2-22. This system is the stand alone system of humanoid robot. The robot is independent from the peripheral circuits and cables. The user can observe the sensing data via the wireless communications. The electronic circuit diagram of wireless sensing data observer system and the whole system circuit are shown in Figure 2-23 and 2-24 respectively. The main parts of proposed system are described as follows;

2.5.1. Humanoid robot
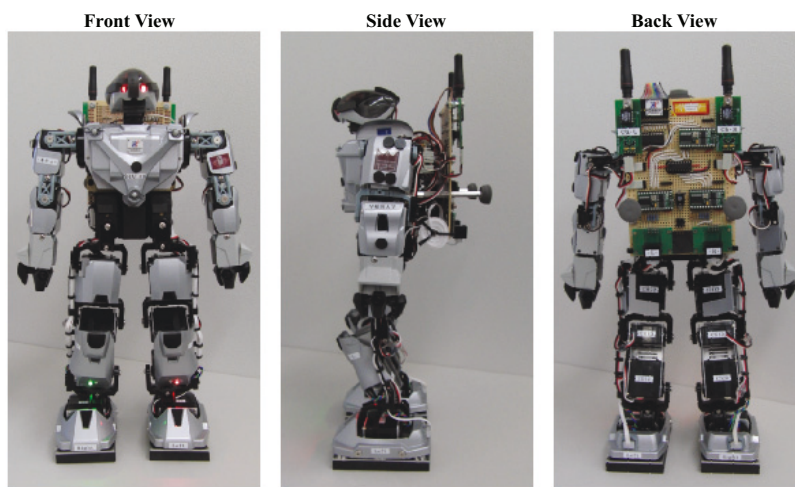
Figure 2-25. Various views of a prototype autonomous humanoid robot
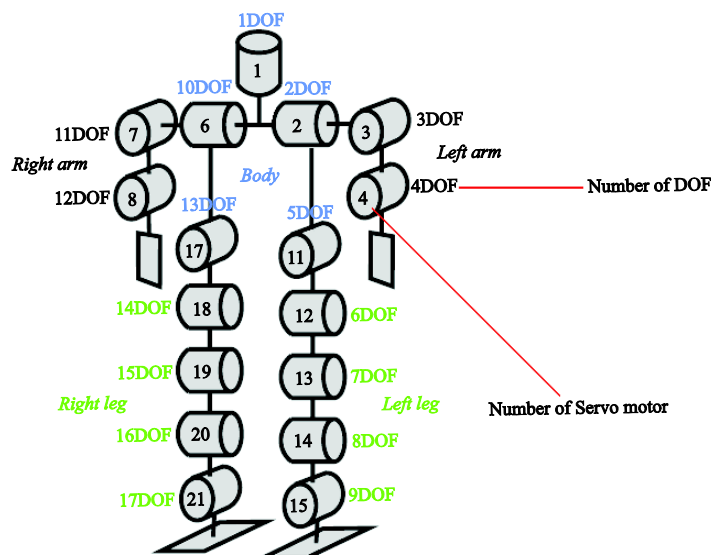
Figure 2-26. Detailed kinematics of prototype humanoid robot

The humanoid robot is specially improved for this research based on Japanese company Kondo Kagaku Co., Ltd, "*KHR-2HV*". The robot chassis is made of aluminum plates, allowing for a lightweight and rigid structure. Frontal, side and back views of a prototype of autonomous humanoid robot are shown in Figure 2-25. The humanoid robot has 17 degrees of freedom (DOF), 4 DOFs for body and each leg, 2 DOFs for each arm and 1 DOF for the head joint as shown in Figure 2-26. The autonomous robotic system must manage its motion automatically rather than playing the sequences motion which is stored in a memory. Due to this reason, the robotic legs need to have the load torque capabilities during the sensing and possessing tasks and to avoid the heating problems. I modified each joint of robotic legs with digital metal gear servomotor model "*KRS-2350HV*". These servos were changed from the standard digital plastic gear servomotor model "*KRS-788HV*" to increase the maximal load torque of each joint from 10kg/cm to 29.5kg/cm. Another aim is to avoid the melting problem of the plastic gears. I used the original servos for the arm and head joints. In total this system contains 17 servos which are connected and controlled by the robot controller unit "*Motion Processor-2HV*" which is allows me to create the control programs and functions regarding to the receiving 8 bits input signal from the sensor interfacing board.

2.5.2. Tactile sensor feet

The structure of the prototype tactile sensing feet for humanoid robot is shown in Figure 2-27. The tactile sensor units are equipped at the back of two robotic feet. Each foot has an individual sensing circuit to detect the three sensing values. As the proposed sensor unit works together with the robot system, it can scan the environment space. The sensor foot unit does not require a lot of sensing elements. The minimum number of the sensing point required for detecting the ground slope and orientation is three. The prepared devices are "*Flexi Force*" which is a sort of the force sensitive resistor produced by Tekscan Inc., which is described on the section 2.2(Sensing element). The sensor resistance has decreases, when applied the pushing force on the sensing area of element sheet. The resistances of three force sensitive resistors have similar values when applied the pushing force to the center of all the elements. Hence, I can detect the gradient of the contacted ground surface by utilizing the differences between these three force sensitive
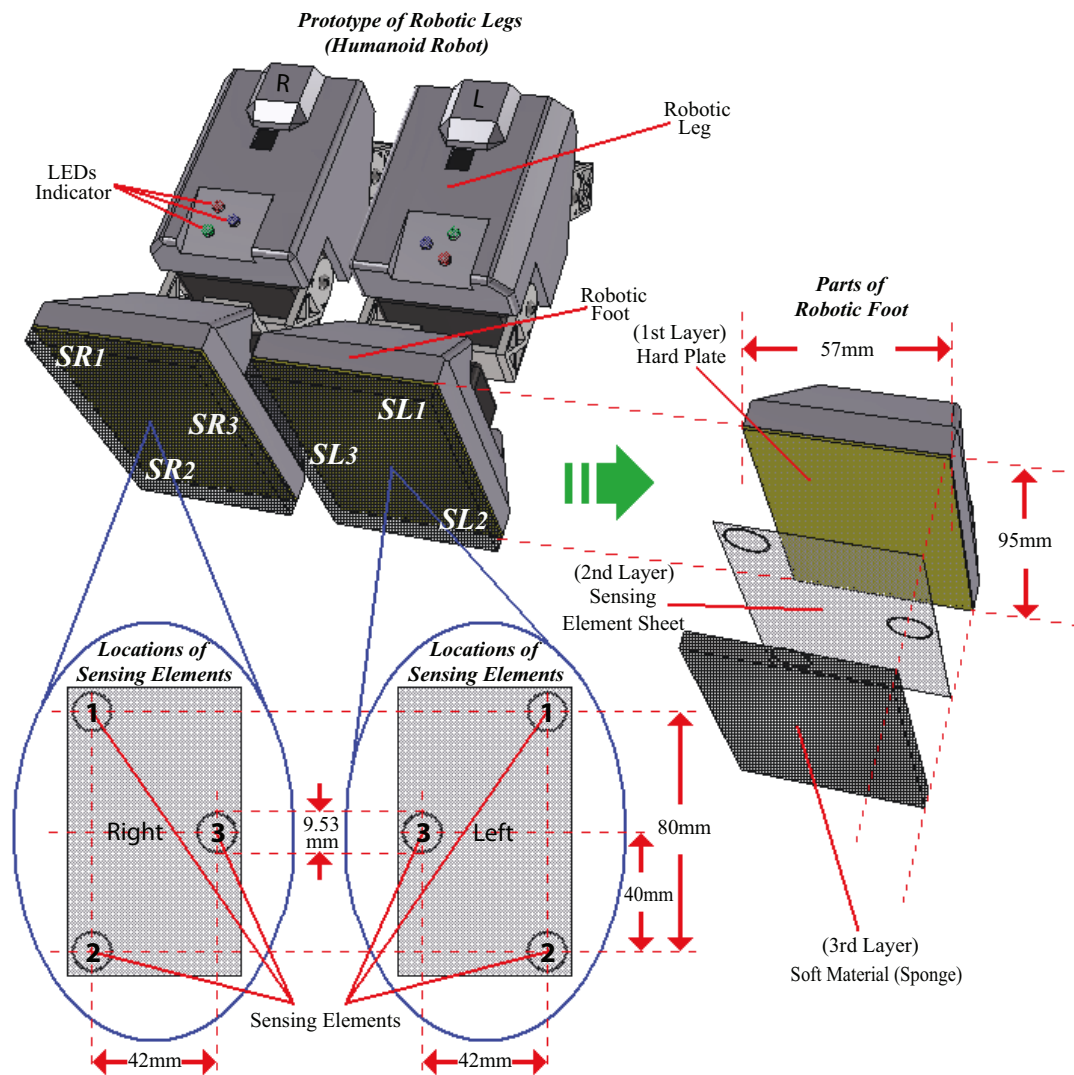
Figure 2-27. Structure of the prototype tactile sensor feet for humanoid robot

resistors. As shown in Figure 2-27, this figure demonstrates the detailed structure of the prototype robotic tactile sensing feet. The installed locations of all sensing elements for two sensing feet are also shown in this figure. The three sensing elements are fixed to make triangular position on each foot. They are covered with a sponge rubber plate (soft material). I employed a sponge whose thickness is 10mm (Young's modulus: 0.496N/mm^2) for the prototype development. The other side of these elements is covered with the hard steel plate and fixed on the end-effector of the robot foot. The sensor signals are digitized by a resistance measuring method using RC time constant technique.

The measurements are carried out in real time with sensor interfacing unit. The resistance value is measured by using the charge and discharge of RC circuit as shown in Figure 2-24. To simplify the functional check, the sensing devices circuit has LED indicators to show the sensing area which received the strongest force. The colors of LEDs are different to simply inform the users of the point where the force is strongest, i.e. red means that the force on back side is the strongest, green means that the force on front side is the strongest, red and green means that the force on their leg side is strongest, and blue means that the force on the opposite of their leg side is the strongest.

2.5.3. Interfacing unit

(Robot Controller Unit)

(Sensor Interfacing Unit)
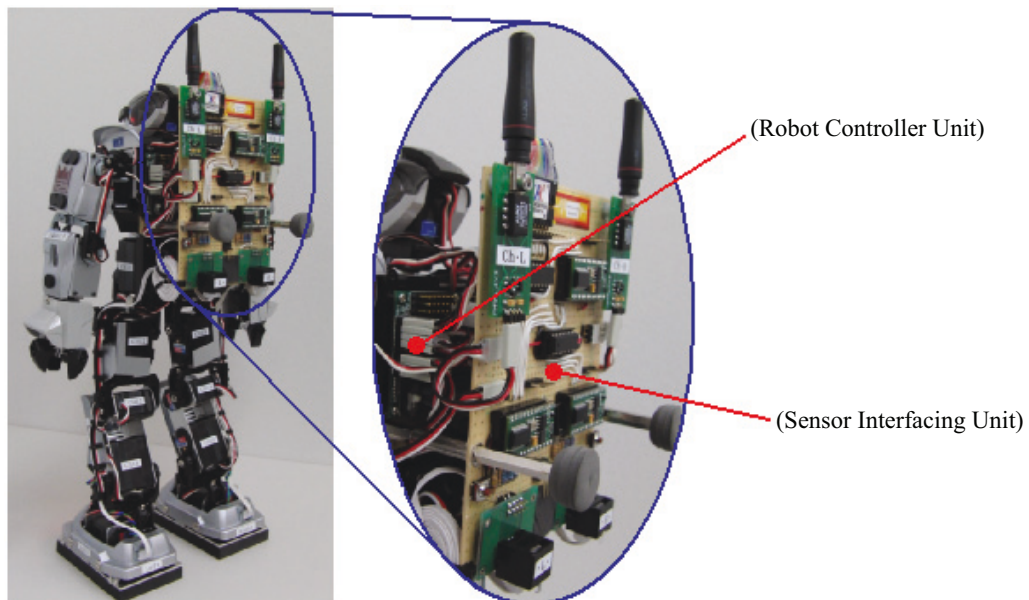
Figure 2-28. Installation of the controller and interfacing boards on humanoid robot

I aim to develop a sensing system for stand-alone robotic system to let the humanoid robot free from the peripheral circuits. To achieve this function, I have integrated the peripheral circuits into one unit and equipped them on the back of a humanoid robot body. Figure 2-28 shows the installation of controller and interfacing boards. The sensor interfacing unit is located on the sensor interfacing board. This board is connected to the robot controller board with 8 bits address bus.
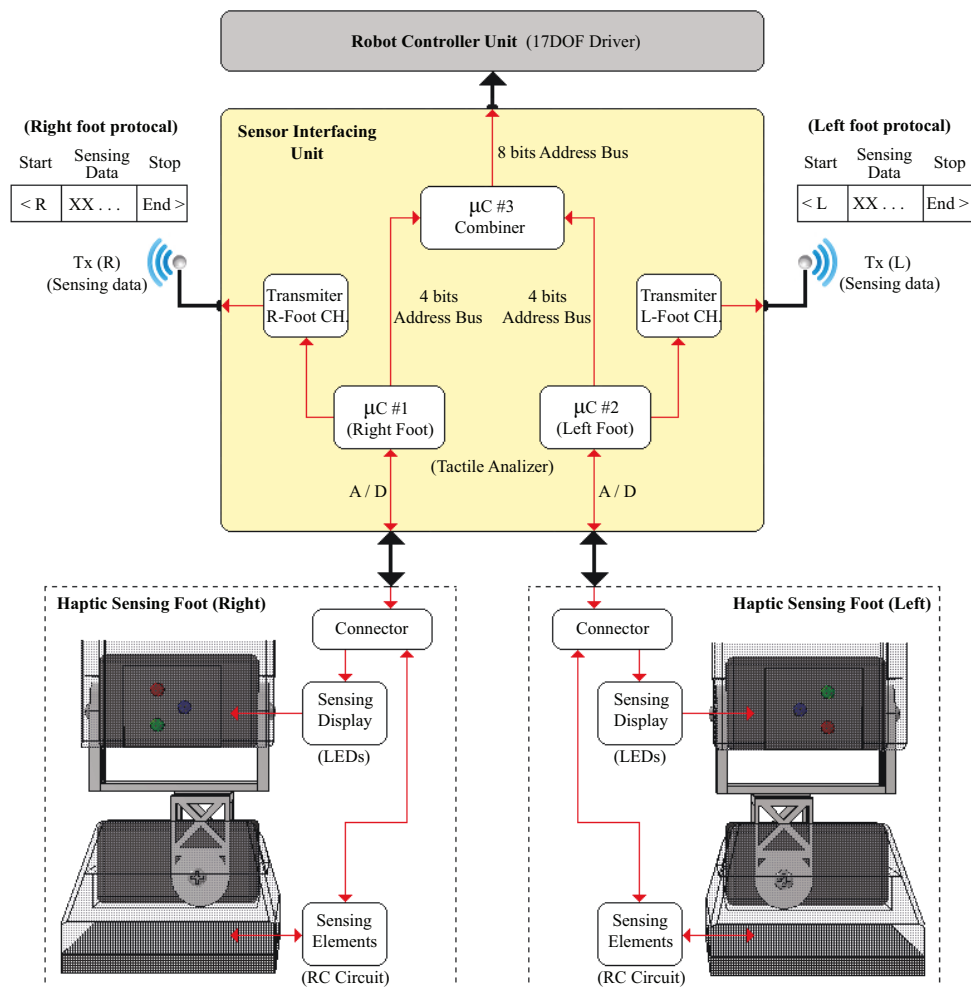
Figure 2-29. System architecture and data flow of embedded tactile sensing feet

Strongest receiving force	Left foot	Right foot	Both feet
Sensing element #1	00010000	00000001	00010001
Sensing element #2	00100000	00000010	00100010
Sensing element #3	01000000	00000100	01000100

Table 2-2. Coding of 8 bits data for humanoid robot motion controls

The system architecture and data flow of embedded tactile sensing feet is shown in Figure 2-29. This sensor interfacing unit carries out the processing task with three *BasicStamp2* microcontrollers with peripheral circuits. Microcontroller 1 and 2 are to analyze the tactile data of right and left foot respectively. The sensing signals are digitized by a resistance measuring method using RC-time constant technique. The

measurements are carried out in real time with developed program installed on microcontrollers 1 and 2. These two processors compare the three sensing data and then generate the 4 bits digital signal regarding to the strongest receiving force position. These two signals will send to combine at microcontroller 3 as 8 bits digital signal. Then this generated signal is sent to the robot controller board for controlling the robot motions. Table. 2-2 is shows all the generating digital from three microcontrollers. In this work, I aim to develop the stand-alone system, thus the sensing monitor was designed out of the robotic system. If the communication is done with the cable links, it affects the dynamic movement of the robot. In order to allow the user to observe the tactile sensing data for researching purpose, hence, the system should connect by utilizing the wireless radio links between the sensor interfacing unit and PC. This wireless radio links contain two channels, left and right foot channels. In order to transmit these two sensing data at the same time, I developed the suitable protocol for two wireless communicating channels. (Left and right foot protocols) These protocols are also shown in Figure 2-29.

2.6. Preliminary Experiments

2.6.1. Sensor linearity test
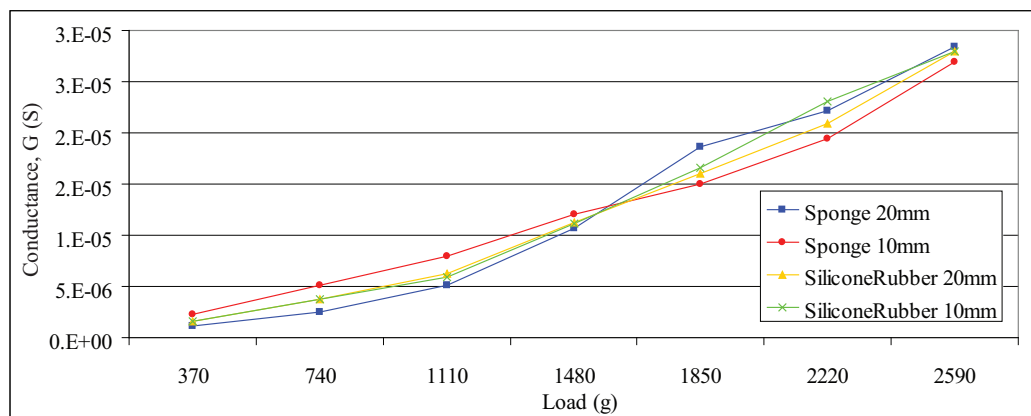
Figure 2-30. Relationship between the conductance and load for different soft materials

To test sensor linearity, I prepared four different kinds of soft material, such as 10mm and 20mm thick pieces of sponge with $0.496 N/mm^2$ young's modulus. I also prepared 10mm and 20mm thick pieces of silicone rubber. In this test, I fixed the sensor unit and set loads of between 0.37 and 2.59 kg on it. The load was normal to the surface
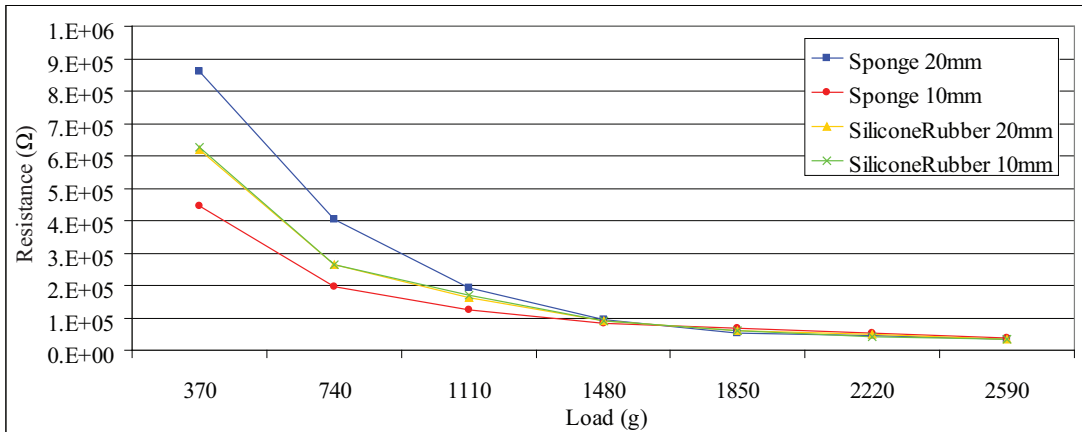
Figure 2-31. Relationship between the resistance and load for different soft materials

(A)   (B)
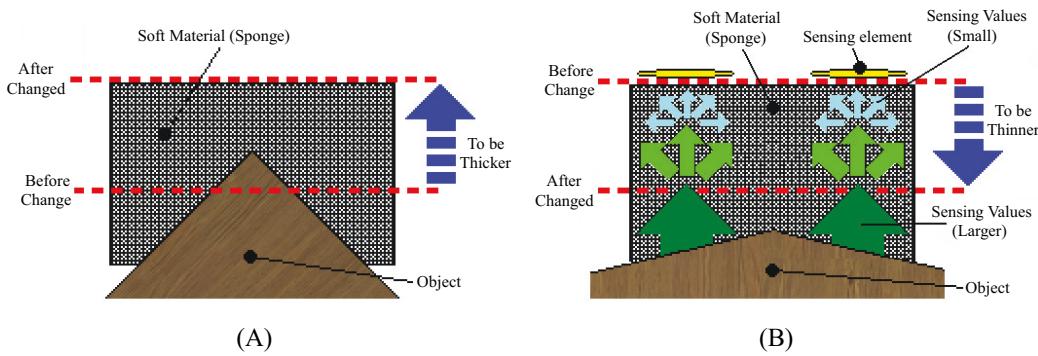
Figure 2-32. Effect of sponge (soft material) thickness

and the three sensing elements received the same load force. The relationship between the conductance and load is shown in Figure 2-30. The conductance of the sensor unit gradually increases with an increase of load for all kinds of soft materials. Linearity is nearly maintained in all cases. Next, a suitable material was chosen.

Figure 2-31 shows the relationship between the resistance and load. I found that the range of the resistance change in the case of a 10mm sponge was half as large as that in the case of a 20mm sponge. On the other hand, when I used silicone rubber, this range was not affected by thickness. I therefore selected sponge as the material for the sensor unit because its dynamic range is larger than that of silicone rubber. The thickness of the sponge can be changed for suitable measurements, depending on the object to be touched. The sponge should be thicker to measure a wide object slope, as shown in Figure 2-32(A). The sponge should be thinner for larger sensing values, because when the sponge is very

thick, the sensor obtains a small sensing value due to the force spreading over a wider area as shown in Figure 2-32(B). Based on these results, I decided on a sponge thickness of 20mm (Young's modulus 0.496N/mm^2) for the following experiments.

2.6.2. Filtering effect test
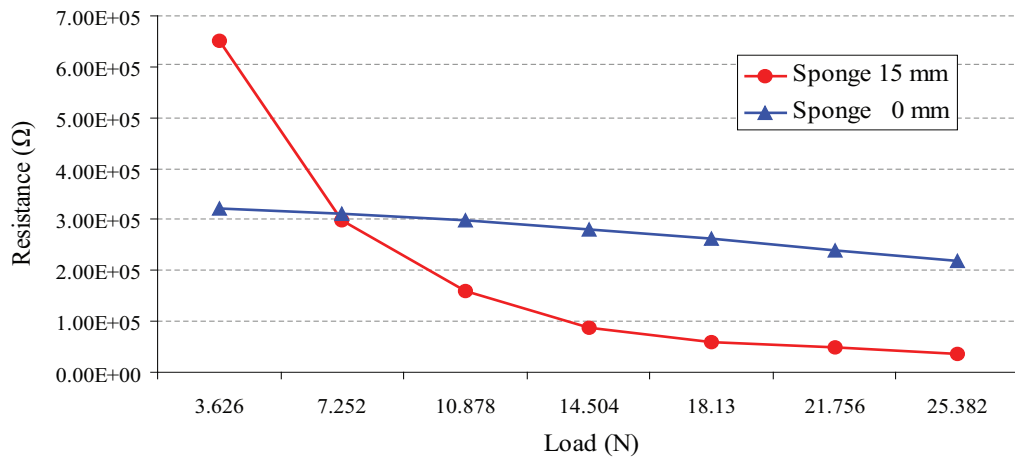
Figure 2-33. Relationship between the resistance and load of filtering effect test

This experiment aims to confirm the filtering effect from the soft material of the proposed sensor unit by observing the quantitative relation between sensing outputs and applying load forces. To evaluate the filtering effect, the two different kinds of sensor unit with and without soft material were used for performing the experiments. The prepared soft material is 15mm thick sponge with 0.496N/mm^2 young's modulus. First the sensor unit was fixed. Then the applying load force is increased from 3.626N to 25.382N with 3.626N interval. The load was normal to the soft material surface, thus the three sensing elements received the same value of load force. The relationship between the resistance and load of this test is shown in Figure 2-33. As shown in this figure, resistance of the sensor unit gradually decreases with the increasing the load for both cases with and without soft materials. Next, a suitable material was chosen. The researchers found that the range of the resistance changes of the sensor unit with soft material was larger than that without soft material. Based on these results, the researchers decided the sensor unit with a sponge for the following experiments. The result shown

here is for the case of static force, while the active touch involves the dynamic forces. However, the sensing system works in real-time. The rise time of the sensing device is less than 20μsec. The conversion time of A/D converter is less than 3ms. Thus, the proposed sensor can be used even when I handle dynamic forces in the applications given in this thesis. As described above, the proposed sensor unit was tested to confirm the practical limitation in preliminary experimental result for industrial purpose. And as a result, the researchers confirmed that it could work even when the applied force was up to 30N. It is considered that the device was not damaged because the sensing device is made of simple thin polyester film even if the large force condition was applied to the device.

2.7. Summary

This chapter introduced a development of tactile sensor systems. First I described the key idea of this research, followed by the sensor element measuring methods. The sensor signals are digitized using resistance measuring method by utilizing the RC time constant technique described in this section. Then I introduced the proposed sensing system for industrial robotic arm and autonomous humanoid robot respectively. In these two sections provided the details of the main components of this system including, robots, hardware, electronic circuits, software and interface. The inverse kinematics calculation of the developed robotic arm system, preliminary experiments including sensor linearity test and filtering effect test were described in this chapter.

CHAPTER III

3. TACTILE SENSING TECHNIQUES

3.1. Tactile Sensing Technique of Sensor Hand

3.1.1. Object surface normal sensing method
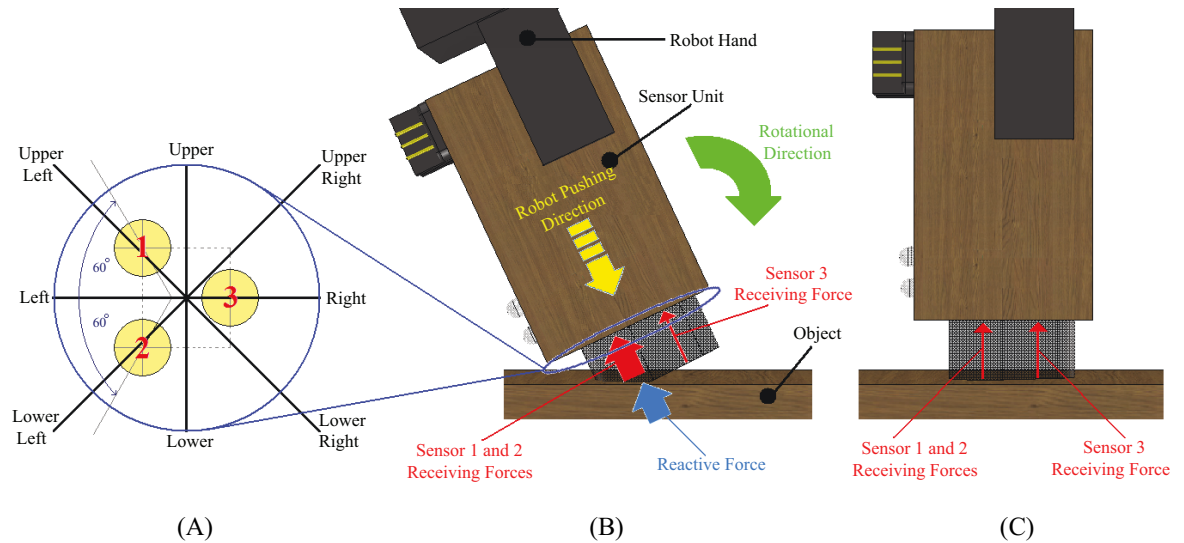
Figure 3-1. Sensing devices location and rotational directions to follow a surface normal

To perform the real-time sensing control of industrial robot to follow an object normal surface in 3-D, the control criterion is to make the three outputs of sensor equal. Table 1 shows the relationship between pushing and received forces. I also show the direction of robot movement based on data from the element sheets in Table 3-1(A) and (B). By utilizing this information, I can detect the gradient of the sponge surface. To keep the robot hand normal to the object surface, the force data from three sensor devices is used to compute the robot hand direction control together with the current hand direction. Figure 3-1(A) displays the layout of three sensing elements constraint to the moving directions. Figure 3-1(B) and (C) shows the side views of the three sensing elements with the robot before and after the object following, respectively. Figure 3-1(B) and (C) shows the relationship between the receiving force, the reactive force from the object, and the robot rotational directions. The robot start pushes the object in the typical direction of

47

Object touching position (Relation pushing and received forces)	Relation of the sensing elements values	Robot moving directions (Finding object normal surface)
(1) Center	S1 = S2 = S3	Keep Position (No Move)
(2) Right	S3 > (S1 = S2)	Move Left
(3) Left	(S1 = S2) > S3	Move Right
(4) Upper	S1 > S3 > S2	Move Lower
(5) Lower	S2 > S3 > S1	Move Upper

Arrow Meaning		
Push Force	Receive Force	Moving Direction

Table 3-1(A). Analysis of tactile feedback to define a touching position for robot control
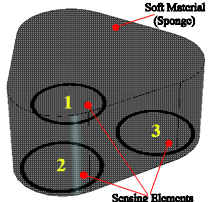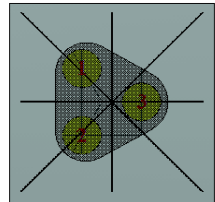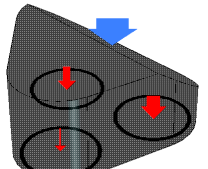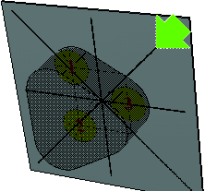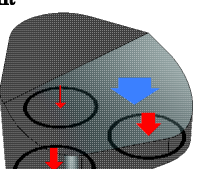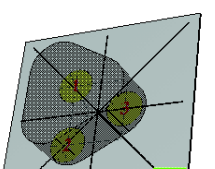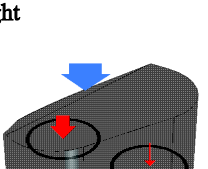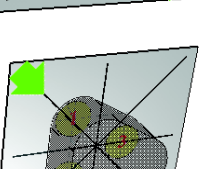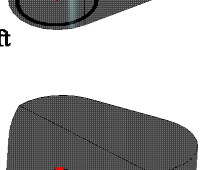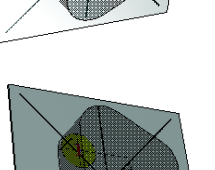
Object touching position (Relation pushing and received forces)	Relation of the sensing elements values	Robot moving directions (Finding object normal surface)
(1) Center	S1 = S2 = S3	Keep Position (No Move)
(2) Upper-Right	S3 > S1 > S2	Move Lower-Left
(3) Lower-Right	S3 > S2 > S1	Move Upper Left
(4) Upper-Left	S1 > S2 > S3	Move Lower-Right
(5) Lower-Left	S2 > S1 > S3	Move Upper-Right

Arrow Meaning		
Push Force	Receive Force	Moving Direction

Table 3-1(B). Analysis of tactile feedback to define a touching position for robot control

robot motion to touch the object. After touched, the sensors receive force from this touch. In this situation, the forces on Sensors 1 and 2 are larger than that that on Sensor 3. The robot moves the hand to the rotational direction to make the forces on all sensors equal, as shown in Figure 3-1(C). For each element, three sensing devices are fixed in a triangular configuration at 120◦ intervals. To complete 3-D movement, I need to move in eight directions as shown in Figure 3-2. Table 3-1(A) and (B) show an analysis of tactile sensing feedback to define an object touch position for robot control. The left column shows the object plane touch position, and provides the relationship between the pushing force and the received forces of the three sensing elements. The middle column shows the relationship among the values of the sensing statements. The right column shows the directions of robot movement directions to make the hand normal to the object surface.

As shown in Table 3-1(A.1), when the object touches the center of the sponge, the pushing force appears at the center. Consequently, the received forces of the three sensing elements are equal when the position of the robot hand is set normal to the surface. In other words, the robot only has to keep the received forces of all three sensing elements equal to keep the position of the robot normal to the surface. As shown in Table 3-1(A.2), when the object touches on the right side of the sponge, a pushing force appears on the right side as well. Consequently, the force on Sensor 3 is greater than those on Sensors 1 and 2, which are equal. That means that to follow the object surface normal, the robot hand needs to move left until the forces on all three sensing elements are equal. The moving directions have shown in the right column. Similarly, as shown in Table 3-1(A.3), when the object touches on the left side of the sponge, a pushing force appears on the left side as well. Therefore, the robot hand needs to move to the right. The direction of movement can be seen on the right column. As shown in Table 3-1(A.4), when the object touches the upper side of the sponge, the pushing force appears on the upper side as well. Consequently, the force on Sensor 1 is greater than that on Sensor 3 and the force on Sensor 3 is greater than that on Sensor 2. In other words, to follow the object surface normal the robot hand needs to move down until the forces on all three sensing elements are equal. The moving directions have shown in the last column of Table 3-1(A). Similarly, as shown in Table 3-1(A.5), when object touches the lower side, a pushing

force appears on the lower side as well. Therefore, the robot hand needs to move up to make it normal to the object surface. Direction of movement figures are shown in the right column of Table 3-1(A).

Table 3-1(B.1) is the same as Table 3-1(A.1) for reference. In Table 3-1(B.2), when the object touches the upper right side of the sponge, a pushing force appears on the upper right side as well. Consequently, the force on Sensor 3 is stronger than that on Sensor 1 and the force on Sensor 1 is also stronger than that on Sensor 2. That means that to follow the object surface normal the robot hand needs to move to the lower left until the forces on the three sensing elements are equal. The moving directions have shown in the right column. Similarly, as shown in Table 3-1(B.3), when the object touches on the lower right side, a pushing force appears on the lower right side as well. Therefore, the robot hand needs to move to the upper left. The direction of movement figures can be seen in the right column. As shown at Table 3-1(B.4), when the object touches the upper left side of the sponge, a pushing force appears on the upper left side as well. Consequently, the force on Sensor 1 is more than that on Sensor 2 and the force on Sensor 2 is more than that on Sensor 3. That means that to follow the object surface normal, the position of the robot hand needs to move to the lower right until the forces on the three sensing elements are equal. The direction of movement can be seen in the right column. Similarly, as shown in Table 3-1(B.5), when the object touches the lower left side, a pushing force appears on the lower left side as well. Therefore, the robot hand needs to move to the upper right to make it normal to the object surface. The moving directions have shown in the right column.

Figure 3-2 shows a flowchart of sensing data analysis to define an object position for robot movement control. To complete the movement in 3-D, I introduce the eight directions of moving controls as shown in Figure 3-2. This figure shows an analysis of tactile sensing feedback to define an object touch position for robot control. It also provides the relationship between the pushing force and the received forces of the three sensing elements. The relationship among the values of the sensing statements is also given. For example, as shown in Figure 3-2, when object touches on the right side of sponge, a pushing force appears on the right side as well. Consequently, the force on
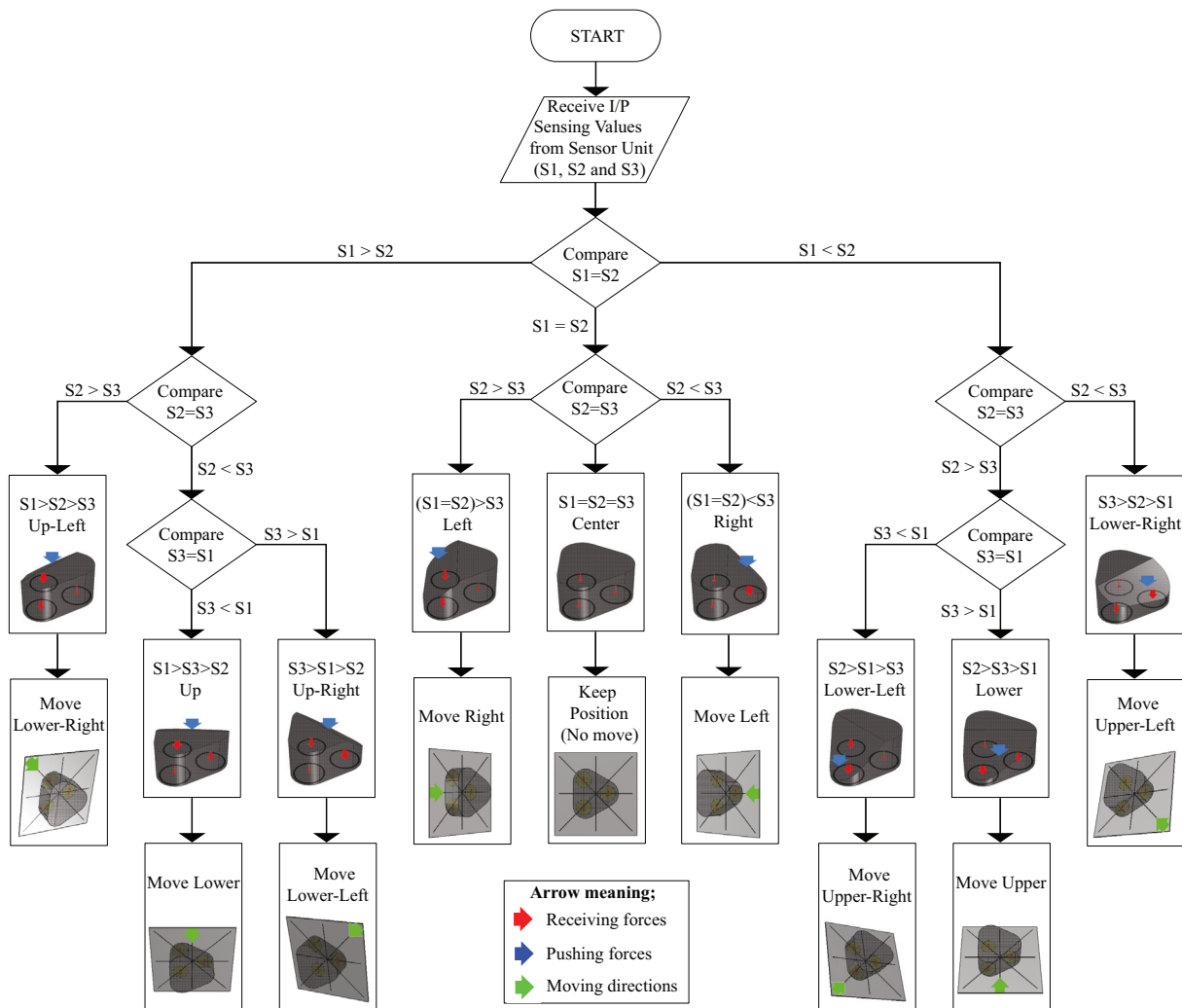
Figure 3-2. Flow chart of sensing data analysis for robot motion control

Sensor 3 is greater than those on Sensors 1 and 2, which are equal. To follow the object surface normal, the robot hand needs to move left until the forces on all three sensing elements are equal. In the same way, the robot hand is controlled to the appropriate direction based on the sensor outputs of RC circuit as shown in Figure 2-20 (Electronic circuit diagram of the tactile sensor hand). In order to verify the tactile information and sensing performance as a tactile interface, the program for analyzing the distributed pressure patterns was created. The load force is applied to the sensor unit. The receiving forces patterns are used for deciding the robot movements automatically following the flowchart to control the hand pose normal to the object surface.

(A)   (B)
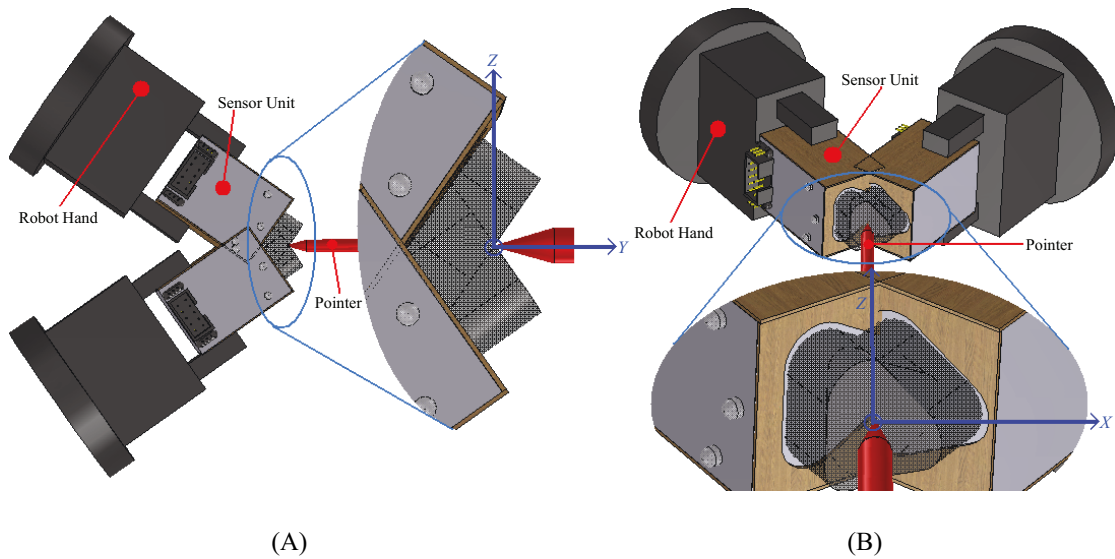
Figure 3-3. Robot control action during the object surface normal sensing motion

Figure 3-3 shows a robot action control during the object surface normal sensing motion. Robot hand poses are controlled to keep the direction of movement normal to the object. The sensing position should be fixed throughout all procedures. To follow an object normal to its surface, the robot only adjusts the sensor angle. During robot movement, I must keep the position of the robot end-effector the same at all times in this process. Figure 3-3(A) illustrates the robot's movement in the y–z plane. The robot hand keeps its position while it moves up or down. Figure 3-3(B) illustrates the robot's movement in the x–y plane. The robot hand keeps its position while it moves left or right. Therefore the robot control program functions to compute moving cases. These cases are classified into eight directions, including up, down, left, right, upper right, lower right, upper left and lower left, as shown in Table 3-1(A) and (B). In this system I realized movement in 3-D directions by combining the movement in the x–y and y–z planes.

3.1.2. Object edge sensing method

To perform real-time sensing control for the hand pose and motion control for object edge tracing as shown in Figure 3-4, the difference among the resistances values of those sensing elements sheets was used. The coordinate system is also shown in this figure. The robot controls its hand pose direction based on the sensor values. The object

53
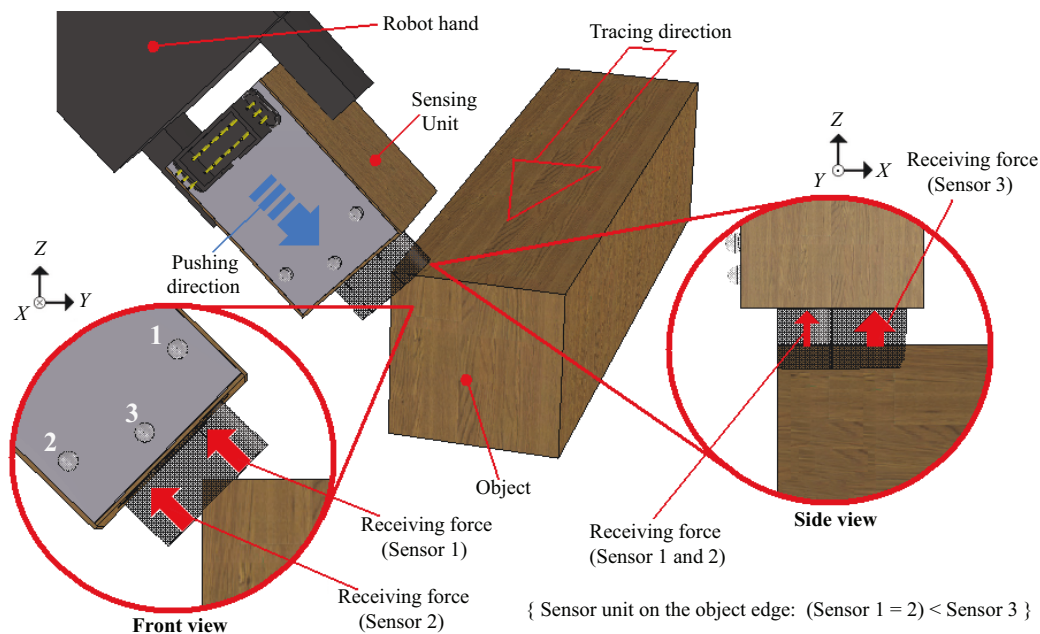
Figure 3-4. Robot control action during the object edge sensing motion

edge is found by scanning. The angle change is large when the robot hand reaches an edge. At the object edge, the force on the sensor 1 should be equal to that on the sensor 2 as shown in Figure 3-4 (Front view). Based on the sensor values, when the force on sensor 2 is larger than that on sensor 1, the robot recognizes that the position of its hand is above the object edge. On the other hand, when the force on sensor 1 is larger than that on sensor 2, the robot recognizes that the position of its hand is under the object edge.

The object edge recognition can be performed by utilizing the two signals from sensor 1 and sensor 2. However, there are two important advantages of using three sensing elements. The first advantage is to keep the robot hand on along the edge when tracing the object edge. The relation of three outputs should be kept so that the output of the central sensing device (Sensor 3) is smaller than that of the other two (Sensors 1 and 2) as shown in Figure 3-4 (Side view), while these two outputs should be the same as shown in Figure 3-4 (Front view). Another advantage of proposed tactile sensing technique is for scanning the end object. After finding the edge, the outputs of sensors 1 and 2 are the same. Then the difference between the sensor 3 and the sensors 1 and 2 was used for scanning the end of object. The tracing motion continues to (−1, 0, 0) direction

until it reaches the rough end point, that is, no forces appear on the sensors 1 and 2. In other words, only the sensor 3 has touched an object. To recognize the details of the end point, the robot then moves back to (1, 0, 0) direction to detect the sensing force on the sensors 1 and 2 again. After the robot detected the hand position on the object, it moves to (−1, 0, 0) direction for fine scanning. The movement continues until the robot does not detect any forces from all three sensors, that is, the sensors do not contact the object. Then the robot moves back to (1, 0, 0) direction by 26 mm, which is the length of the sensing unit. Then the robot moves 13 mm forward to (−1, 0, 0) direction, which means that the center of sensing unit is set to the end of object.

To perform the sensing technique efficiently, the sensor unit should keep the orientation as shown in Figure 3-4. Otherwise, the edge sensing will fail. For example, let us consider that the line contacts to the center of two sensors parallel to the object edge. In this case, there is no difference between two sensors output. If only two sensors are used, the method has a limitation. Therefore, the three sensing elements are used to keep the correct orientation as described before.

3.2. Tactile Sensing Technique of Sensor Feet

3.2.1. Ground slope sensing method

To perform real time sensing control for robot to adjust its foot normal to the ground surface, the control criterion is to make the receiving forces from three sensing elements equal. Note that the robot leg position is fixed. Only foot position moves followed by the received sensing information.

Figure 3-5 shows a flowchart of sensing data analysis to define a contacting slope condition for robot motion control. This flowchart gives an analysis example on the right foot of robot. On the left foot, the same method can also be used. However, the flowchart becomes symmetric about the right foot analysis. In Figure 3-5, S_i represents the output of sensing element i (i = 1, 2 and 3). By using this information, I can detect the gradient of the sponge surface. To keep the robot foot normal to the ground surface, the force data from three sensing elements are used to control the robot foot direction together
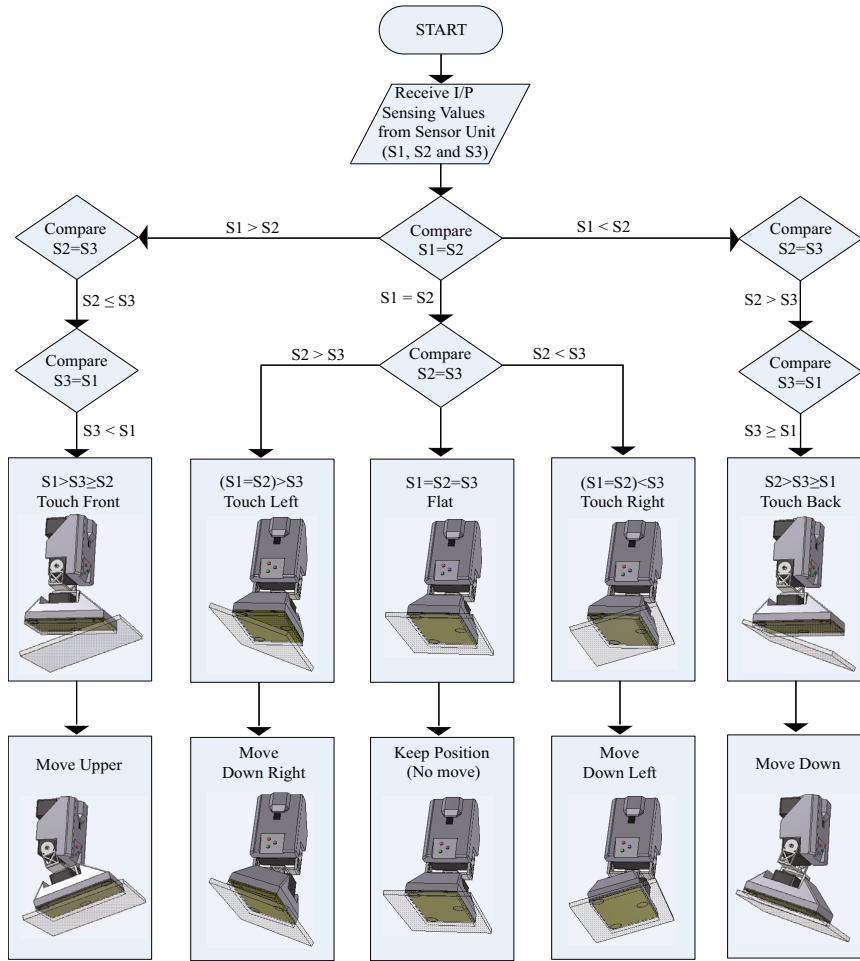
Figure 3-5. Flow chart of sensing data analysis to define a contacted ground slope condition for robot motion control (Right foot case)

with the current foot direction. To complete the movement in 3-D, I introduce the four directions of movements as shown in Figure 3-5. These figures show the analysis results of tactile sensing feedbacks to determine the robot position against the ground based on the values of the sensing elements. As shown in this figure, when the robot foot touched the ground floor on the right side of the sponge, a pushing force appears on the right side. Consequently, S_3 is greater than S_1 and S_2. S_1 is equal to S_2. Hence, to follow the ground surface normal, the robot foot needs to move down left until the forces on all three sensing elements are equal. In a similar fashion, when the robot foot approaches the ground from other direction, it can also be controlled to the appropriate direction based on the sensor outputs as well.
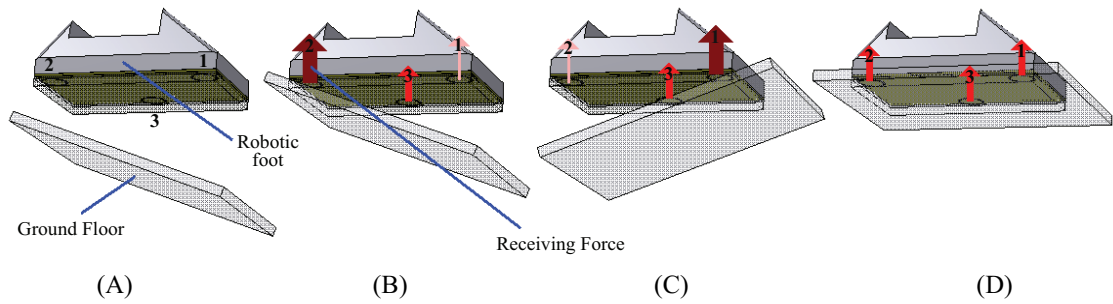
Figure 3-6. Methodology of recognizing the ground slope (Upward/Downward)
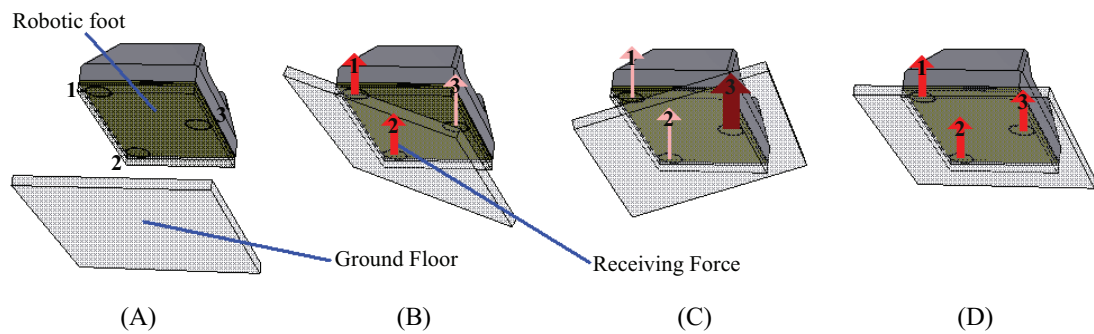
Figure 3-7. Methodology of recognizing the ground slope (Leftward/Rightward)

Figure 3-6 shows the methodology of recognizing slope in cases of upward and downward slopes. Figure 3-6(A) shows the case that robot foot has not contacted to the ground and therefore no forces appear for all sensors. Figure 3-6(B) the robot foot touched the ground floor on the back side of the sponge, thus the relation between the sensor outputs is as, $S_2 > S_3 \geq S_1$. Figure 3-6(C) the robot foot touched the ground floor on the front side of the sponge, thus the relation between the sensor outputs is as, $S_1 > S_3 \geq S_2$. Figure 3-6(D) the robot foot touched normal to the ground floor, thus all forces are equal. Figure 3-7 shows the methodology of recognizing the slope in cases of leftward and rightward slopes. Figure 3-7(A) shows the case that the foot has not contact the ground and therefore no forces appear for all sensors. Figure 3-7(B) shows the case that the robot foot touched the ground floor on the right side of the sponge, thus the relation between the sensor outputs is as $(S_1 \approx S_2) > S_3$. Figure 3-7(C) shows the case that the robot foot touched the ground floor on the left side of the sponge, thus the relation between the sensor outputs is as $(S_1 \approx S_2) < S_3$. Figure 3-7(D) shows the case that the robot foot touched normal to the ground floor, thus all forces are equal. To verify the

57

tactile information sensing performance as a tactile interface, I created the program for analyzing the distributed pressure patterns when a robot put its foot on the ground floor. The applied force will be detected by the sensor unit and can be used for deciding the robotic foot movement automatically for assisting the robot to achieve the natural foot posture motions to be balanced on the different environments.

3.2.2. Balance sensing method
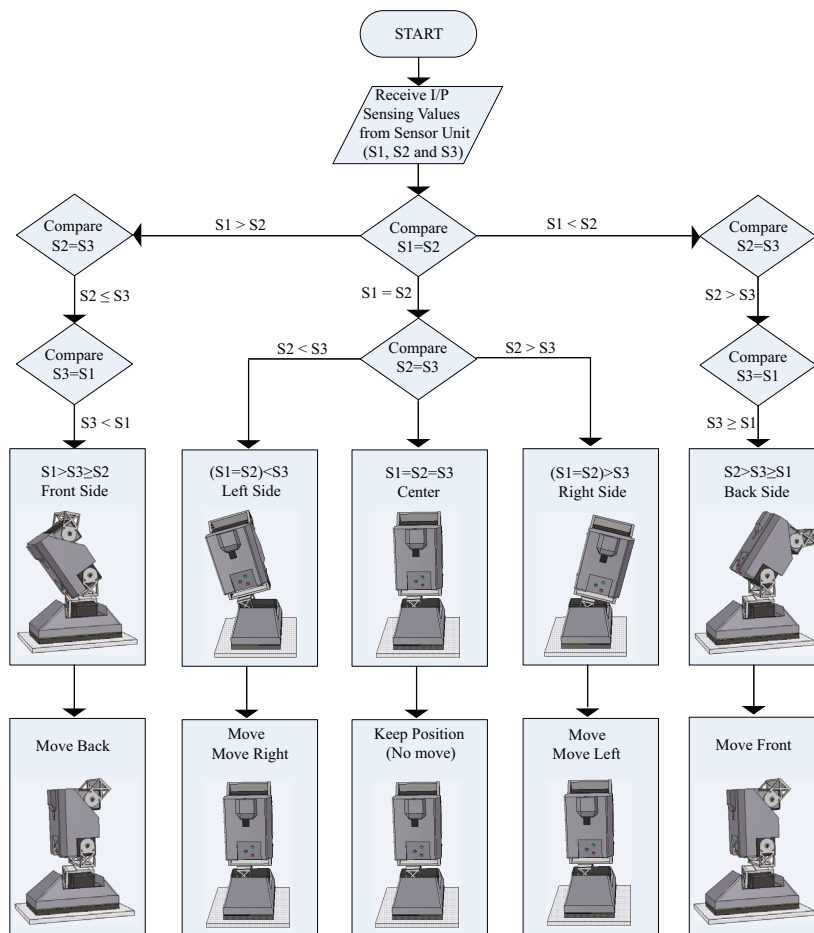
Figure 3-8. Flow chart of sensing data analysis to define the strongest force position for robot balancing control (Left foot case)

To perform real time sensing control for robot to adjust its body balanced with one leg, the control criterion is to make the receiving forces from three sensing elements equal. Note that the robot foot poses must be normal to the ground surface using previous

sensing method. Its foot position is then fixed and only body pose motions are controlled by the received sensing information.

Figure 3-8 shows a flowchart of sensing data analysis to define the strongest force position which appeared depending on a body movement condition. This flowchart gives an analysis example concerning the left foot of robot. On the right foot, the same method can be used. However, the flowchart becomes symmetric about the right foot analysis. In Figure 3-8, S_i represents the output of sensing element i (i = 1, 2 and 3). By using these data, I can detect the gradient of the sponge surface. To keep the robot body balance with one leg, the force data from three sensor devices is used to control the robot body direction together with the current foot direction. To complete the movement in 3-D, I introduce the four directions of movements as shown in Figure 3-8. This figure displays the analysis results of tactile sensing feedbacks to determine the robot position against the ground based on the sensing values of sensing elements. As shown in this figure, when robot changes its weight into right side of the sponge, a pushing force appears on the right side. Consequently, S_3 is smaller than S_1 and S_2, while S_1 is equal to S_2. Hence, to follow the ground surface normal, the robot needs to move its weight into left side until the forces on all three sensing elements are equal. In a similar fashion, when the robot foot approaches the ground from other direction, it can also be controlled to the appropriate direction based on the sensor outputs shown in Figure 3-8.
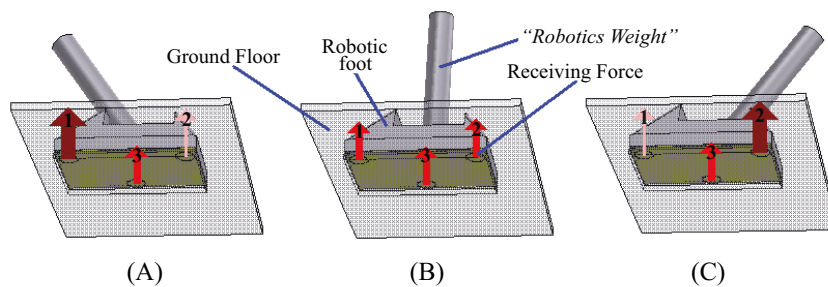
Figure 3-9. Methodology of recognizing the robot weight (Front/Back)

Figure 3-9 shows the methodology of recognizing the robot weight in cases of front and back side. In Figure 3-9(A), the robot moves its weight into front side, thus the relation between the sensor outputs is as, $S_1 > S_3 \geq S_2$. Figure 3-9(B) shows the robot
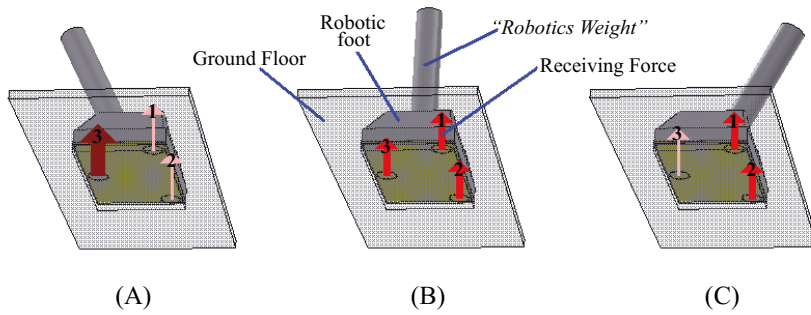
Figure 3-10. Methodology of recognizing the robot weight (Left/Right)

weight in the center, thus all forces are equal. In Figure 3-9(C), the robot moves its weight into back side, thus the relation between the sensor outputs is as, $S_2 > S_3 \geq S_1$. Figure 3-10 displays the methodology to recognize the robot weight in cases of left and right sides. Figure 3-10(A), the robot moves its weight into right side, thus the relation between the sensor outputs is as, $(S_1 \approx S_2) < S_3$. Figure 3-10(B) shows the robot weight in the center, thus all forces are equal. In Figure 3-10(C), the robot moves its weight into left side, thus the relation between the sensor outputs is as, $(S_1 \approx S_2) > S_3$. To verify the tactile information sensing performance as a tactile interface, I created the program for analyzing the distributed pressure patterns when a robot moves its weight along the foot. The applied force will be detected by the sensor unit and can be used for deciding the robot body movement automatically for assisting the robot to achieve the natural body poses motions to be balanced on the different ground slopes.
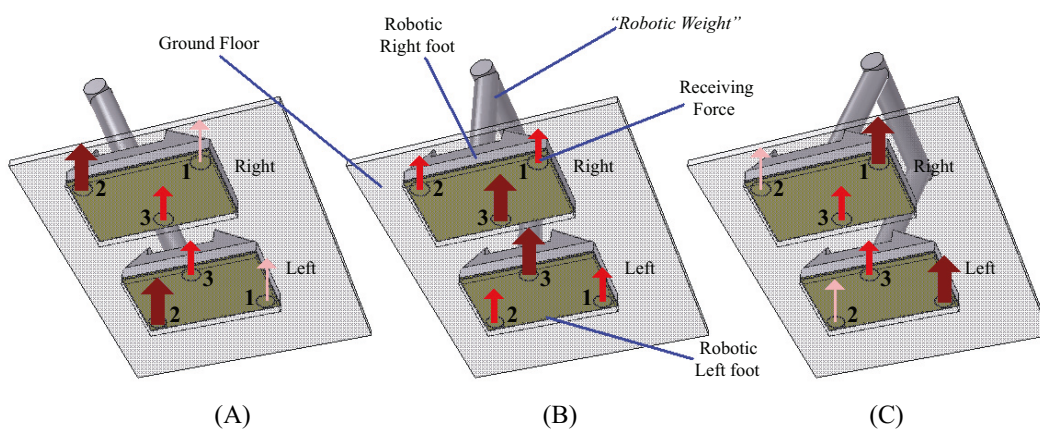
Figure 3-11. Methodology of recognizing the robot weight in case of the robot moving to the frontward and backward of its body in case of stand with two legs
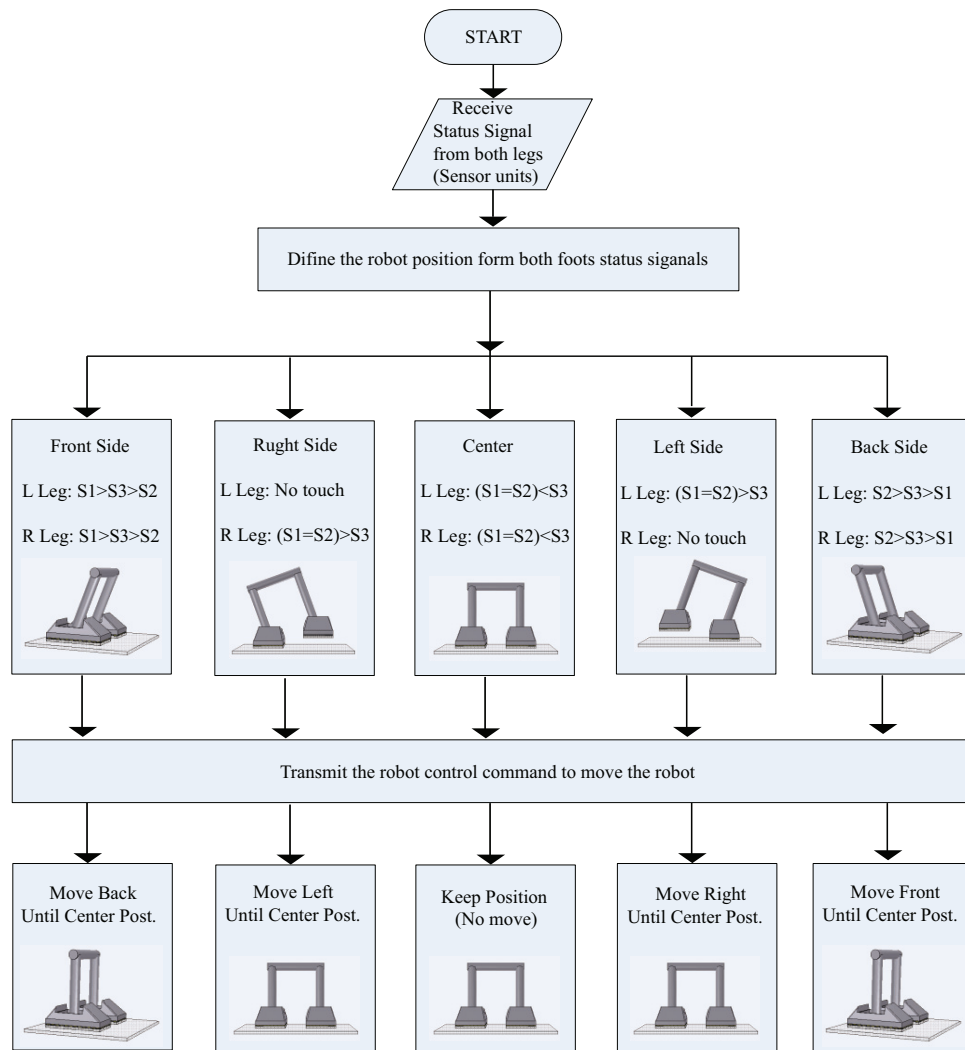
Figure 3-12. Methodology of recognizing the robot weight in case of stand with two legs

Figure 3-11 shows the methodology of recognizing the robot weight when robot stands with two legs, and moves to the front and the back side of its body. Figure 3-11(A) shows the case that the robot moves its weight into the back side. In this case, the force relation between the sensor outputs is described as, $S_2, > S_3 > S_1$ concerning both legs. Hence, to make a balance, the robot needs to move its weight into the front side until the forces on both legs as $(S_1 = S_2) < S_3$. Figure 3-11(B) shows the robot weight in the center. In this case, the forces on both legs are constrained as $(S_1 = S_2) < S_3$. Figure 3-11(C) shows that the robot moves its weight into front side. The force relation between the sensor outputs is described as, $S_1, > S_3 > S_2$ concerning both legs. Hence, to make it

balance, the robot needs to move their weights into the back side until the relation among the forces on both legs are, $(S_1 = S_2) < S_3$. To verify the performance of the proposed tactile interface, I created the program for analyzing the distributed pressure patterns. The applied force will be detected by two sensor units (left and right foots). These data can be used for deciding the robot position automatically for assisting the robot to be balanced on the different environments such as flat floor, upward and downward slopes.

Figure 3-12 shows the relation between the receiving force and robot legs when a robot stands with two legs and balance control method based on the postures. When a robot stands with two legs, it is difficult to make the forces on all three sensing elements equal due to the constraint between right and left legs. To solve the problem, I make two legs work together to realize the balance control. I can make the balance with two legs when both sensing feet receive the forces on both legs as $(S_1 = S_2) < S_3$. In order to complete this task, I implement the main CPU interface unit on the system for collecting information from two sensing feet, and determine the robot position from the collected data. After that, the unit will decide the appropriate control motion based on the sensor outputs as shown in Figure 3-12. Figure 3-13 shows methodology to recognized the robot weight when the robot stands on the upward and downward slope with two legs. In Figure 3-13, β represents the angle between the robot body and foot before touch the ground slope. While, θ represents the slope angle. SLR_i represent the receiving force of left and right foot sensing element i (i = 1, 2, 3). Figure 3-13(A) shows the case that robot stands on the upward slope. This position makes the robot unbalance. The robot will fall down to the back side. In this case, the force relation between the sensor outputs is described as, $SLR_2, > SLR_3 > SLR_1$ concerning both legs. Hence, to make it balance, the robot needs to move its weight into the front side until the forces on both legs as $(SLR_1 = SLR_2) < SLR_3$. Figure 3-13(B) shows the robot weight in the balance situation. This case is the same as standing balance on the flat surface, and the forces on both legs are constrained as $(SLR_1 = SLR_2) < SLR_3$ as shown in Figure 3-13(C). Figure 3-13(D) shows case that robot stands on the downward slope. This position makes the robot unbalance. The robot will fall down to the front side. In this case, the force relation between the sensor outputs is described as, $SLR_1 > SLR_3 > SLR_2$

62
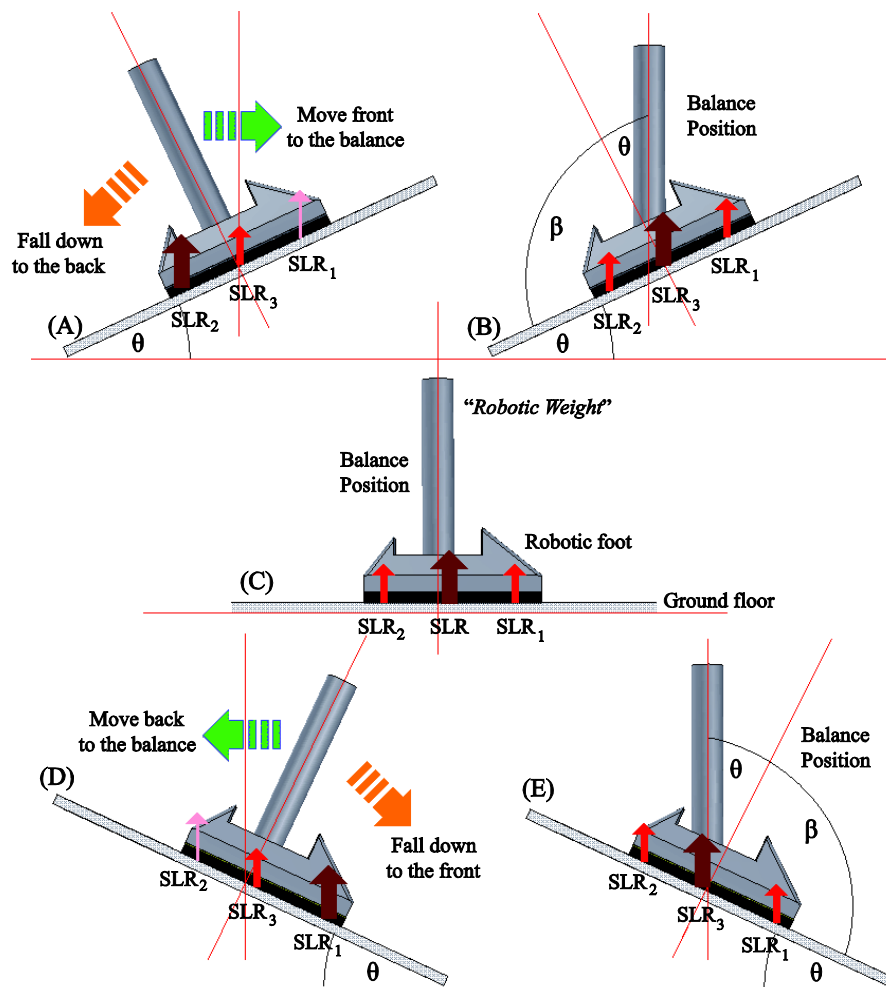
Figure 3-13. Methodology of recognizing the robots weight in case of the robot stands on the upward and downward slopes

concerning both legs. Hence, the humanoid robot needs to move its weight into the back side to be balanced until the receiving forces condition of both legs as ($SLR_1 = SLR_2$) < SLR_3 as shown in Figure 3-13(E). As shown in the balancing position on the upward and downward slopes in Figure 3-13, the robot can maintain its balance on the slopes by moving its weight with the slope angle, θ. For the upward slope case (+ angle), the balancing position angle is equal as the ($\beta - \theta$) angle. On the other hand, for the downward slope case (– angle), the balancing position angle is equal as the ($\beta + \theta$) angle. Thus, the robot must keep the balancing position angle between the robot body and foot to enable the robot to walk on the slope before moving to the next step of walking motion.

3.3. Summary

This chapter introduced the tactile sensing techniques. The tactile sensing techniques for industrial robot applications by utilizing the developed tactile sensor hand were described in this section. The sensing method for surface normal detection was described, followed by the real-time sensing control of robot arm to follow an object surface normal in 3-D, the control criterion is to make the three outputs of sensor equal which is require the pushing action constantly. This technique can be used for object handling by machine to machine cooperation (robot-robot) or man to machine interaction (human-robot). Then I described the sensing technique to obtain object information and the hand pose control for object's edge detection and tracing. This technique can be used instead of manual teaching by a person, which is often necessary to obtain object information for welding points before carrying out the welding process. Then I introduced the tactile sensing technique by utilizing the developed tactile sensor feet of humanoid robot was introduced. The ground slopes sensing method and balance sensing method were also introduced in this section.

CHAPTER IV

4. INDUSTRIAL APPLICATIONS

4.1. Object Recognizing Applications

To confirm the ability of the proposed tactile sensing system, three experiments were conducted for object recognizing applications. First experiment is to measure the angle of the object surface. Second experiment is to measure the object shape using a mechanical scan method. Third experiment is to search an object surface and to keep the sensor unit orientation normal to the object surface. As the first two experiments aims to confirm the principle of proposed system, the first developing version of sensor hand with two sensing elements is used to simplify the experiments. For the next experiments, the sensor hand with three sensing elements is decided to detect an object surface and to keep the sensor unit orientation normal to the object surface in 3-D.

4.1.1. Surface angle measurement

This experiment aims to test the effectiveness of the proposed sensor for surface angle measurement. Figure 4-1 shows the experiment setup. The sensor unit has two sensing elements with the soft material (sponge). The thickness of the sponge was
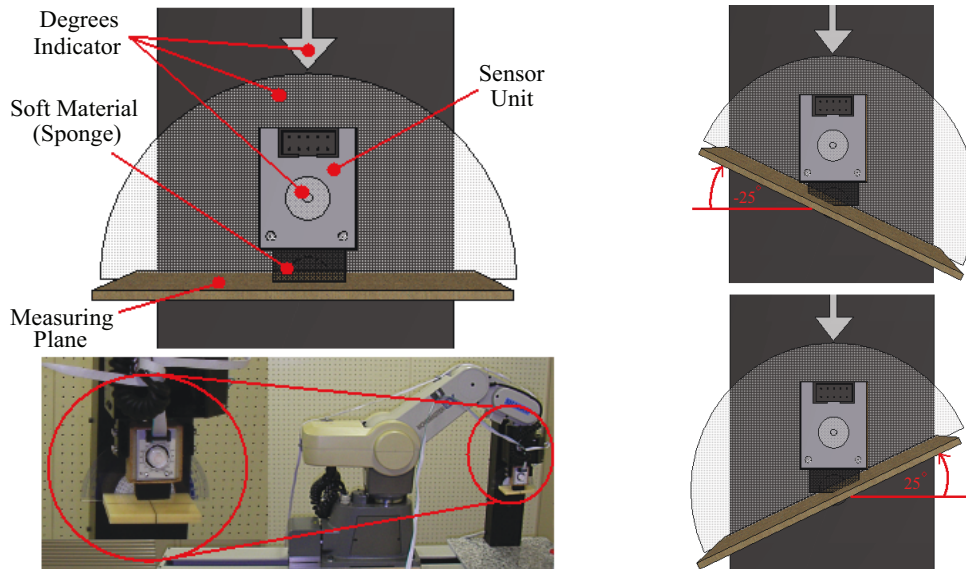
Figure 4-1. Experiment setup for surface angle measurement
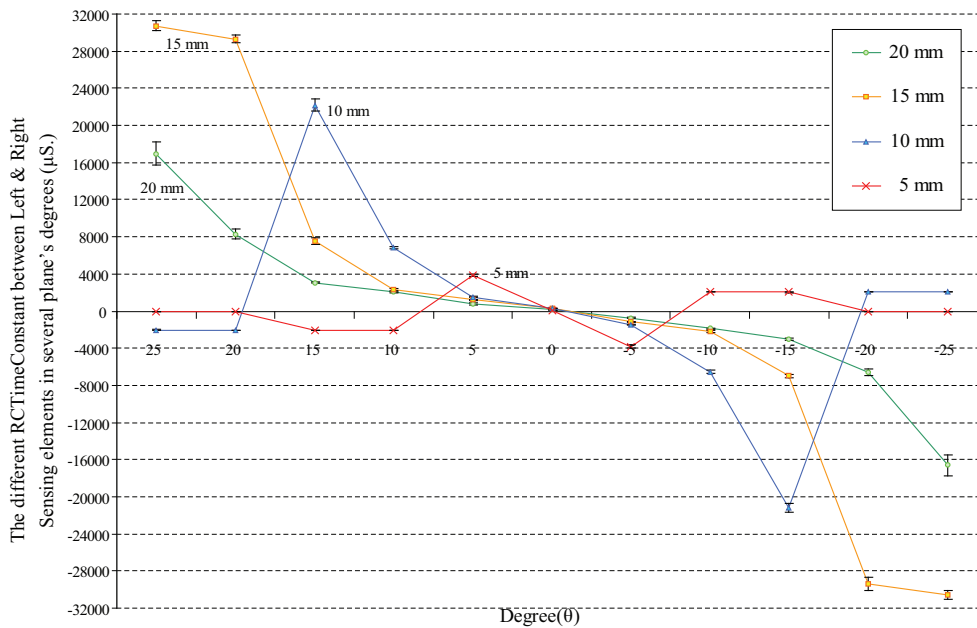
Figure 4-2. Surface angle measurement experimental results

changed from 5mm to 20 mm with 5mm interval in this experiment. To collect the data, the robot pushed its hand on the measuring plane. The plane was tilted at 0˚ (Flat), ±5˚, ±10˚, ±15˚, ±20˚ and ±25˚ angles. The right side on Figure 4-1 shows the measuring plane movement in example angle degrees at ±25˚. The resistances of two sensing elements were used to detect the attached surface angle. The experiments were conducted ten times for each sponge sizes and plane degrees.

Figure 4-2 shows the average of results. The vertical axis in this figure shows the different reading RC-time constant between two sensing elements while the horizontal axis shows the measuring degrees. According to the experimental results, the measurable angle is limited by the thickness of the soft material. As shown in the Figure 4-2, the measurable limitation angles of the 5mm, 10mm, 15mm and 20mm thickness sponge are within ±5˚, ±15˚, ,±20˚and ±20˚, respectively. This experiment also shows that the characteristic becomes linear for every thickness of soft materials in the small degrees. If the thickness of soft materials is 15 mm, the linear region is around from −10 to 10 degrees. According to the experiments, the range of the measurable angle is limited in large degrees due to the nonlinear characteristics of the sensor unit structure.

4.1.2. Object shape measurement
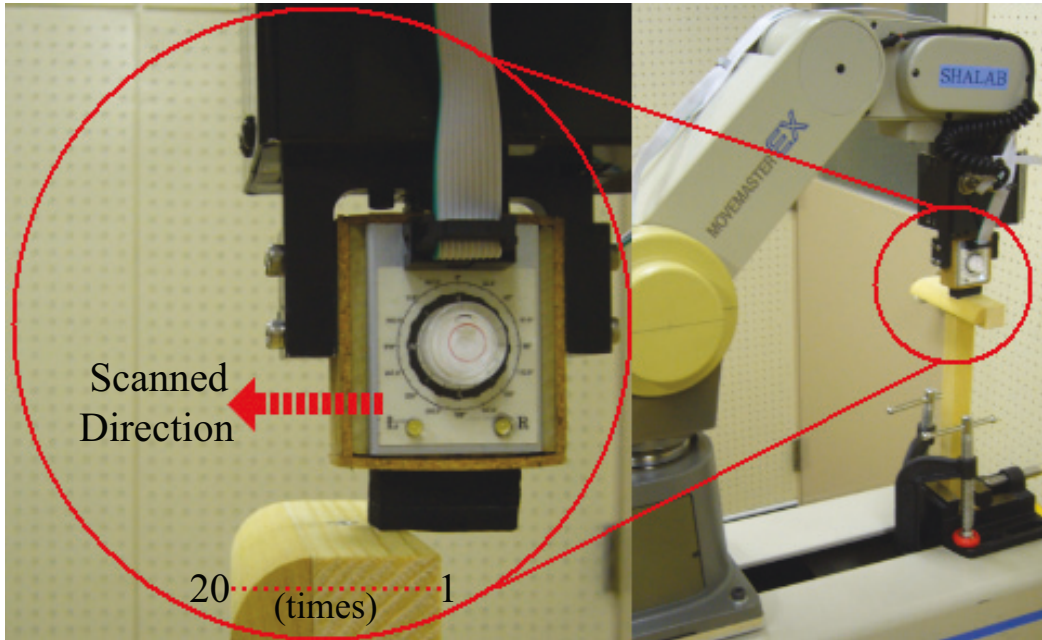
Figure 4-3. Experiment setup for shape measurement
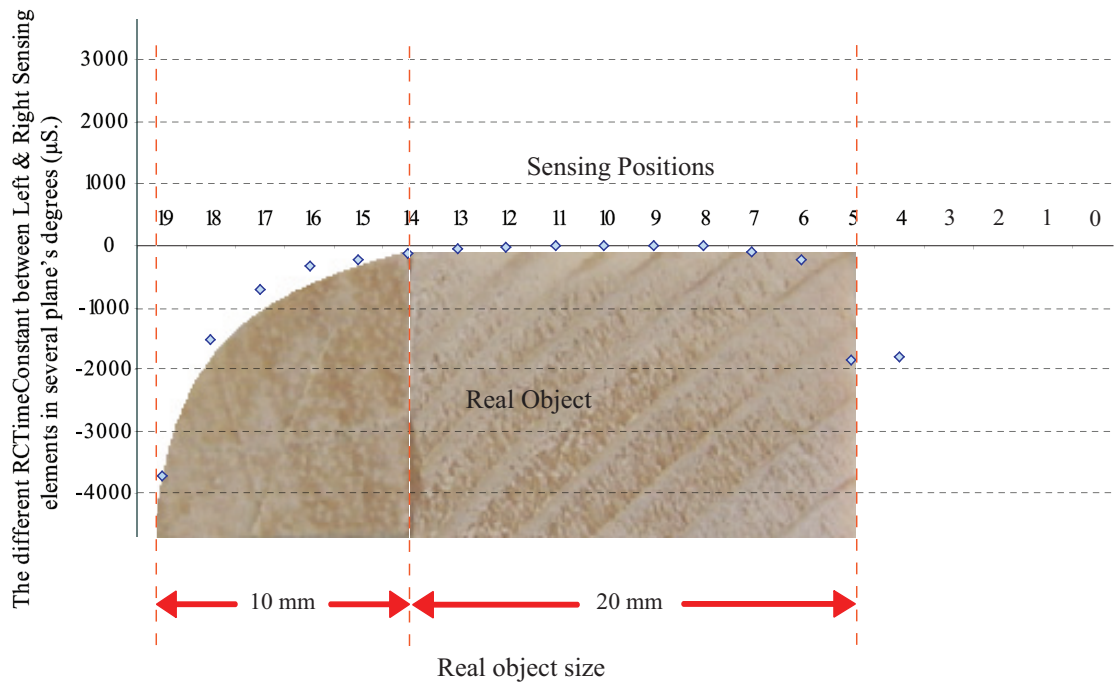
Figure 4-4. Shape measurement experimental results

This experiment aims to test the effectiveness of the proposed sensor for shape measurement. Figure 4-3 shows experiment setup. In this experiment, sensor unit has two sensing elements with the soft material (sponge). The thickness of the sponge was set to 15mm. In this experiment, the robot scanned the surface of the object by measuring the angle along the object surface. The system collects data by pushing the robot hand on the object surface. The scanning motion starts with the tip position controlled by pushing the robot hand down in vertical axis to be touched with an object, and continues pushing until the force becomes the certain value. Then the robot releases its hand from the object by moving the robot hand up in vertical axis. The robot then moves its hand 2mm forward in horizontal axis. It repeats this process until the scan for the whole object is finished. The shape of the surface is obtained by integrating the angle data along the scan direction. Experimental results and photograph of the measured object can be seen at Figure 4-4. As result, resistance change between two sensing elements could be used for shape measurement. As can be seen at Figure 4-4, the scanned result (Tactile image) is similar to real object surface. This result shows that the proposed system can be used to obtain the shape recognition.

4.1.3. Surface normal following

This experiment aims to apply the proposed tactile sensing system to control a hand pose in order to keep the hand direction normal to the object surface in 3-D (Surface Normal Following in $X–Y$ and $Y–Z$ Planes). Two robot arms, i.e., a sensing robot and an object holder robot, which were not connected, were used. Interaction was only *via* the object and the sensing device. Experimental setup is shown at Figures 4-5 and 4-6. To follow the object surface normal smoothly, the speed of robot motion is controlled proportional to the angle between the arm and the object plane. Figure 4-5(Left) shows a side view of device location in the $Y–Z$ plane. Figure 4-6(Left) shows a top view of devices location in the $X–Y$ plane. Figures 4-5(Right) and 4-6(Right) show the experimental setup in the $Y–Z$ and $X–Y$ planes, respectively.

The sensing robot firstly moves to the object surface. The robot sets its hand at $0°$ and then moves in to the $(0, 1, 0)$ direction to contact surface of object held by the

68
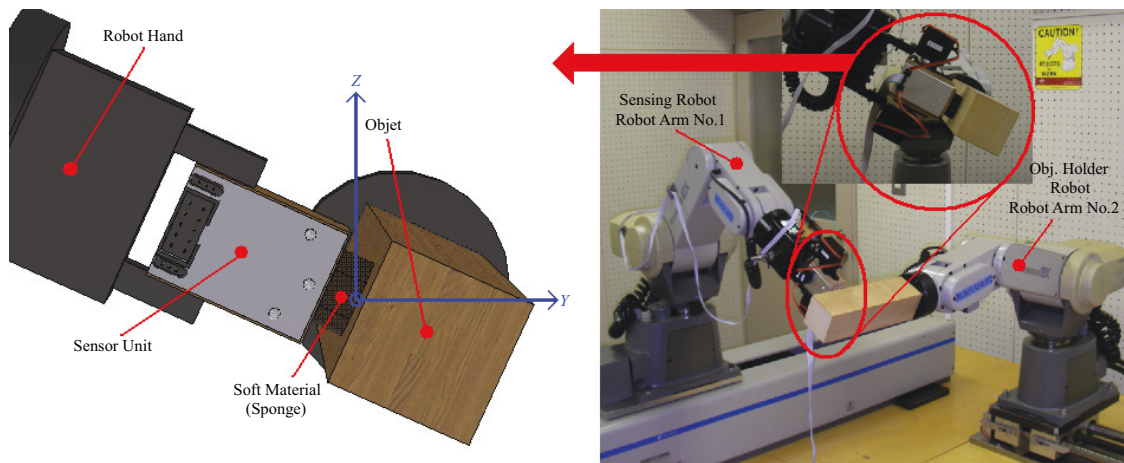
Figure 4-5. Experiment setup for following the surface normal in *Y-Z* plane
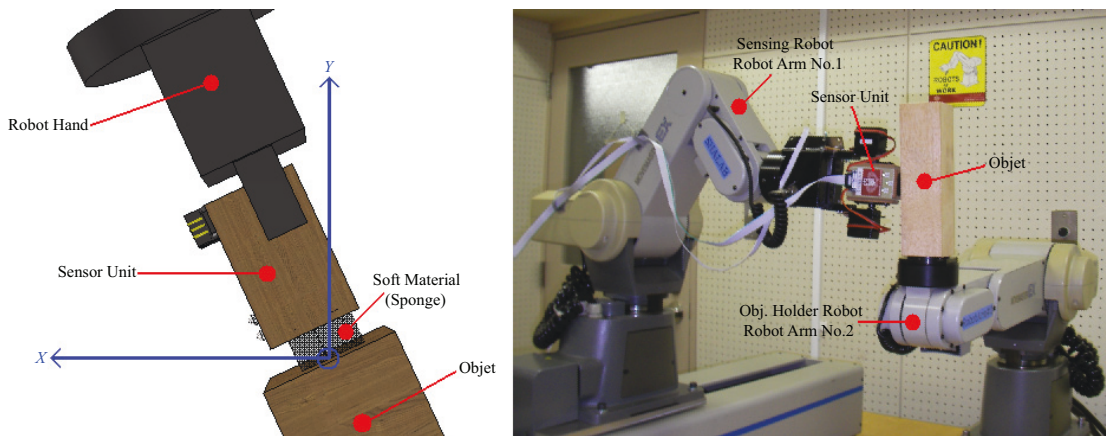
Figure 4-6. Experiment setup for following the surface normal in *X-Y* plane

object holder robot. After that, the object holder robot begins turning the object with a sine function between ±20◦ for two cycles with 147 sensing times. It then keeps the attitude at 0◦ for 30 sensing times. The term "sensing times" means the number of sensing times for each moving step of the object holder robot. In this experiment, I set the sampling interval to 550ms. Hence, the total experiment time was equal to 96.250 seconds (175 sensing times). Figure 4-7(A), (B) and (C) show the sensing elements output 1, 2 and 3, respectively. During object movement, the sensing robot moves its hand to follow the object surface normal as in Figure 4-7(D). The dotted line shows the
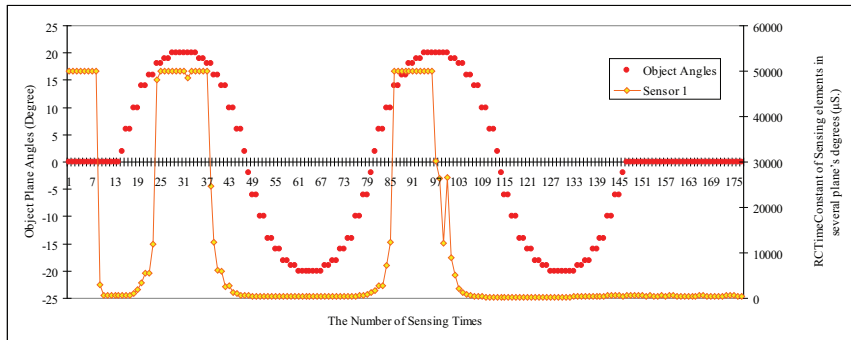
(A) Output of Sensor 1 and object angles
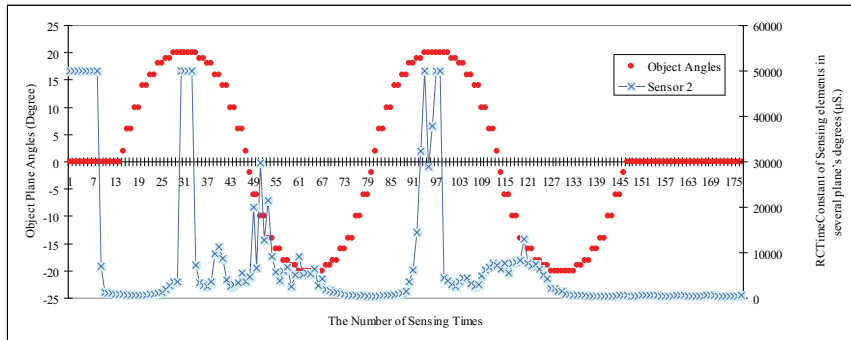
(B) Output of Sensor 2 and object angles
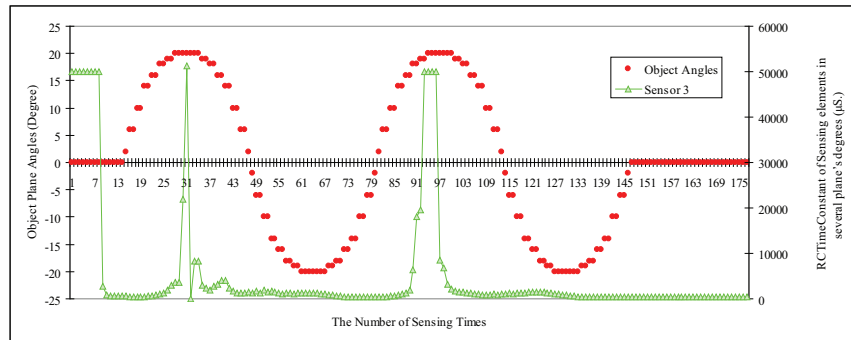
(C) Output of Sensor 3 and object angles
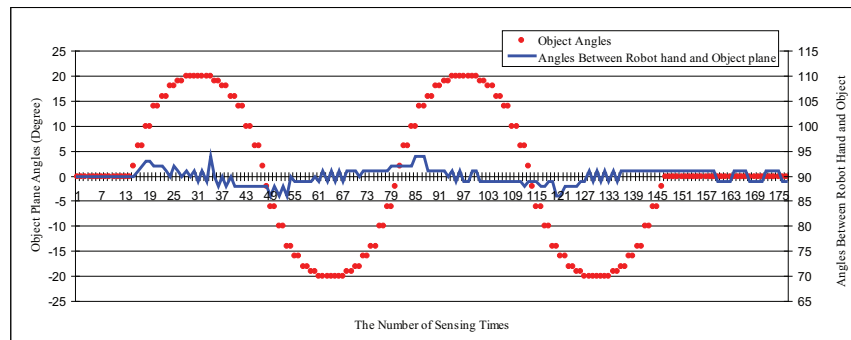
(D) Angles between the robot hand and object plane, and object angles

Figure 4-7. Surface normal following experimental results

70
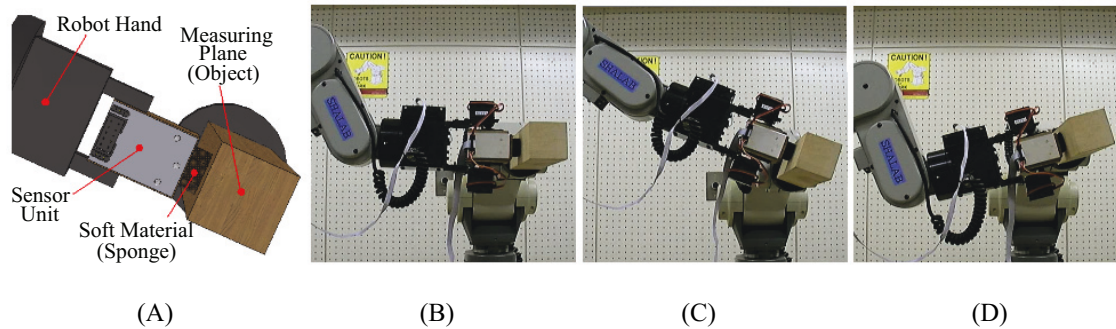
Figure 4-8. Actual robot motion of Surface normal following experimental results

object angle and the solid line shows the angle between the robot hand and the object plane angle. The robot was able to keep the angle between the robot hand and the object surface at 90°, within 5° of error, which means that the robot could follow the object surface normal while object angles changed, as shown in Figure 4-7(D). However, graphs in Figure 4-7(A) to (C) do not look smooth because these graphs are the sensing output of Sensors 1 to 3 during the robot motion to follow the object's movement. During the motion, these three sensing outputs are used to control the robot and make it follow the object surface normal. Thus, some of these sensing elements may sometimes not be in contact with the object because the object has moved.

As shown in Figure 4-8, two robot arms can interact with each other only through the objects. This figure shows the actual robot motion of Surface normal following experimental results. Experimental setup details are shown in Figure 4-8(A). In order to make the sensing robot follow to object surface normal smoothly, the speed of robot motion is controlled proportionally to the angle between the robot hand and the object plane. The controller unit controls to move the robot hand to change the orientation following the changes of the attached object plane. The robot hand turns the angle larger and increases the speed of robot motion when the attached angle becomes larger. On the other hand, the robot hand turns the angle smaller and decreases the speed of robot motion when the attached angle becomes smaller. The sensing robot firstly moves to the object surface. It sets its hand at zero degrees and then moves in (0, 1, 0) direction to contacted surface of object held by the object holder robot. After that, the object holder

robot begins turning the object with a sine function from 0, +20 and –20 degrees as shown in Figure 4-8(B), (C) and (D) respectively

4.2. Welding Applications

To confirm the ability of the proposed sensing system, I conducted three experiments. The first experiment is the object edge recognition to confirm the accuracy of the edge detection. To show the robustness of the proposed system, I conducted the experiments from three kinds of initial points, that is, the point above the edge, the point under the edge and the point on the edge. The second experiment is the object edge detection starting from the object surface. The last experiment is an object edge tracking to obtain the object information and then repeat them for simulated welding motion. The tactile sensing system diagram for welding application is shown at Figure 4-9.
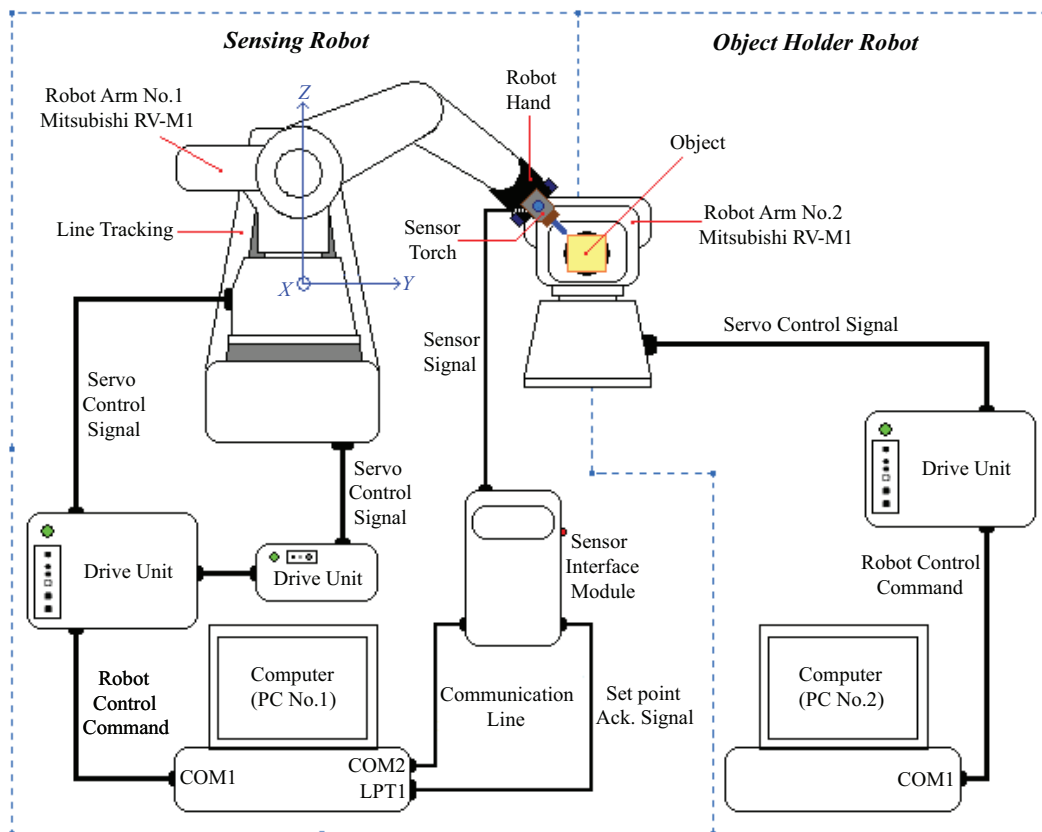
Figure 4-9. Diagram of tactile sensing system for welding application

4.2.1. Object edge recognition

(A)   (B)   (C)
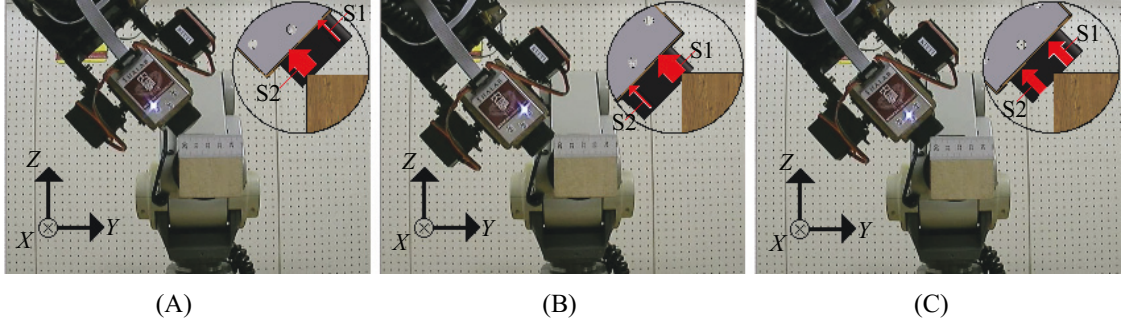
Figure 4-10. Actual robot motions of recognizing an object edge
(Starting point is around an object edge)

Figure 4-10 depicts the object edge detecting procedure and shows the actual robot movement during the sensing process parallel to X axis. As shown in Figure 4-10, the robot detects the edge utilizing the difference between the received forces on the sensors 1 and 2. To confirm the robustness of the proposed method, the average error can be calculated as follows;

$$E_{(Avg)} = \frac{1}{n} \sum_{i=0}^{n} \sqrt{\left(X_i - X_{Avg}\right)^2 + \left(Y_i - Y_{Avg}\right)^2 + \left(Z_i - Z_{Avg}\right)^2} \qquad (4\text{-}1)$$

where $E_{(Avg)}$ represents the mean square error. (X_i, Y_i, Z_i) represents the object edge coordinates in the ith measurement. n represents the data length. $(X_{Avg}, Y_{Avg}, Z_{Avg})$ represents the average coordinates of the object edge throughout all the measurements.

4.2.1.1. When the initial point is set above the edge

The robot firstly sets its hand 45 degrees and moves to (0, 1, −1) direction to move its hand to contact the object. At the object edge, the force on the sensor 1 and 2 should be equal. However, in this case the force on sensor 2 is larger than that on sensor 1 as shown in Figure 4-10(A). The robot recognizes position of its hand based on the sensor values. After recognizing the position of its hand, the robot moves to (0, −1, 1) direction until all forces on three sensors are equal to 0, that is, the sensors do not contact the object. The robot then moves to (0, −1, −1) direction with 1 mm interval based on the

force difference between the sensors 1 and 2. The robot repeats the movements until the force on the sensor 1 and 2 are equal 2 as shown in Figure 4-10(C). At this stage, robot finds the object edge. This experiment was conducted 10 times. The mean square error, $E_{(Avg)}$ was 0.29 mm.

4.2.1.2. When the initial point is set under the edge

In this case, when the robot touched the object, the force on sensor 2 is smaller than that on sensor 1 as shown in Figure 4-10(B). Based on the sensor values, the robot can recognize that the position of its hands is under object edge position. After recognizing the hand position on the object, the robot moves to $(0, -1, 1)$ direction until all forces on three sensors are equal to 0, that is, the sensors do not contact the object. The robot then moves to $(0, 1, 1)$ direction with 1 mm interval based on the force difference between the sensors 1 and 2. The robot repeats movements until the forces on sensor 1 and 2 are equal as shown in Figure 4-10(C). This experiment was conducted 10 times. The mean square error, $E_{(Avg)}$ was 0.44 mm.

4.2.1.3. When the initial point is set on the edge

In this case, when the robot touched the object, the force on the sensor 1 and 2 should be equal as shown in Figure 4-10(C). If these sensing values different, the robot should do an object edge finding procedure as described in the previous two sections. This experiment was conducted 10 times. The mean square error, $E_{(Avg)}$ was 0.32 mm.

4.2.2. Object edge finding

(A)   (B)   (C)
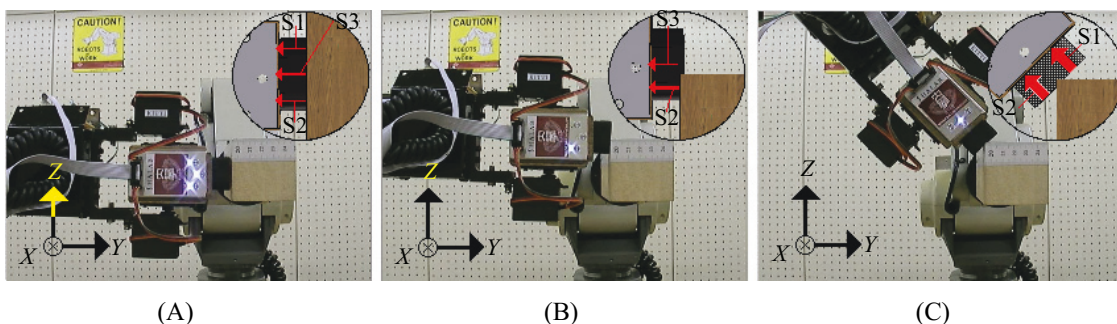
Figure 4-11. Actual robot motions of recognizing an object edge
(Starting point is on an object edge)

Figure 4-11 depicts the procedure of finding the edge from the object surface and shows the actual robot movement when the robot finds the object edge from the object surface. In this case, the robot first sets its hand at 0 degree and then move to (0, 1, 0) direction to contact its hand on the object surface. At this contacted point, the force on three sensors should be equal as shown in Figure 4-11(A). The robot recognizes hand position. Then the robot keeps moving up along the Z axis until reaching the rough edge point as shown in Figure 4-11(B). In other words, it keeps moving until the force on sensor 1 is equal to 0 and that on the sensor 2 is the biggest of all. Then the robot turns its hand –45 degrees and then the robot uses the object edge finding procedure as described in the previous section to reach an exact object edge as shown in Figure 4-11(C). This experiment was conducted 10 times. The mean square error, $E_{(Avg)}$ was 0.43 mm.

4.2.3. Object edge tracking and welding

This experiment aimed to obtain object information by tracing an object edge continuously. Welding is one potential application of this hand pose and motion control technique for finding and tracing the edge and shape of a 3-D object. This technique can be used instead of manual teaching by a person, which is often necessary to obtain object information for welding points before carrying out the welding process.

Figure 4-12 shows the actual movement when the robot tracks an object edge and does simulated welding automatically. Figure 4-13 shows the tracking positions along an object edge during the automatic object searching process. Cross points in Figure 4-13 are the positions of the center of the sensing area shown in Figure 4-12. Dot points are the points on the object edge. The numbers in Figure 4-12 correspond to those in Figure 4-13. In the sensing process, I used the feedback control loop with sensor values to realize the object edge tracking and tracing task.

The robot firstly sets its hand 45 degrees at start position as shown in Figure 4-12(A) and Figure 4-13 (Position 1) and then moves to (0, 1, –1) direction to contact its hand on the object. At the object edge, the forces on the sensors 1 and 2 should be equal. If not equal, the robot repeats the edge recognizing procedure described in section 4.2.1(Object edge recognitions). At this stage, the sensors already set on the object edge.
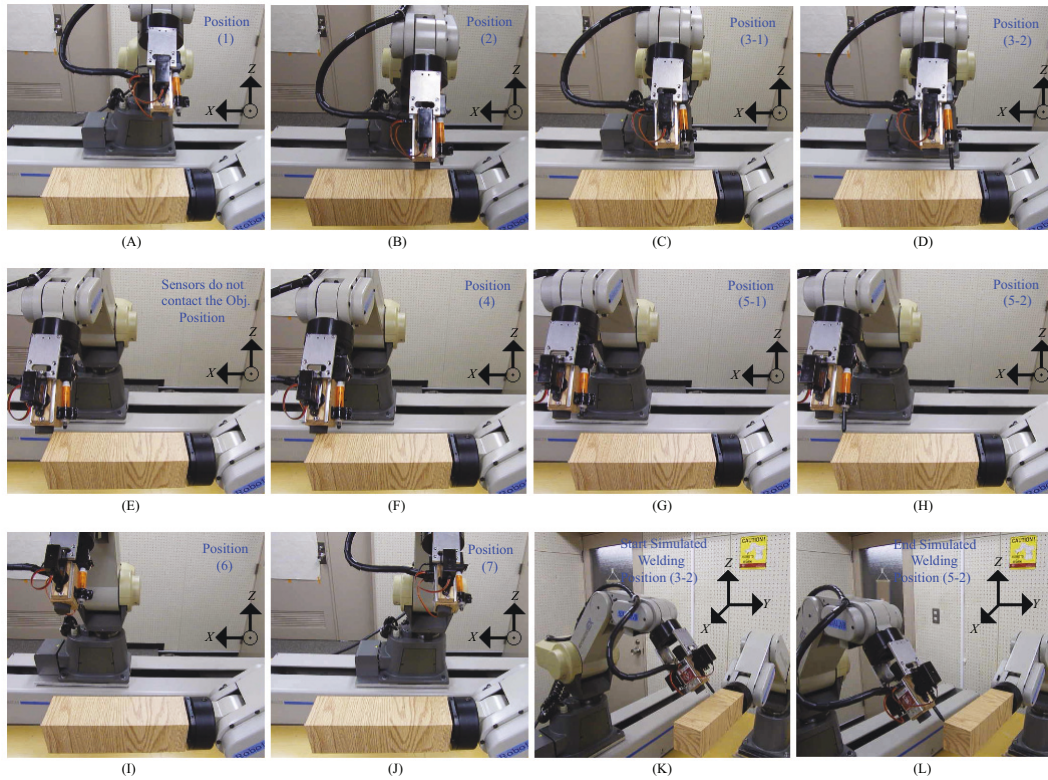
Figure 4-12. Actual autonomous robot motions for tracking an object edge and welding

However the sensor depth position must keep at the same depth. The robot pushes (0, 1, –1) direction and moves back (0, –1, 1) direction to find the depth position from the setting pressure value on the sensor 3. After the edge and depth position are found, the object starting point is show as position 2 Figure 4-12(B) and Figure 4-13(Position 2). Then robot additionally moves by (35 mm, –17 mm, 17 mm) offset as shown in Figure 4-12(C) and Figure 4-13 (Position 3). Then the servo mechanism drives the tip of the simulated welding torch to the object edge in order to give a user visual feedback from proposed system as shown in Figure 4-12(D) and Figure 4-13(Position 3). Hence, positions 3-1 and 3-2 in Figure 4-12 are same as the position 3 in Figure 4-13. The robot records the (X, Y, Z) points for calculating an absolute error of that position as the start point of welding process (X= 0 mm). Then the robot returns the tip of the torch into the case, and moves the sensor back to position 2. After that, robot continues tracing the object edge. The robot moves to (1, 0, 0) direction with 10 mm interval to trace an object edge. The robot also records the (X, Y, Z) points for calculating an absolute error of all tracing path.

Position (2)

Position (4)

Position (3)
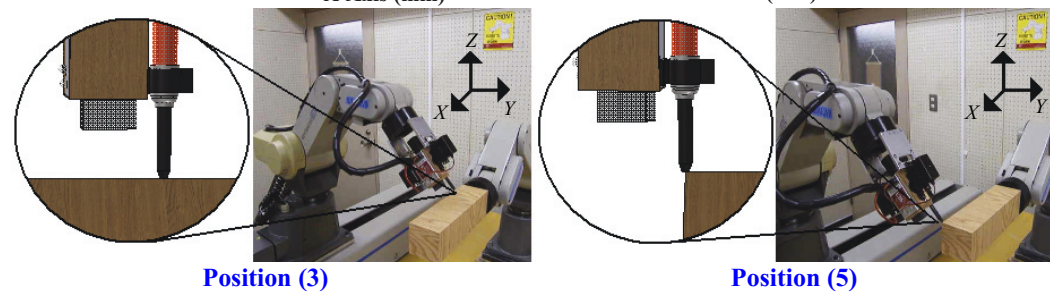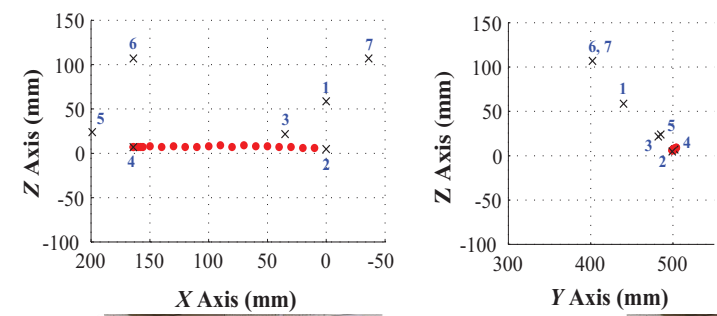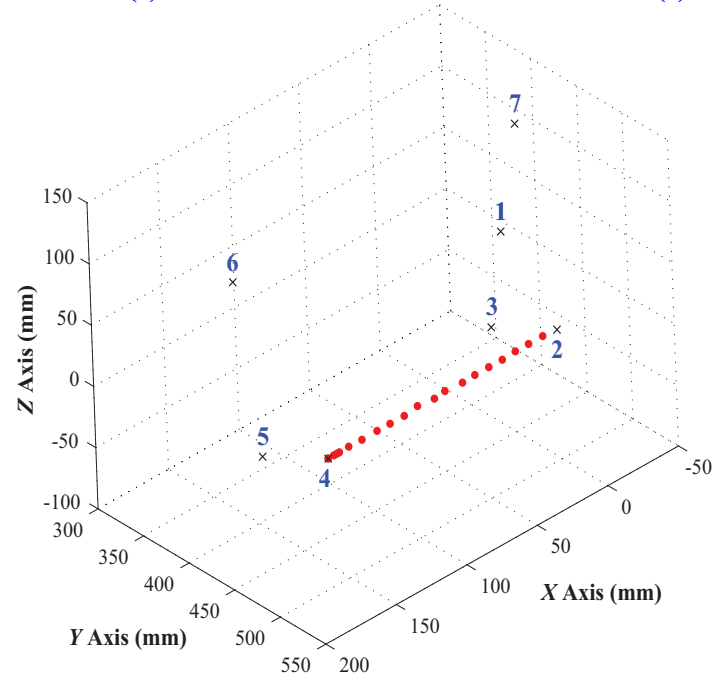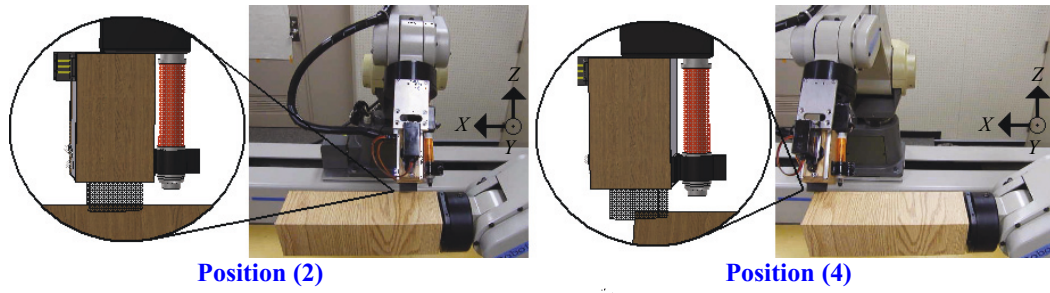
Position (5)

Figure 4-13. Experimental result (Tracking positions along an object edge)

It continues the process until it reaches the rough end point ($X=$ 160 mm), that is, no forces on the sensor 1 and 2, which means that only the sensor 3 has touched an object. To recognize the details of the end point, the robot then moves back to (–1, 0, 0) direction with 1 mm to detect the sensing force on the sensors 1 and 2 again ($X=$ 158 mm). After that, the robot moves forward to (1, 0, 0) direction with 1 mm interval for fine scanning. The movement continues until all the forces on three sensors are equal to 0, that is, the sensors do not contact the object ($X=$ 172 mm) as shown in Figure 4-12(E).

The robot then moves back to (–1, 0, 0) direction by 26 mm, which is the length of the sensing unit ($X=$ 146 mm). At this position the robot confirms the object edge again. If not equal, the robot repeats the edge recognizing procedure. Then the robot moves 13 mm forward to (1, 0, 0) direction, which means that the center of sensing unit is set to the end of object ($X=$ 159 mm) as shown in Figure 4-12(F) and Figure 4-13(Position 4). Then, it additionally moves by (35 mm, –17 mm, 17 mm) offset as shown in Figure 4-12(G) and Figure 4-13(Position 5). Then servo mechanism drives the tip of the simulated welding torch to the object edge and records the (X, Y, Z) points as the end point of welding as shown in Figure 4-12(H) and Figure 4-13(Position 5). Hence, positions 5-1 and 5-2 shown in Figure 4-12 are same as the position 5 in Figure 4-13. Then the robot returns to (Position 4) to confirm the object edge again.

After that, the robot moves to the safety position (Position 7) shown in Figure 4-12(J) and Figure 4-13 through the position 6 shown in Figure 4-12(I). The distances from position 5 to 6 and from position 6 to 7 are (0 mm, –100 mm, 100 mm) and (–200 mm, 0 mm, 0 mm) respectively. When the robot received a welding command from a user, it moves following the recorded points along the object edge through the positions 3-2 and 5-2 as shown in Figures 4-12 (K), (L), (D) and (H). Figures 4-12 (K) and (L) are the overall views, and Figures 4-12(D) and (H) are the front views of those positions respectively. In this case, as the trajectory is a straight line, I set the start and end point by using the memorized trajectory and control the robot movement from the start point to the end point. When a user utilizes this system, s/he can repeat the welding times with various travel speeds. In this experiment, I set the robot repeats the movement 5 times with 477 cm/min travel speed. As the results, the object edge was set in parallel to the X
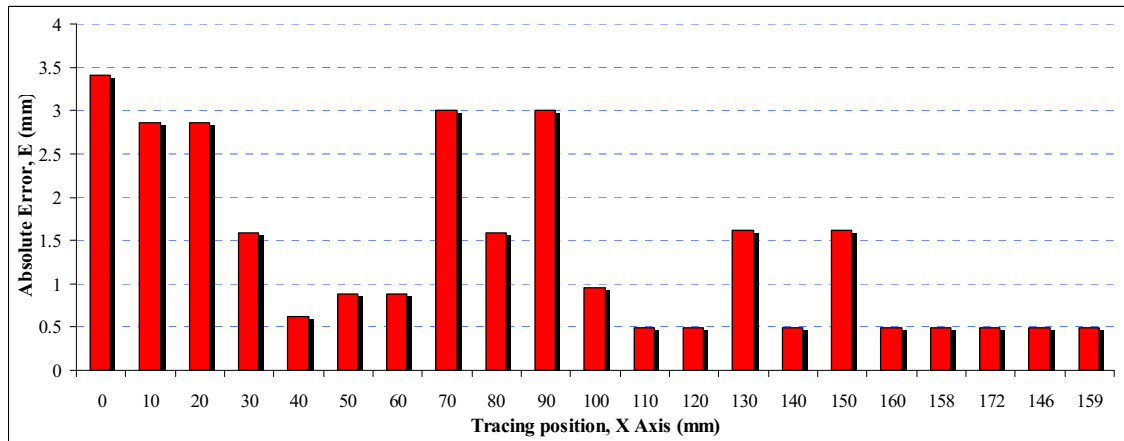
Figure 4-14. Experimental result (Absolute error along an object edge)

axis and the robot moved by 159 mm and obtained 21 tracing points with average 12 sensing times for each tracing point. The term "*sensing times*" means the number of sensing times for each moving step of the object holder robot. In this experiment, I set the sampling interval to 550 ms. Hence, the total experiment time was equal to 138.6 s (252 sensing times). Thus the motion velocity to recognize the object edge in this experiment was 6.9 cm/min. The average of the obtained object edge (Y_{Avg}, Z_{Avg}) was (501.6 mm, 7.2 mm) while the actual object edge (Y_{Avg}, Z_{Avg}) was set to (500 mm, 5 mm). The absolute error for each sensing points from 0 mm to 159 mm along X axis are illustrated in Figure 4-14. The average absolute error of all sensing points was 1.37 mm.

4.3. Summary

This chapter introduced the applications of the proposed tactile sensing system for the industrial purpose. Three possible applications of tactile sensing technique for object recognitions with experimental results are first presented. Such as, the surface angle measurement, the object shapes measurement and the surface normal following. Then an approach for welding application with experimental results was introduced next. Welding is one potential application for finding and tracing the edge and shape of 3-D object. As the result, the proposed technique can use for automatic obtain the welding points and then does the simulated welding task. Thus the proposed technique can be use instead of manual teaching.

CHAPTER V

5. HUMANOID ROBOT APPLICATIONS

5.1. Ground Slopes Recognizing Application

I conducted some experiments to confirm the ability of the proposed tactile sensing system for humanoid robot to move its foot in 3-D. I mainly examined four cases, the downward slope, upward slope, rightward slope and leftward slope. In these applications, I do not need the information about the contacted ground slopes conditions or orientation in advance.

5.1.1. Experiment on robot foot poses action (Downward-Upward slopes)

5.1.1.1. Downward slope case

This experiment aims to confirm that humanoid robot can detect downward slope by using the proposed system. Figure 5-1 displays an actual movement when the robot recognizes a downward slope. Figure 5-2 demonstrations robotic foot's sensing data when robot recognizes a downward slope. The sensing data is the RC time constant value in the RC circuit of each sensing element. When the sensor has no-load, sensing value is high (In case of no-load, I set maximum detecting values as 5,000μs). RC time constant value decreased when applied force into the sensor. In this experiment, the right foot was first set above the 20 degrees downward slope as shown in Figure 5-1(A). As this state the sensor has no-load, and thus all three sensing values are 5,000μs as can be seen at the beginning (0 second) in Figure 5-2. In other words, when all sensing values are maximal values, the robot foot is free from the ground. Next, the robot moved its foot down to touch the ground slope as shown in Figure 5-1(B). When the robot did this action, the sensing value on sensor 2 decreased as shown at 1.5s in Figure 5-2. After the first touch, the robot began turning its foot by utilizing the analyses of the distributed pressure patterns. In this case, the outputs of the sensor elements are constrained as follows,

$$SR_2 > SR_3 \geq SR_1 \tag{5-1}$$

where the SR_i represents the sensor output from the ith sensor on the right foot.

(A)	(B)	(C)	(D)
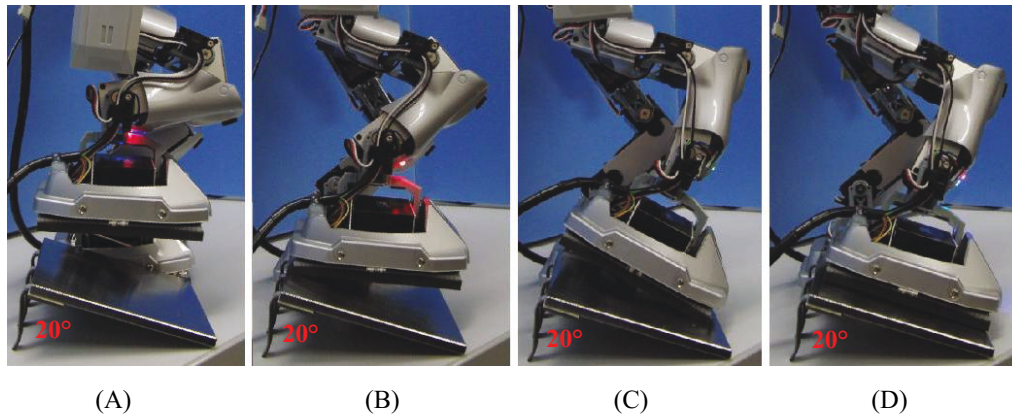
Figure 5-1. Actual robot motion when the robot recognizes a downward slope
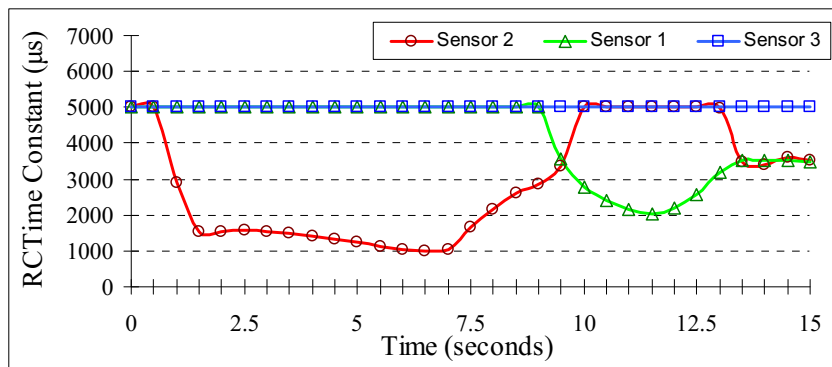
Figure 5-2. Sensing data of robotic foot when the robot recognizes a downward slope

To follow the ground surface normal in this condition, the robot foot needs to move up until all three sensing data are equal or the forces between sensor 1 and 2 are equal. These actions are shown at 9.5s in Figure 5-2. However, to confirm the correctness of the results, I temporarily controlled the robot foot to overshoot the point where the receiving forces are equal as shown in Figure 5-1(C). The graph at 10 seconds in Figure 5-2 shows the three sensors data when the robot did the overshoot. Finally, the robot turned its foot back to the position where the receiving forces are equal as shown in Figure 5-1(D). The graph at 13.5s in Figure 5-2 shows the three sensors data when the robot did the action. Throughout this experiment, the robot can detect the ground slope and move its foot normal to the ground surface in case of following the downward slope.

5.1.1.2. Upward slope case

This experiment aims to confirm that the humanoid robot can detect the upward

slope by using the proposed system. Figure 5-3 shows the actual movement when the robot recognizes an up slope. Figure 5-4 shows the sensing data of robotic foot when the robot recognizes an upward slope.

(A)　　　　　　　(B)　　　　　　　(C)　　　　　　　(D)
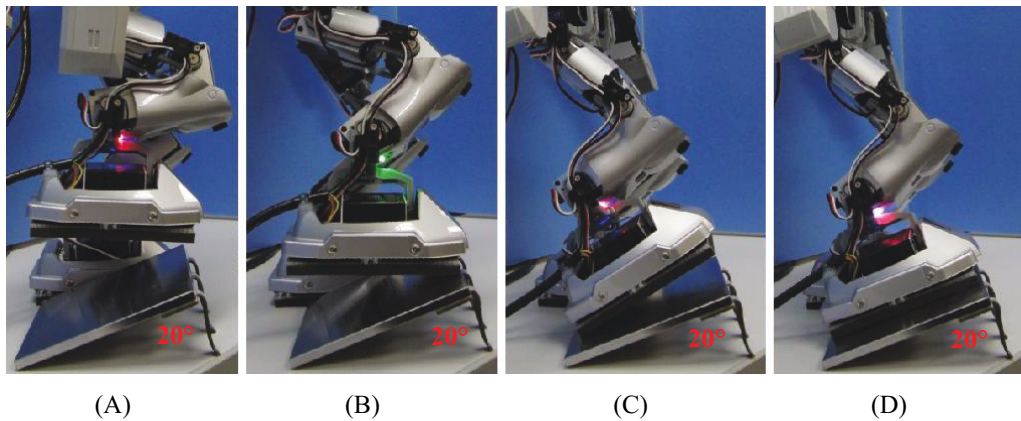
Figure 5-3. Actual robot motion when the robot recognizes an upward slope
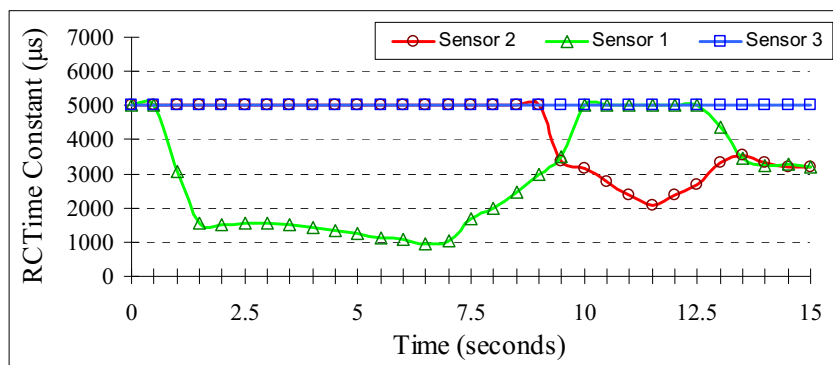
Figure 5-4. Sensing data of robotic foot when the robot recognizes an upward slope

In this experiment, the right foot was first set above the 20 degrees up slope as shown in Figure 5-3(A). At this state the sensor is no-load, thus all three sensing values are 5,000μs as can be seen at the beginning (0 second) in Figure 5-4. Next, the robot moved its foot down to touch the ground slope as shown in Figure 5-3(B). When robot did this action, the sensing value on sensor 1 decreased as shown at 1.5s in Figure 5-4. After the first touch, the robot began turning its foot by utilizing the analyses of the distributed pressure patterns. In this case, the outputs of the sensor elements are constrained as follow;

$$SR_1 > SR_3 \geq SR_2 \qquad\qquad (5\text{-}2)$$

Based on the sensor values, to follow the ground surface normal, the robot foot needs to move up until the forces on all three sensing elements are equal or the forces between sensor 1 and 2 are equal. These actions are shown at 9.5s in Figure 5-4. However, to confirm the correctness of the results, I temporally controlled the robot foot to overshoot the point where the receiving forces are equal as shown in Figure 51(C). The graph at 10 seconds in Figure 5-4 shows the three sensors data when the robot did the overshoot. Finally, the robot turned its foot back to the position where the receiving forces are equal as shown in Figure 5-3(D). The graph at 13.5s in Figure 5-4 shows the three sensors data when the robot can detect the ground slope and move its foot normal to the ground surface in case of following the upward slope.

5.1.2. Experiment on robot foot poses action (Leftward-Rightward slopes)

5.1.2.1. Leftward slope case

This experiment aims to confirm that the humanoid robot can detect the left slope by using the proposed system. Figure 5-5 shows the actual movement when the robot recognizes a left side slope. Figure 5-6 shows the sensing data of robotic foot when the robot recognizes a leftward slope (Figure direction).

| (A) | (B) | (C) | (D) |
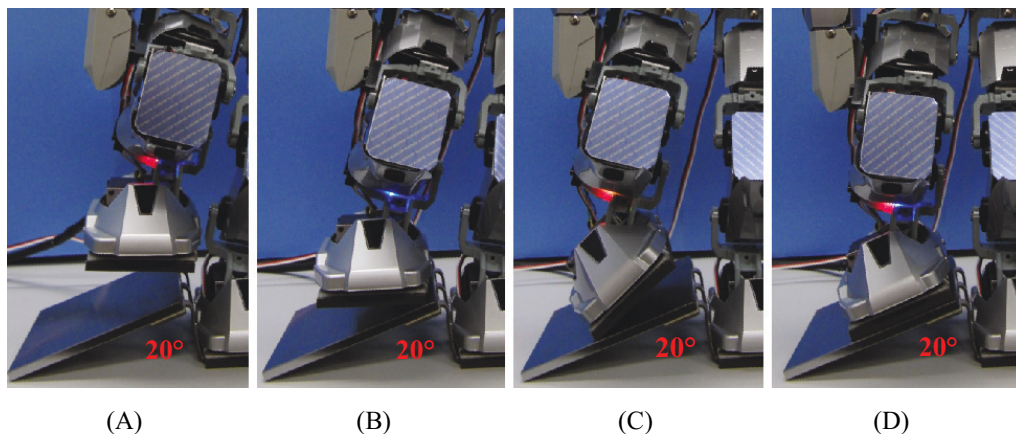
Figure 5-5. Actual robot motion when the robot recognizes a leftward slope

In this experiment, the right foot was first set above the 20 degrees leftward slope as shown in Figure 5-5(A). At this point the sensor is unloaded, and therefore all three

sensing values are 5,000μs as can be seen at the beginning (0 second) in Figure 5-6. Next, the robot moved its foot down to touch the ground slope as shown in Figure 5-5(B). Graph at 1.5s in Figure 5-6 shows sensor output throughout the movement. At this point the sensing value on sensor 3 decreased. After the first touch, the robot began turning its foot by using the analyses of the distributed pressure patterns. In this case, the outputs of the sensor elements are constrained as follows,

$$(SR_1 \approx SR_2) > SR_3 \tag{5-3}$$
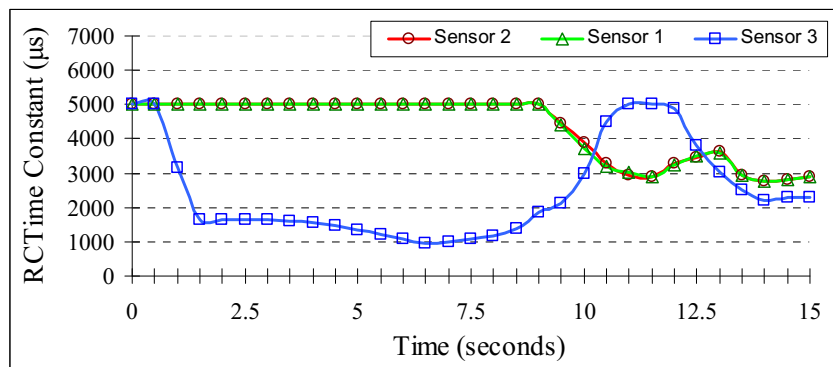
Figure 5-6. Sensing data of robotic foot when the robot recognizes a leftward slope

To follow the ground surface normal, the robot foot needs to move turn left until the forces on all three sensing elements are equal. The sensor outputs throughout the movements are shown around 10 seconds in Figure 5-6. However, I also temporally controlled the robot foot to overshoot the detected point as shown in Figure 5-5(C) and at 10.5s in Figure 5-6. Finally, the robot turned its foot back to the position where the receiving forces are equal as shown in Figure 5-5(D) and at 12.5s in Figure 5-6. Throughout this experiment, the robot also can detect the ground slope and move its foot normal to the ground surface in case of following the leftward slope.

5.1.2.2. Rightward slope case

This experiment aims to confirm that the humanoid robot can detect the right slope by using the proposed system. Figure 5-7 shows the actual movement when the robot recognizes a rightward slope. Figure 5-8 shows the sensing data of robotic foot when the robot recognizes a rightward slope (Figure direction).

(A) (B) (C) (D)
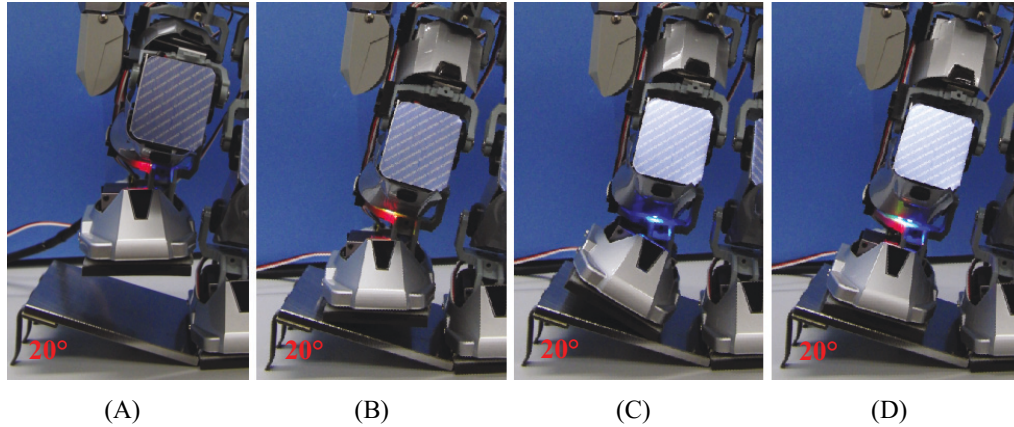
Figure 5-7. Actual robot motion when the robot recognizes a rightward slope
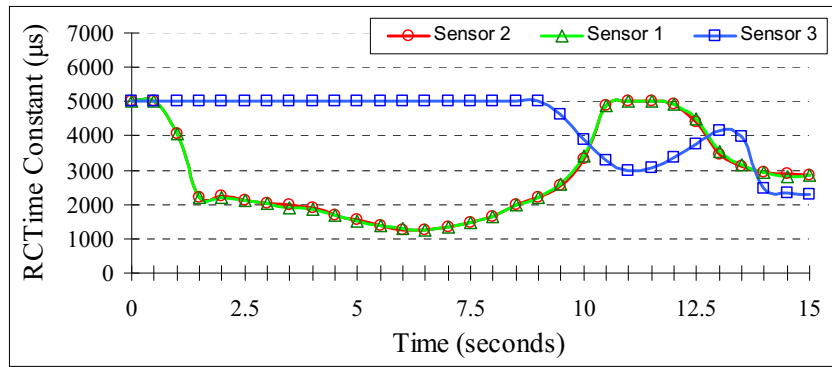
Figure 5-8. Sensing data of robotic foot when the robot recognizes a rightward slope

In this experiment, the right foot was first set above the 20 degrees right side slope as shown in Figure 5-7(A). At this point the sensor is unloaded, and therefore all three sensing values are 5,000μs as can be seen at the beginning (0 second) in Figure 5-8. Next, the robot moved its foot down to touch the ground slope as shown in Figure 5-7(B). Graph at 1.5s in Figure 5-8 shows three sensors data when the robot did the movement. At this point the sensing values on sensor 1 and 2 decreased. After the first touch, the robot began turning its foot by utilizing the analyses of the distributed pressure patterns. In this case, the outputs of the sensor elements are constrained as follows,

$$(SR_1 \approx SR_2) < SR_3 \tag{5-4}$$

To follow the ground surface normal, the robot needs to move turn right until the

86

forces on all three sensing elements are equal. The data from three sensors in the above control process is shown around 10 seconds in Figure 5-8. However, I also temporally controlled the robot foot to overshoot the detected point as shown in Figure 5-7(C) and at 10.5s shown in Figure 5-8. Finally, the robot turned its foot back to the position where the receiving forces are equal as shown in Figure 5-7(D) and at 12.5s shown in Figure 5-8. Throughout this experiment, the robot can also detect the ground slope and move its foot normal to the ground surface in case of following the rightward slope.

5.2. Balancing Applications
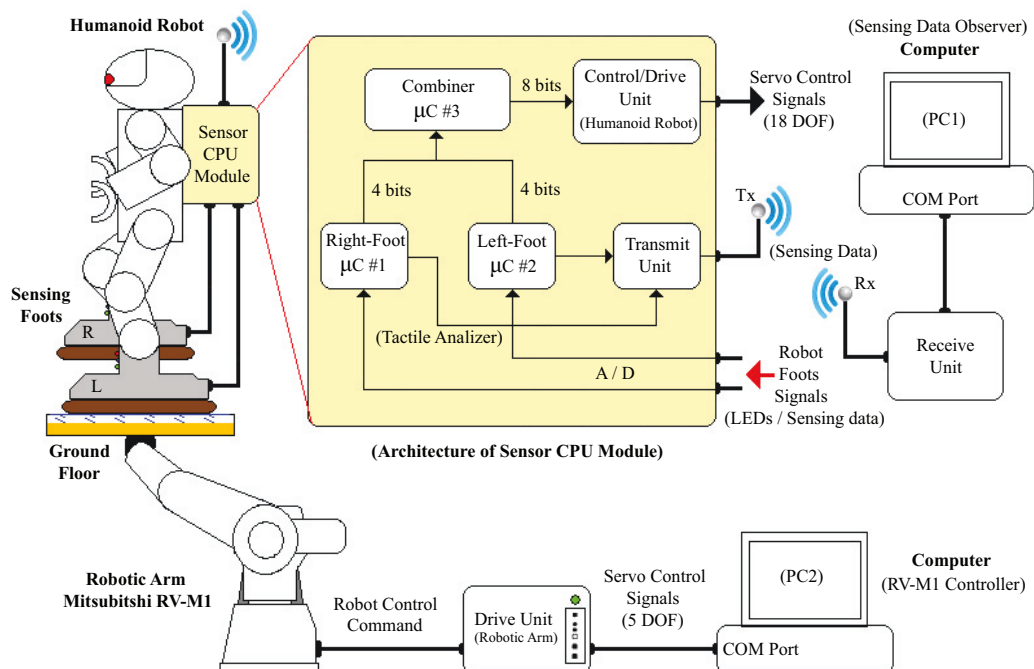
Figure 5-9. Diagram of tactile sensing system for two legs balancing test

In this application, I conducted the experiments to confirm the two legs balance control of the humanoid robot with the proposed tactile sensing feet on the different ground environments such as flat, upward slopes, downward slopes. The diagram of tactile sensing system for two legs balancing test of humanoid robot and experimental setup is shown in Figure 5-9. Humanoid robot was interacted with moving ground floor by using its sensing feet. As shown in this figure, a humanoid robot is put on the flat

plastic plate (Thickness: 15mm) at the end-effector of the arm robot. The equipped flat plate is used as the ground floor for testing the two legs balancing control. I also attempted some other experiments to realize one leg balance control of the humanoid robot during it does the swinging motions. In additions, to confirm the ability of the proposed system for humanoid robot motion control effectively, I also attempted some other experiments to realize effective balancing actions, especially to avoid the robot damages which cause the falling down due to the unpredicted external pushing force from the human on both one leg and two legs balance actions. In these applications, the robots do not need any information about the contacted ground slope or orientation in advance.

5.2.1. Humanoid robot kinematics for balancing controls

5.2.1.1. Balancing Algorithm

A) Zero Moment Point (ZMP)
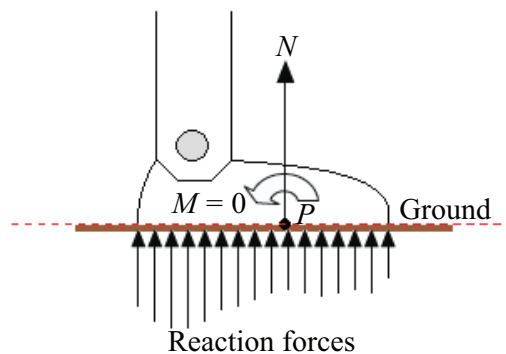
Figure 5-10. Diagram of *Zero Moment Point* (ZMP) concept

The *Zero Moment Point* (ZMP) is the important concept to realize the balancing algorithm for biped robots. ZMP used for analyze the dynamic motion is equivalent to *center of gravity* (COG). COG is a projection of *center of mass* (CM) on ground plane in static circumstance. Thus, COG should maintain to keep within the supporting area for static balance control, while ZMP should maintain to keep within the supporting area for dynamic balance control. The ZMP trajectory of robot foot is a key criterion for robot

stability walking. In many studies, ZMP coordinates have computed using robot model and joint angle information read from encoders. Conversely, in this research I employed a direct approach and simpler technique which is tactile feedback measured by using tactile sensors mounted under the robot's feet instead. The tactile sensor units are equipped at the back of two robotic feet. Each foot has an individual sensing circuit to detect the three sensing values which is describe on Section 2.5.2(Tactile sensor feet). The distribution of the ground is reaction force beneath the robot's foot is complicated. However, at any point P on the sole of the foot to the reaction can be represented by a force N and moment M, as shown in Figure 5-10. Basically, ZMP is center of pressure of robot foot project on the ground, and moment applied by ground about zero in this point. In other words, the point P on the ground is the point which the net moment of the inertial and gravity forces has no component along the axes which is parallel to the ground plane.

B) Center of Mass (CM)

For every system and at every instant in time, there is a unique location in space that is the average position of the system mass. This place is called the *Center of mass*, commonly designated by c.o.m., COM, CM, G, c.g., and ◕ (in the diagram). According to the previous section, I emphasized that ZMP used for analyze the dynamic motion is equivalent to *center of gravity* (COG). COG is a projection of *center of mass* (CM) on ground plane in static circumstance. Thus COG and ZMP should be kept within the supporting area for static and dynamic balancing controls respectively. In other words, to maintain the balance, the system should also keep the *total center of mass* (*T-CM*) inside the supporting area. *T-CM* position of the system n particles can be obtained as:

$$X_{T-CM} = \frac{(M_1 * X_1) + (M_2 * X_2) + ... + (M_n * X_n)}{M_1 + M_2 + ... + M_n} = \frac{1}{M_T} \sum_{i=1}^{n} (M_i * X_i) \qquad (5\text{-}5)$$

$$Y_{T-CM} = \frac{(M_1 * Y_1) + (M_2 * Y_2) + ... + (M_n * Y_n)}{M_1 + M_2 + ... + M_n} = \frac{1}{M_T} \sum_{i=1}^{n} (M_i * Y_i) \qquad (5\text{-}6)$$

$$Z_{T-CM} = \frac{(M_1 * Z_1) + (M_2 * Z_2) + ... + (M_n * Z_n)}{M_1 + M_2 + ... + M_n} = \frac{1}{M_T} \sum_{i=1}^{n} (M_i * Z_i) \qquad (5\text{-}7)$$

C) Single and Double supporting phases

I employed a direct approach and simpler technique which is to use tactile feedback measured using the sensors mounted on the robot's feet. Each foot has an individual sensing circuit to detect the three sensing values. The position of *center of mass* (*CM*) on the single and double supporting phases is shown in Figure 5-11. This figure, SL_i and SR_i represent the receiving force of left and right foot sensing element i ($i = 1, 2, 3$) respectively.
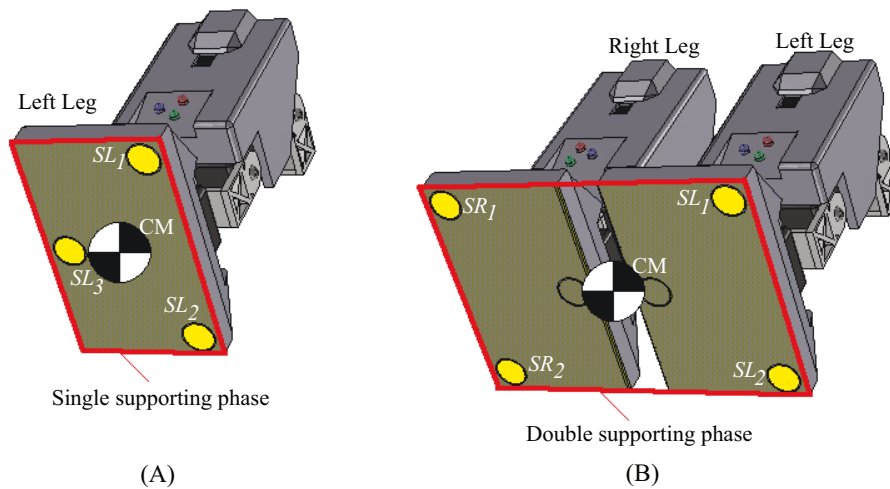
Figure 5-11. Center of mass on the single and double supporting phases

The proposed technique is to control the robot motion to keep the three sensing values of supporting foot equal when the robot standing with one leg (single supporting phase). The relation forces between the sensor outputs is described as, $SL_1 = SL_2 = SL_3$ as shown in Figure 5-11(A). This technique also can be further extended to the double supporting phases, when the robot stands with two legs. In this case, the four sensing values of left and right foots are considered to make equally. The relation forces between the sensor outputs in this case is described as, $SL_1 = SL_2 = SR_1 = SR_2$ as shown in Figure 5-11(B). Hence, in both cases when the concern sensing values are the same, the *CM* point is also in the middle of the supporting area. In other words, this technique can be employed to control the robot to keep the *CM* constantly in the center of single and double support phases and that is correspondence to the method to keep the COG and ZMP within the supporting area for static and dynamic balance controls in advance.

D) Humanoid robot model
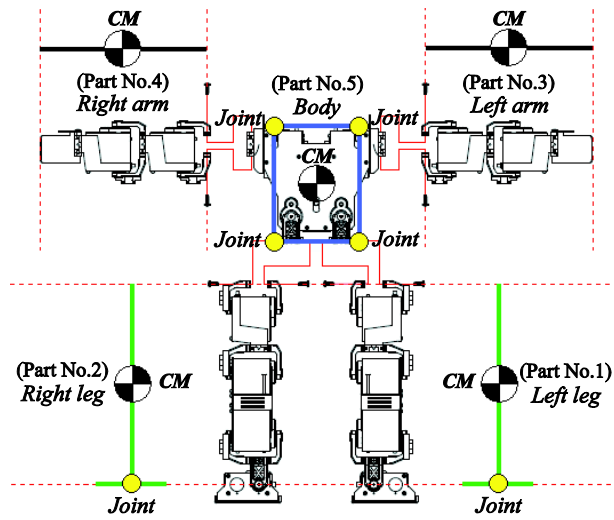
Figure 5-12. Diagram of humanoid robot parts
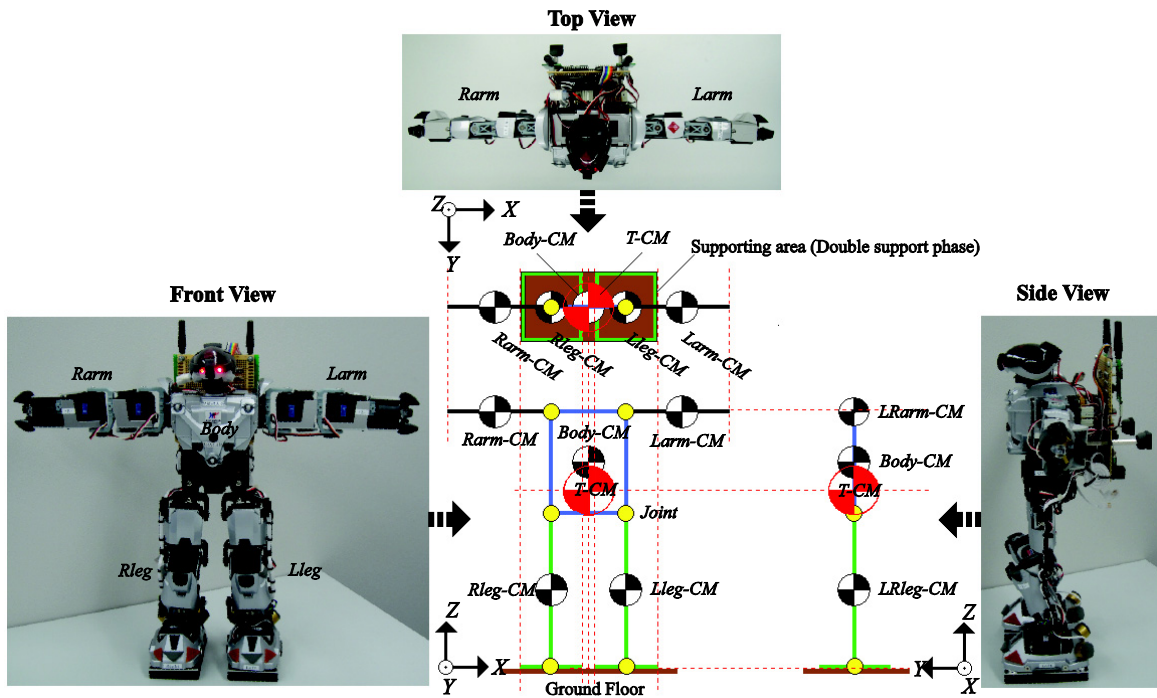
Figure 5-13. The relation between the actual robot and the robot model in 3-D

In order to perform the successful computation, I have divided the humanoid robot into five separated parts including, left and right legs, left and right arms, and the body as part number 1 to 5 respectively as shown in Figure 5-12. The relation between the actual robot and the equivalence model in 3-D are shown in Figure 5-13.

91

E) Total CM calculation from humanoid robot model
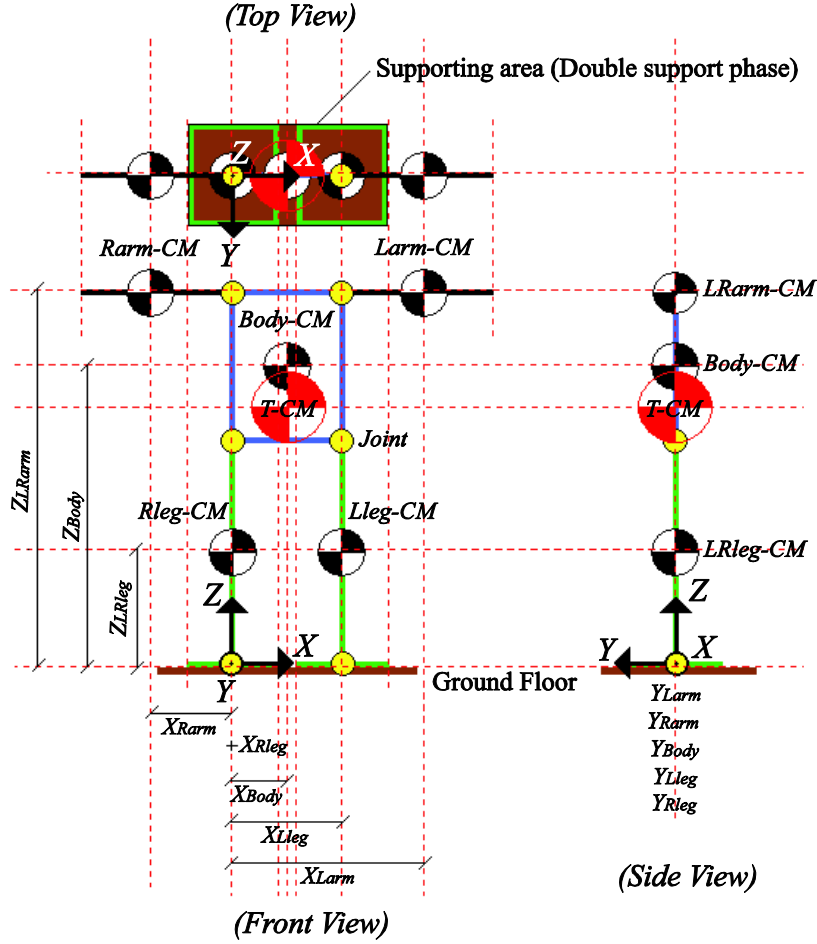
Figure 5-14. Parameters definition for center of mass calculation in 3-D

Figure 5-14 shows the definition for center of mass calculation. The *total center of mass* (*T-CM*) position of the humanoid robot model above can be obtained as:

$$X_{T-CM} = \frac{(M_{Lleg} * X_{Lleg}) + (M_{Rleg} * X_{Rleg}) + (M_{Larm} * X_{Larm}) + (M_{Rarm} * X_{Rarm}) + (M_{Body} * X_{Body})}{M_{Lleg} + M_{Rleg} + M_{Larm} + M_{Rarm} + M_{Body}} \quad (5\text{-}8)$$

$$Y_{T-CM} = \frac{(M_{Lleg} * Y_{Lleg}) + (M_{Rleg} * Y_{Rleg}) + (M_{Larm} * Y_{Larm}) + (M_{Rarm} * Y_{Rarm}) + (M_{Body} * Y_{Body})}{M_{Lleg} + M_{Rleg} + M_{Larm} + M_{Rarm} + M_{Body}} \quad (5\text{-}9)$$

$$Z_{T-CM} = \frac{(M_{Lleg} * Z_{Lleg}) + (M_{Rleg} * Z_{Rleg}) + (M_{Larm} * Z_{Larm}) + (M_{Rarm} * Z_{Rarm}) + (M_{Body} * Z_{Body})}{M_{Lleg} + M_{Rleg} + M_{Larm} + M_{Rarm} + M_{Body}} \quad (5\text{-}10)$$
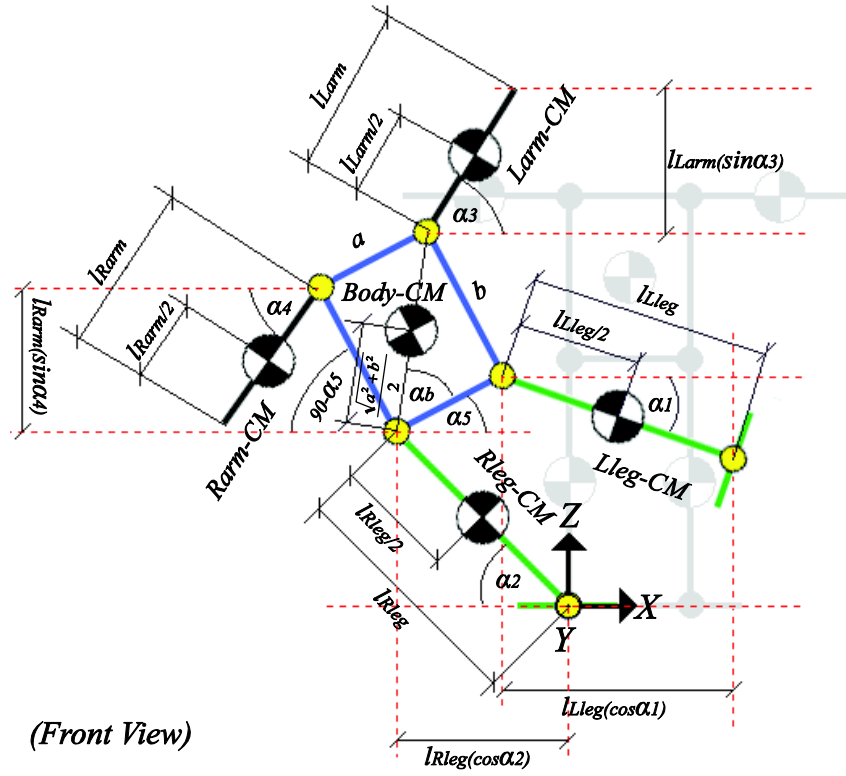
Figure 5-15. Parameters definitions for center of mass calculation in *X* direction

Figure 5-15 illustrates the parameters definitions for calculating the *total center of mass* position respect to *X* direction ($X_{T\text{-}CM}$). This figure shows the front view of equivalence humanoid robot which is provides the solving idea for the joint angles of five links including, Left leg, Right leg, Left arm, Right arm and Body. The summation of mass multiply with *X* length of all constraint parts from the equivalence humanoid robot model above can be obtained as:

$$\sum_{i=1}^{n}(M_i * X_i) = M_{Lleg} * \left[(\frac{-l_{Rleg}}{2}\cos\alpha_2) + (a\cos\alpha_5) + (\frac{l_{Lleg}}{2}\cos\alpha_1) \right] + M_{Rleg} * (\frac{-l_{Rleg}}{2}\cos\alpha_2)$$

$$+ M_{Larm} * \left[(\frac{-l_{Rleg}}{2}\cos\alpha_2) + (\sqrt{a^2+b^2}\cos(\alpha_b+\alpha_5)) + (\frac{l_{Larm}}{2}\cos\alpha_3) \right]$$

$$+ M_{Rarm} * \left[(\frac{-l_{Rleg}}{2}\cos\alpha_2) - (b\cos(90-\alpha_5) + (\frac{-l_{Rarm}}{2}\cos\alpha_4) \right]$$

$$+ M_{Body} * \left[(\frac{-l_{Rleg}}{2}\cos\alpha_2) + \frac{\sqrt{a^2+b^2}}{2}\cos(\alpha_b+\alpha_5) \right]$$

(5-11)

93

Figure 5-16. Parameters definitions for center of mass calculation in *X-Y* directions

Figure 5-16 illustrates the parameters definitions for calculating the *total center of mass position* respect to *X* and *Y* directions as ($X_{T\text{-}CM}$) and ($Y_{T\text{-}CM}$) respectively. This figure shows the top view of the robot model which provides the solving idea for the joint angles of four links, left-right legs and left-right arms accept the robot body. Both legs will not have constraint effect regarding to *X-Y* plane (top view), when the robot not swing the legs left-rightwards (*X* Axis) or front-backwards (*Y* Axis). Due to, when the robot standing normal α_1, α_2, β_1 and $\beta_2 = 90°$. The lengths of left and right legs are $\sqrt{(l_{Lleg}\cos\alpha_1)^2 + (l_{Lleg}\cos\beta_1)^2}$ and $\sqrt{(l_{Rleg}\cos\alpha_2)^2 + (l_{Rleg}\cos\beta_2)^2}$ respectively, which are obtained from the kinematics analysis of front and side views. The summations of mass multiply with *X* and *Y* length of all parts from the robot model above can be obtained as:

$$\sum_{i=1}^{n}(M_i * X_i) = M_{Lleg} * (a + \frac{\sqrt{(l_{Lleg}\cos\alpha_1)^2 + (l_{Lleg}\cos\beta_1)^2}}{2}\cos\theta_1)$$
$$+ M_{Rleg} * (\frac{-\sqrt{(l_{Rleg}\cos\alpha_2)^2 + (l_{Rleg}\cos\beta_2)^2}}{2}\cos\theta_2) + M_{Larm} * (a + \frac{l_{Larm}}{2}\sin\theta_3) + M_{Rarm} * (\frac{-l_{Rarm}}{2}\sin\theta_4)$$

(5-12)

$$\sum_{i=1}^{n}(M_i * Y_i) = M_{Lleg} * (\frac{\sqrt{(l_{Lleg}\cos\alpha_1)^2 + (l_{Lleg}\cos\beta_1)^2}}{2}\sin\theta_1)$$
$$+ M_{Rleg} * (\frac{-\sqrt{(l_{Rleg}\cos\alpha_2)^2 + (l_{Rleg}\cos\beta_2)^2}}{2}\sin\theta_2) + M_{Larm} * (\frac{-l_{Larm}}{2}\cos\theta_3) + M_{Rarm} * (\frac{l_{Rarm}}{2}\cos\theta_4)$$

(5-13)

94

Figure 5-17. Parameters definitions for center of mass calculation in *Y* direction

Figure 5-17 illustrates the parameters definitions for calculating the *total center of mass* position respect to *Y* direction ($Y_{T\text{-}CM}$). This figure also shows the side view of robot model which provides the solving idea for all joint angles. The lengths of left and right arms are $\sqrt{(l_{Larm} \sin \alpha_3)^2 + (l_{Larm} \cos \theta_3)^2}$ and $\sqrt{(l_{Rarm} \sin \alpha_4)^2 + (l_{Rarm} \cos \theta_4)^2}$ respectively, which are obtained from an analysis of top and front views. These arms will not have constraint effect regarding to *Y* direction, when the arms not swing front-backward (*Y* Axis) or up-downward (*Z* Axis). Due to, when the robot standing normal α_3 and $\alpha_4 = 0°$, θ_3 and $\theta_4 = 90°$. The summation of mass multiply with *Y* length of all parts from the robot model above can be obtained as:

$$
\begin{aligned}
\sum_{i=1}^{n}(M_i * Y_i) = {} & M_{Lleg} * \left[\left(\frac{-l_{Rleg}}{2} \cos\beta_2 \right) + \left(\frac{l_{Lleg}}{2} \cos\beta_1 \right) \right] + M_{Rleg} * \left(\frac{-l_{Rleg}}{2} \cos\beta_2 \right) \\
& + M_{Larm} * \left[\left(\frac{-l_{Rleg}}{2} \cos\beta_2 \right) + (b * \cos\beta_5) + \left(\frac{-\sqrt{(l_{Larm}\sin\alpha_3)^2 + (l_{Larm}\cos\theta_3)^2}}{2} \cos\beta_3 \right) \right] \\
& + M_{Rarm} * \left[\left(\frac{-l_{Rleg}}{2} \cos\beta_2 \right) + (b * \cos\beta_5) + \left(\frac{\sqrt{(l_{Rarm}\sin\alpha_4)^2 + (l_{Rarm}\cos\theta_4)^2}}{2} \cos\beta_4 \right) \right] + M_{Body} * \left[\left(\frac{-l_{Rleg}}{2} \cos\beta_2 \right) + \frac{b}{2} \cos\beta_5 \right]
\end{aligned}
$$

(5-14)

95

The *total center of mass position in X direction*, ($X_{T\text{-}CM}$) can be obtained by combined those $X_{T\text{-}CM}$ equations from those three images as;

$$X_{T-CM} = \frac{(M_{Lleg} * X_{Lleg}) + (M_{Rleg} * X_{Rleg}) + (M_{Larm} * X_{Larm}) + (M_{Rarm} * X_{Rarm}) + (M_{Body} * X_{Body})}{M_{Lleg} + M_{Rleg} + M_{Larm} + M_{Rarm} + M_{Body}}$$

$$= M_{Lleg} * \left[(\frac{-l_{Rleg}}{2} \cos\alpha_2) + (a\cos\alpha_5) + (\frac{l_{Lleg}}{2}\cos\alpha_1) + (a + \frac{\sqrt{(l_{Lleg}\cos\alpha_1)^2 + (l_{Lleg}\cos\beta_1)^2}}{2}\cos\theta_1) \right]$$

$$+ M_{Rleg} * \left[(\frac{-l_{Rleg}}{2}\cos\alpha_2) + (\frac{-\sqrt{(l_{Rleg}\cos\alpha_2)^2 + (l_{Rleg}\cos\beta_2)^2}}{2}\cos\theta_2) \right]$$

$$+ M_{Larm} * \left[(\frac{-l_{Rleg}}{2}\cos\alpha_2) + (\sqrt{a^2 + b^2}\cos(\alpha_b + \alpha_5)) + (\frac{l_{Larm}}{2}\cos\alpha_3) + (a + \frac{l_{Larm}}{2}\sin\theta_3) \right]$$

$$+ M_{Rarm} * \left[(\frac{-l_{Rleg}}{2}\cos\alpha_2) - (b\cos(90 - \alpha_5)) + (\frac{-l_{Rarm}}{2}\cos\alpha_4) + (\frac{-l_{Rarm}}{2}\sin\theta_4) \right]$$

$$\frac{+ M_{Body} * \left[(\frac{-l_{Rleg}}{2}\cos\alpha_2) + \frac{\sqrt{a^2 + b^2}}{2}\cos(\alpha_b + \alpha_5) \right]}{M_{Lleg} + M_{Rleg} + M_{Larm} + M_{Rarm} + M_{Body}} \qquad (5\text{-}15)$$

The *total center of mass position in Y direction*, ($Y_{T\text{-}CM}$) can be obtained by combined those $Y_{T\text{-}CM}$ equations from those three images as;

$$Y_{T-CM} = \frac{(M_{Lleg} * Y_{Lleg}) + (M_{Rleg} * Y_{Rleg}) + (M_{Larm} * Y_{Larm}) + (M_{Rarm} * Y_{Rarm}) + (M_{Body} * Y_{Body})}{M_{Lleg} + M_{Rleg} + M_{Larm} + M_{Rarm} + M_{Body}}$$

$$= M_{Lleg} * \left[(\frac{-l_{Rleg}}{2}\cos\beta_2) + (\frac{l_{Lleg}}{2}\cos\beta_1) + (\frac{\sqrt{(l_{Lleg}\cos\alpha_1)^2 + (l_{Lleg}\cos\beta_1)^2}}{2}\sin\theta_1) \right]$$

$$+ M_{Rleg} * \left[(\frac{-l_{Rleg}}{2}\cos\beta_2) + \frac{-\sqrt{(l_{Rleg}\cos\alpha_2)^2 + (l_{Rleg}\cos\beta_2)^2}}{2}\sin\theta_2 \right]$$

$$+ M_{Larm} * \left[(\frac{-l_{Rleg}}{2}\cos\beta_2) + (b*\cos\beta_5) + (\frac{-\sqrt{(l_{Larm}\sin\alpha_3)^2 + (l_{Larm}\cos\theta_3)^2}}{2}\cos\beta_3) + (\frac{-l_{Larm}}{2}\cos\theta_3) \right]$$

$$+ M_{Rarm} * \left[(\frac{-l_{Rleg}}{2}\cos\beta_2) + (b*\cos\beta_5) + (\frac{\sqrt{(l_{Rarm}\sin\alpha_4)^2 + (l_{Rarm}\cos\theta_4)^2}}{2}\cos\beta_4) + (\frac{l_{Rarm}}{2}\cos\theta_4) \right]$$

$$\frac{+ M_{Body} * \left[(\frac{-l_{Rleg}}{2}\cos\beta_2) + \frac{b}{2}\cos\beta_5 \right]}{M_{Lleg} + M_{Rleg} + M_{Larm} + M_{Rarm} + M_{Body}} \qquad (5\text{-}16)$$

F) Balancing control in X direction with CM analysis

F-1) Unbalanced motion analysis
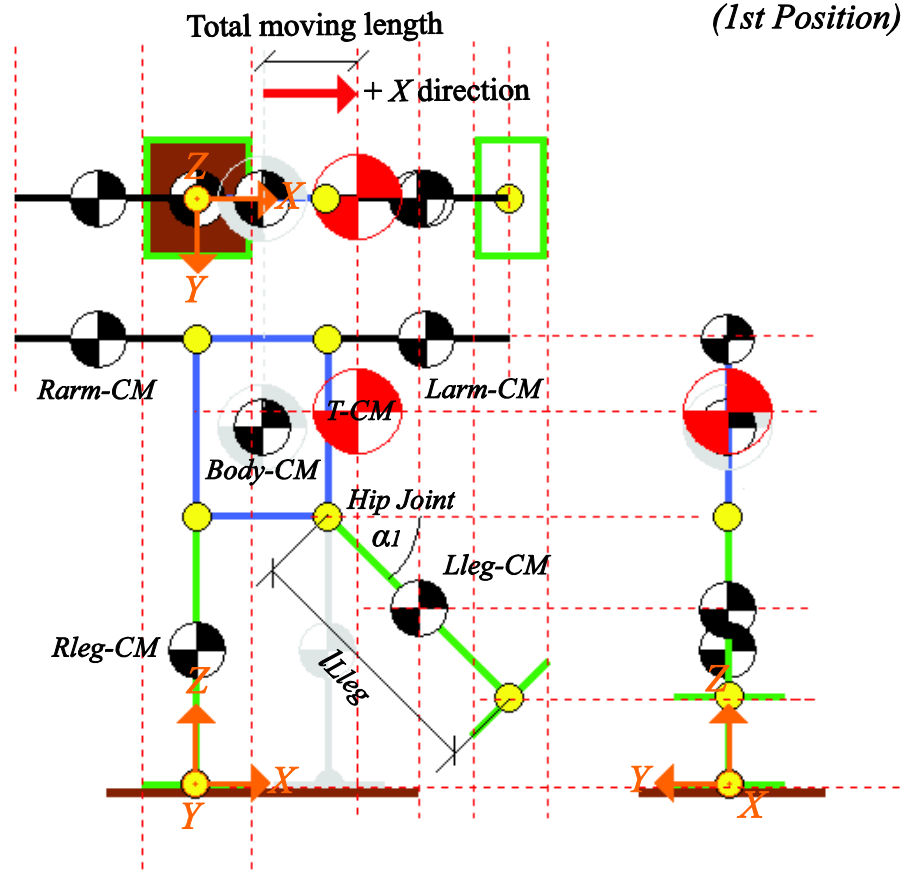
Figure 5-18. A change of *T-CM* point, when the left leg swing up leftward (1st position)

$$X_{T-CM} = M_{Lleg} * \left[\left(\frac{-l_{Rleg}}{2} \cos\alpha_2 \right) + (a\cos\alpha_5) + \left(\frac{l_{Lleg}}{2}\cos\alpha_1 \right) + \left(a + \frac{l_{Lleg}\cos\beta_1}{2}\cos\theta_1 \right) \right]$$

$$\frac{+ (M_{Rleg} * X_{Rleg}) + (M_{Larm} * X_{Larm}) + (M_{Rarm} * X_{Rarm}) + (M_{Body} * X_{Body})}{M_{Lleg} + M_{Rleg} + M_{Larm} + M_{Rarm} + M_{Body}} \qquad (5\text{-}17)$$

Figure 5-18 shows the first example of the robot motion in unbalance situation (1st position). In this case the projection of (*T-CM*) position will be out of the supporting area in +*X* direction due to the swinging motion of the left leg up leftward (−α_1 degree at left leg's hip joint). Thus, the robot will fall to +*X* direction. As the other joint angles are kept,

97

the constraint effect is caused only by this angle. According to the equation (5-17), especially on the term surrounded by the green dot line, the $X_{T\text{-}CM}$ position is increasing when the α_1 has decreasing. The maximum effect to *T-CM* position in $+X$ and $-X$ directions are when $\alpha_1 = 0$ and 180 degrees respectively. Hence, there is no effect of left leg to the *T-CM* position in X directions when $\alpha_1 = 90$ degree.

F-2) Recovering balance motion analysis

Figure 5-19. The robot motion to recover the balance position from the change of *T-CM* point, when the left leg swing up leftward (2nd position)

The first example motion on the Figure 5-18 shows the unbalance situation by swing the left leg up leftward which make the *T-CM* position moved out of the supporting area in $+X$ direction. In order to recover the system balance, the robot should move the whole body rightward ($-X$ direction) by turning the right leg's ankle joint rightward with $-\alpha_2$ degree and swing up the left arm ($+\alpha_3$ degree at left shoulder's joint)

98

until the projection of (*T-CM*)'s position is within the supporting area. Figure.5-19 shows the balance situation after recovered as 2nd position. According to this figure, the other joint angles are constant (no move), thus the constraint effect is caused by these two angles only. Although, the constraint effect depends on these angles, however it's also depending on the links which are attached to particular concerning joint angles as:

$$X_{T-CM} =$$

$$= M_{Lleg} * \left[\left(\frac{-l_{Rleg}}{2} \cos\alpha_2 \right) + (a\cos\alpha_5) + \left(\frac{l_{Lleg}}{2}\cos\alpha_1 \right) + \left(a + \frac{\sqrt{(l_{Lleg}\cos\alpha_1)^2 + (l_{Lleg}\cos\beta_1)^2}}{2}\cos\theta_1 \right) \right]$$

$$+ M_{Rleg} * \left[\left(\frac{-l_{Rleg}}{2}\cos\alpha_2 \right) + \left(\frac{-\sqrt{(l_{Rleg}\cos\alpha_2)^2 + (l_{Rleg}\cos\beta_2)^2}}{2}\cos\theta_2 \right) \right]$$

$$+ M_{Larm} * \left[\left(\frac{-l_{Rleg}}{2}\cos\alpha_2 \right) + \left(\sqrt{a^2+b^2}\cos(\alpha_b+\alpha_5) \right) + \left(\frac{l_{Larm}}{2}\cos\alpha_3 \right) + \left(a + \frac{l_{Larm}}{2}\sin\theta_3 \right) \right]$$

$$+ M_{Rarm} * \left[\left(\frac{-l_{Rleg}}{2}\cos\alpha_2 \right) - (b\cos(90-\alpha_5)) + \left(\frac{-l_{Rarm}}{2}\cos\alpha_4 \right) + \left(\frac{-l_{Rarm}}{2}\sin\theta_4 \right) \right]$$

$$+ M_{Body} * \left[\left(\frac{-l_{Rleg}}{2}\cos\alpha_2 \right) + l_{Body}\cos(\alpha_b+\alpha_5) \right]$$

$$\overline{\quad M_{Lleg} + M_{Rleg} + M_{Larm} + M_{Rarm} + M_{Body} \quad}$$

(5-18)

According to the equation (5-18), especially on the terms surrounded by the green dot line show the constraint effect which are caused by α_2 degree and the links which are attached to the left arm shoulder joint, the X_{T-CM} position decreases when α_2 is deceased. As the calculations of each link angle is relative to the right leg's ankle joint, a change in this joint angle will affect to every angle on each link. The maximum effect to *T-CM* position in $+X$ and $-X$ directions are when $\alpha_2 = 180$ and 0 degrees respectively. Hence, there is no effect of right leg to the *T-CM* position in X directions when $\alpha_1 = 90$ degree.

Another concerned equation term is the term which is surrounded by the black dot line, show the constraint effect which are cause by α_3 degree, the X_{T-CM} position decreases when increasing the α_3. In this case, there is no constraint effect from other links when swinging the left arm shoulder's joint. The maximum effect to *T-CM* position in $+X$ and $-X$ directions are when $\alpha_3 = 0$ and 180 degrees respectively. Hence, there is no effect of left arm to the *T-CM* position in X directions when $\alpha_3 = 90$ degree.

G) Balancing control in Y direction with CM analysis

The system should keep the COG or ZMP within the supporting area (X-Y plane), thus, the *total center of mass position in Z direction*, ($Z_{T\text{-}CM}$) is not of concern. Note that, this definition is only based on physical valid, and works on flat surfaces. The total center of mass position in X and Y directions can analysis from front view, top view and side view images. This section will give the example of unbalanced situation and the balance recovering technique of the system by keeping the projection of (T-CM)'s position within the supporting area in Y direction.

G-1) Unbalanced motion analysis
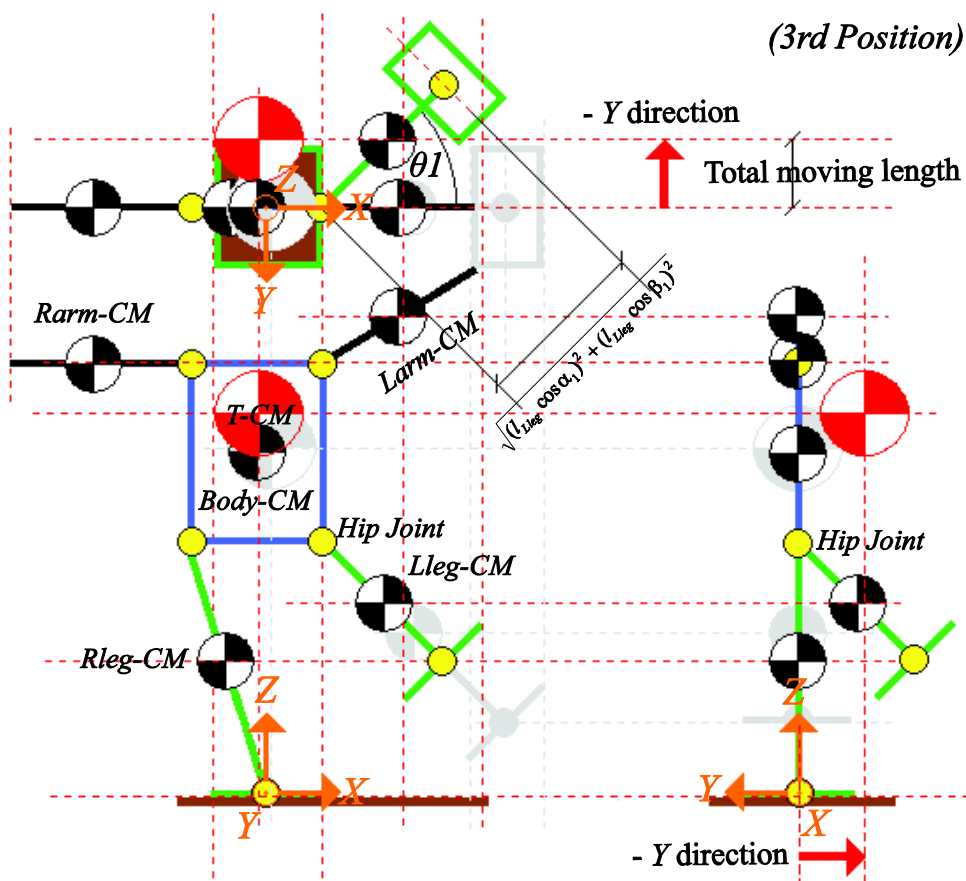
Figure 5-20. A change of T-CM point, when the left leg swing backward (3rd position)

Figure 5-20 shows the third example of robot motion at unbalanced situation (3rd position). This figure is the continue motion from Figure 5-19 in the previous section. In

this case the projection of (*T-CM*) position will be out of the supporting area in −*Y* direction, due to the swinging motion of the left leg's ankle hip backward (+θ₁ degree). Thus, the robot will fall down in −*Y* direction. As the other joint angles are kept, the constraint effect is caused only by turning the left leg's hip joint angle as:

$$Y_{T-CM} = M_{Lleg} * \left[(\frac{-l_{Rleg}}{2} \cos \beta_2) + (\frac{l_{Lleg}}{2} \cos \beta_1) + (\frac{\sqrt{(l_{Lleg} \cos \alpha_1)^2 + (l_{Lleg} \cos \beta_1)^2}}{2} \sin \theta_1) \right]$$

$$\frac{+ (M_{Rleg} * Y_{Rleg}) + (M_{Larm} * Y_{Larm}) + (M_{Rarm} * Y_{Rarm}) + (M_{Body} * Y_{Body})}{M_{Lleg} + M_{Rleg} + M_{Larm} + M_{Rarm} + M_{Body}} \quad (5\text{-}19)$$

According to the equation (5-19), especially on the term surrounded by the green dot line, the $Y_{T\text{-}CM}$ position decreases when the θ₁ is increased. The maximum effect to *T-CM* position in +*Y* and −*Y* directions are when θ₁ = 0 and 180 degrees respectively. Hence, there is no effect of left leg to the *T-CM* position in *Y* directions when θ₁ = 90 degree.

G-2) Recovering balance motion analysis

The third example motion on the Figure 5-20 shows the unbalance situation by swing the left leg's hip joint backward which makes the *T-CM* position moved out of the supporting area in −*Y* direction. In order to recover the balance of the system, the robot should move the whole body forward (+*Y* direction) by turning the right leg's ankle joint forward with −β₂ degree until the projection of (*T-CM*)'s position within the supporting area. Figure.5-21 shows the robot position after the robot recovered the balance as 4th position. According to this figure, the other joint angles are constant (no move), thus the constraint effect is cause by only the right leg ankle's joint angle. However, the constraint effect also depends on the links which are attached to particular concerning joint angles.

According to the equation (5-20), especially on the terms surrounded by the green dot line show the constraint effect which is cause by β₂ degree changes and the links which are attached to the ankle joint of right leg. The $Y_{T\text{-}CM}$ position increases when the β₂

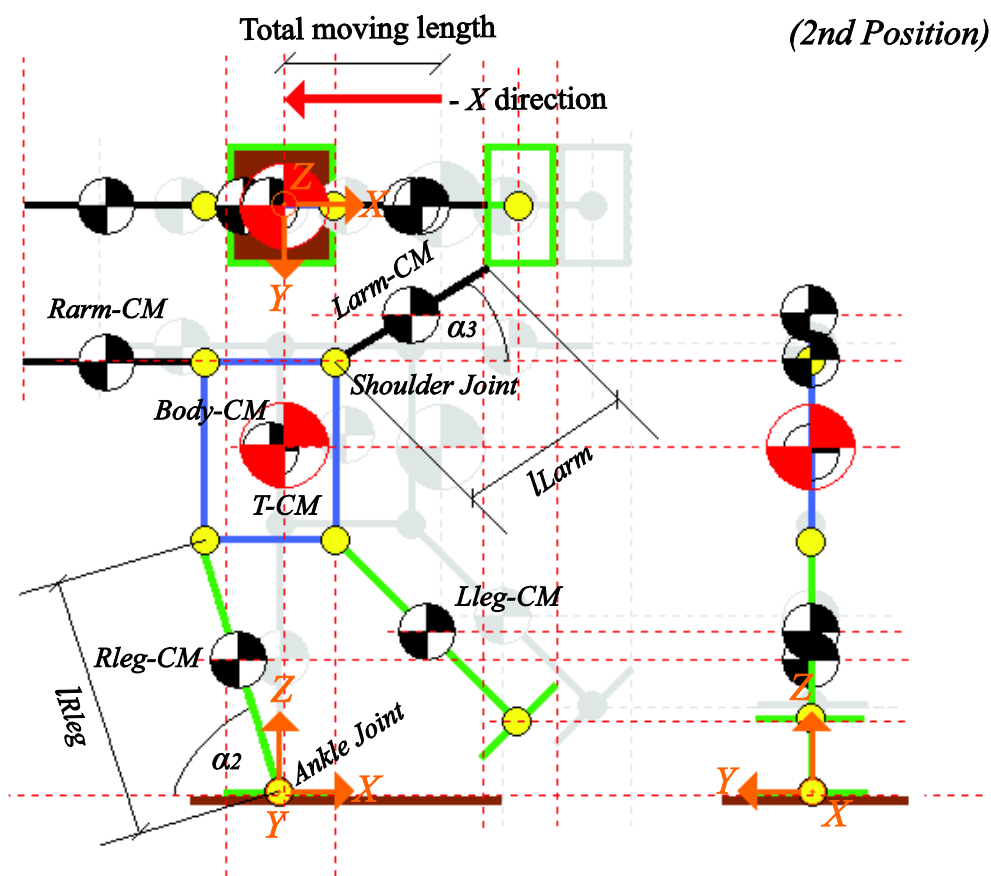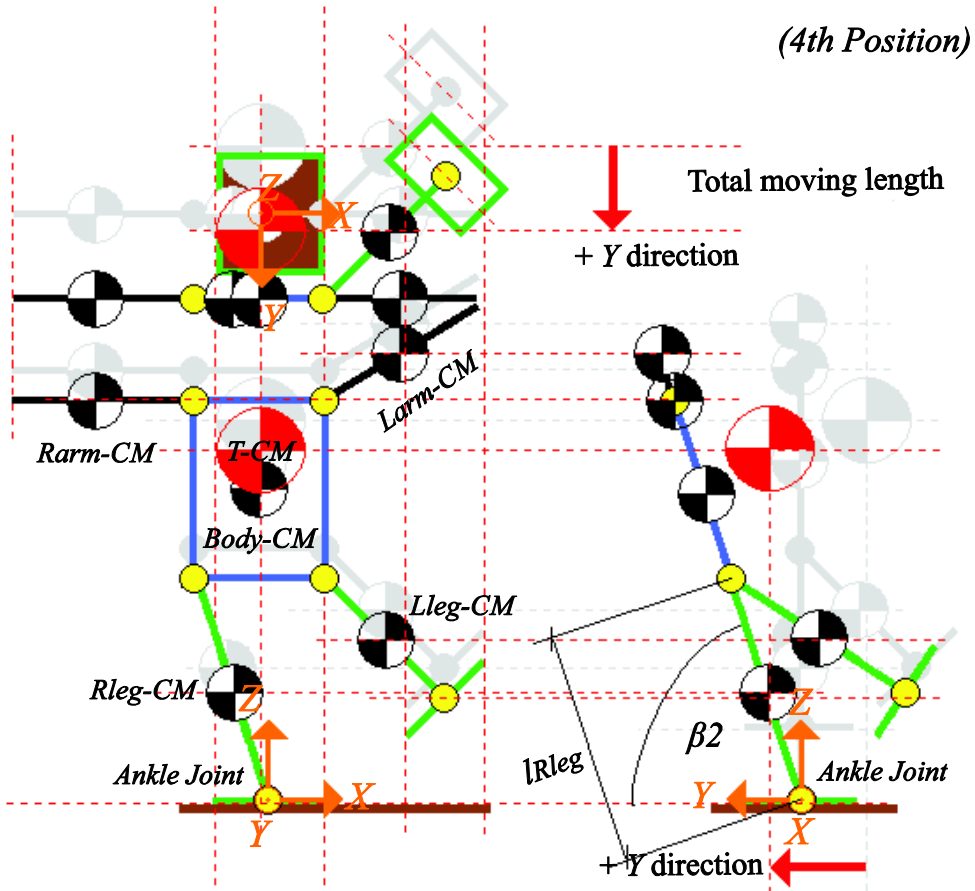**Figure 5-21.** The robot motion to recover the balance position from the change of *T-CM* point, when the left leg swing backward (4th position)

$$Y_{T-CM} =$$

$$= M_{Lleg} * \left[(\frac{-l_{Rleg}}{2}\cos\beta_2) + (\frac{l_{Lleg}}{2}\cos\beta_1) + (\frac{\sqrt{(l_{Lleg}\cos\alpha_1)^2 + (l_{Lleg}\cos\beta_1)^2}}{2}\sin\theta_1) \right]$$

$$+ M_{Rleg} * \left[(\frac{-l_{Rleg}}{2}\cos\beta_2) + \frac{-\sqrt{(l_{Rleg}\cos\alpha_2)^2 + (l_{Rleg}\cos\beta_2)^2}}{2}\sin\theta_2) \right]$$

$$+ M_{Larm} * \left[(\frac{-l_{Rleg}}{2}\cos\beta_2) + (b*\cos\beta_5) + (\frac{-\sqrt{(l_{Larm}\sin\alpha_3)^2 + (l_{Larm}\cos\theta_3)^2}}{2}\cos\beta_3) + (\frac{-l_{Larm}}{2}\cos\theta_3) \right]$$

$$+ M_{Rarm} * \left[(\frac{-l_{Rleg}}{2}\cos\beta_2) + (b*\cos\beta_5) + (\frac{\sqrt{(l_{Rarm}\sin\alpha_4)^2 + (l_{Rarm}\cos\theta_4)^2}}{2}\cos\beta_4) + (\frac{l_{Rarm}}{2}\cos\theta_4) \right]$$

$$+ M_{Body} * \left[(\frac{-l_{Rleg}}{2}\cos\beta_2) + \frac{b}{2}\cos\beta_5) \right]$$

$$\overline{M_{Lleg} + M_{Rleg} + M_{Larm} + M_{Rarm} + M_{Body}}$$

(5-20)

degree decreased. As the calculations of each link angle is relative to the right leg's ankle joint, a change in this joint angle will affect to every angle in each link. According to this equation, the maximum effect to *T-CM* position in $+Y$ and $-Y$ directions are when $\alpha_2 = 0$ and 180 degrees respectively. Hence, there is no effect of right leg to the *T-CM* position in *X* directions when $\alpha_1 = 90$ degree.

5.2.2. Balancing experiments

According to the previous section given an example robot motions which are affected to shift the COG position in and out of the supporting area. COG is the projection of the *center of mass* (CM) on ground plane used in statics. Thus CM should be kept within the supporting area for static balance control, while ZMP should be kept within the supporting area for dynamic balance control. The ZMP trajectory in a robot foot is a significant criterion for the stability of the walk. Thus, in many studies, ZMP coordinates have computed by using robot model and angle information of all joints read from the encoders. The complicate of the ZMP coordinates computation are depending on the structure of the robot. In order to make the more efficient controller, in this research I employed a more direct approach and simpler technique which is to use tactile feedback measured using the sensors mounted under robot's feet instead complicated calculation of robot model. Also it makes the control system free from the angle information on the all joints from the encoders in advanced. The tactile sensor units are equipped at the back of two robotic feet. Each foot has three sensing points.

The proposed technique is to control the robot motion to keep the three sensing values of supporting foot equal when the robot standing with one leg. This technique also can be further extended to the double supporting phases, when the robot stands with two legs. In this case, the four outer sensing values of left and right foots are considered to make equally. Hence, in both cases when the concern sensing values are the same, the *CM* point is also in the middle of the supporting area. In other words, this technique can be employed to control the robot to keep the *CM* constantly in the center of single and double support phases and that is correspondence to the method to keep the COG and ZMP within the supporting area for static and dynamic balance controls in advance. In

other word, this method is the automatic ZMP coordinates computation instead of using robot model and angle information of all joints read from encoders. In order to confirm the proposed technique can be employed instead of the conventional ZMP computation, I conducted some experiments to realize effective balancing actions as following section;

5.2.2.1. Two leg balancing task

A) Robot balancing actions (Weight on front side)

A-1) Uncontrolled case

Figure 5-22. Actual robot motion when the robot arm makes the front slope
(Humanoid robot: Without balancing control)

This experiment aims to show the failed example of two legs balance. In this case, humanoid robot is not controlled by proposed method. I first set the humanoid robot stand two legs on the flat plate at the end-effector of arm robot as shown in Figure 5-22(A). Then, ground inclines to front slope direction from 0 to 25 degrees to make the unbalanced situation. As a result, the humanoid robot fell down from the plate when the plate turned over than 10 degree as shown in Figure 5-22(B) and (C) respectively.

A-2) Controlled case

This experiment aims to show the successful balancing example. In this case, humanoid robot was controlled by utilizing the proposed method.

The experimental procedure is the same as the previous experiment as shown in Figure 5-23(A). The arm robot inclines flat plate to the front direction from 0 to 25 degrees to make the front slope for making the robot unbalanced. At this state, the robot
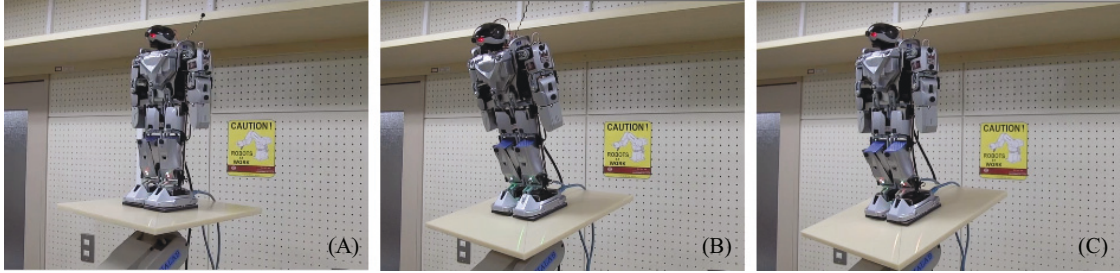
Figure 5-23. Actual robot motion when the robot arm makes the front slope
(Humanoid robot: With balancing control)

began turning its body backward by utilizing the analyses of the distributed pressure patterns as shown in Figure 5-23(B). In this case, the outputs of sensor elements are constrained as,

$$SRL_1 > SRL_3 > SRL_2 \qquad (5\text{-}21)$$

where the SRL_i represents the sensor output from the ith sensor on the right and left foots. Based on the sensor values, the robot needs to move its weight into the back side until the forces on both legs satisfy the sensing relation,

$$(SRL_1 = SRL_2) < SRL_3 \qquad (5\text{-}22)$$

Finally, the robot turned to the balance position as shown in Figure 5-23(C). In these figures, the robot could keep its body balanced by using the proposed method. Figure 5-24 shows the average tactile sensing data of two robotic foots on the moving ground in case of turning the ground slope to the front side. The sensing data is the RC time constant value in the RC circuit of each sensing element. When the sensor is no-load, its value high (I set maximum detecting values as 5,000µs). The RC time constant value decreases when applied force on sensing area of sensing element.

As can be seen from this graph, the point at 0 degree in this figure shows that the robot stands with keeping the balance by bending its foots to make the forces on sensor
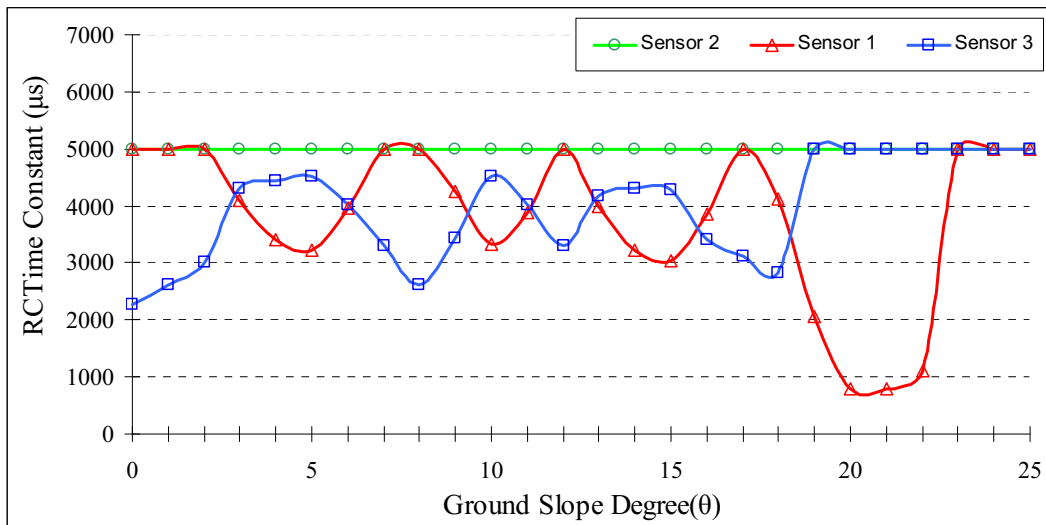
Figure 5-24. Sensing data of robotic foot on the moving slope to the front

number 3 of both legs bigger as I described before. After that, the arm robot inclines the flat plate to the front direction. At this state, RC time constant value of sensor 1 of both legs decreases. Humanoid robot turned its body against the slope from 3 to 6 degree. The robot balanced again around 6 degree. However, the ground slope is still moving to make the humanoid robot unbalanced. Humanoid robot repeat turned its body against the slope from 9 to 11 degree and from 13 to 16 degree again. Finally, humanoid fell down from the plate when the plate reached to 22 degree because to there is no friction between robotic foots and ground anymore.

B) Robot balancing actions (Weight on back side)

B-1) Uncontrolled case

This experiment aims to show the failed two legs balancing example. In this case, humanoid robot is not controlled by the proposed method. I first set the humanoid robot stand on the flat plate at the end-effector of arm robot as shown in Figure 5-25(A). Then, the ground slope inclines to the back slope direction from 0 to −25 degrees to make the unbalanced environment. As a result the humanoid robot fell down from the plate when the plate turned over than −10 degrees as Figure 5-25(B) and (C) respectively.
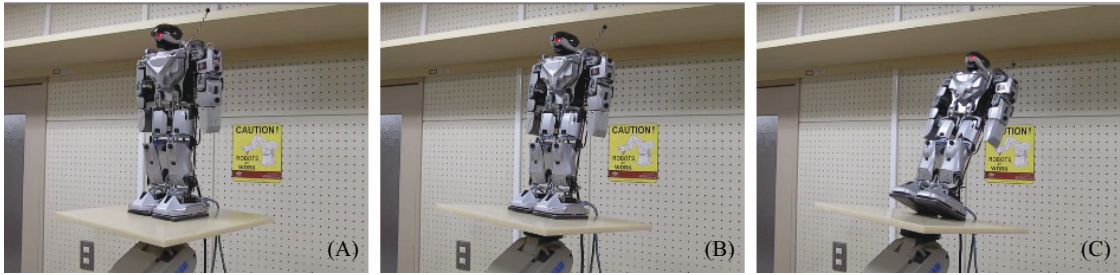
Figure 5-25. Actual robot motion when the robot arm makes the back slope
(Humanoid robot: Without balancing control)

B-2) Controlled case

Figure 5-26. Actual robot motion when the robot arm makes the back slope
(Humanoid robot: With balancing control)

This experiment aims to show the successful balancing example. In this case, humanoid robot was controlled by using the proposed method. The experimental procedure is the same as the previous experiment as shown in Figure 5-26(A). The arm robot inclines the flat plate to the back direction from 0 to −25 degrees to make the robot unbalanced. At this state, the robot began turning its body forward by utilizing the analyses of the distributed pressure patterns as shown in Figure 5-26(B). In this case, outputs of sensor elements are constrained as,

$$SRL_2 > SRL_3 > SRL_1 \tag{5-23}$$

Based on the sensor values, the robot needs to move its weight to the front side until the relation among the forces on both legs is satisfied with Eq(8). Finally, based on the balance control, the robot turned to the balance position as shown in Fig.5-26(C).
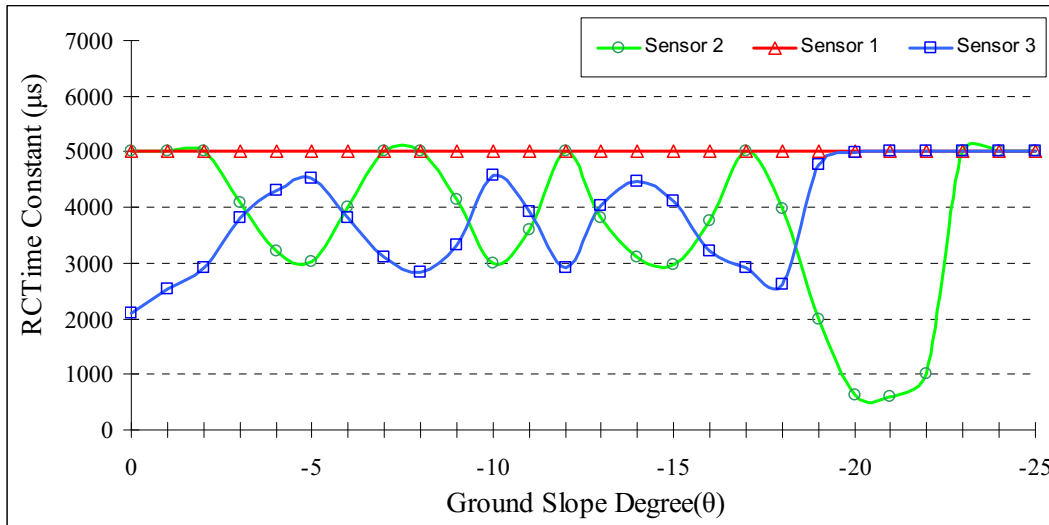
Figure 5-27. Sensing data of robotic foot on the moving slope to the back

Figure 5-27 shows the average tactile sensing data of two robotic feet on the moving ground slope when turning the ground slope to the back side. As can be seen from this graph, the point at 0 degree in this figure shows that the robot stands while keeping the balance by bending its foots to make the receiving forces on sensor number 3 of both legs bigger as I described before. After the arm robot inclines the flat plate to the back direction. At this state, RC time constant value of sensor 2 of both legs decreases. Humanoid robot turned its body against the slope from 3 to 6 degree. The robot balanced again around 6 degree. However, the ground slope is still moving to make the humanoid robot unbalanced. Humanoid robot repeats turning its body against the slope from 9 to 11 degree and from 13 to 16 degree again. Finally, humanoid robot fell down from the plate when the plate reached to -22 degree because there is no friction between robotic feet and ground anymore.

5.2.2.2 One leg balancing task

A) Robot balancing actions (Weight on front side)

A-1) Uncontrolled case

This experiment aims to show the failed example of the robot when the robot turns its body to the front side without the proposed method. In this procedure, first I set

108

(A)　　　　　　　　　　(B)　　　　　　　　　　(C)

Figure 5-28. Actual robot motion when the robot turns front (Without balance control)

(A)　　　　　　　　　　(B)　　　　　　　　　　(C)

Figure 5-29. Actual robot motion when the robot turns front (With balance control)

(A)　　　　　　　　　　(B)　　　　　　　　　　(C)

Figure 5-30. Actual robot keeps the balance when human pushing backside

the robot balance with only the left leg. Then the robot turns its body into the front side by 1 degree/s until 20 degrees to make the robot unbalanced. As a result, after the robot turn to the front without balance control, the robot fell down to the front direction as shown in Figures 5-28(A), (B) and (C) respectively.

Figure 5-31. Sensor data of robot foot when the robot has one leg balance control {Robot turns front itself (5-20s) and Push back-side by human (25s)}

A-2) Controlled case

The experiment aims to show two successful example of the balance control of the robot. One is the same unbalanced situation as the failure case. In this case, the robot turned its body to the front side by itself the same as the previous experiment, the robot could keep its balance. The other is the unbalanced situation caused by the human. In this experiment, human pushed the robot from the back side to realize human-machine interaction. The robot also could balance its body despite the disturbance from the human. Figure 5-29 shows the actual movement of robot when robot turns to the front side by itself based on the sensor values. Figure 5-30 shows the actual movement when the human pushes the robot from the back side. Figure 5-31 shows the sensing data of this experiment. In this procedure, I first set the robot to stand with only left leg as shown in Figure 5-29(A) and at the beginning (0 second) in Figure 5-31. Then the robot starts to turn its body to the front side the same as previous experiment to make the robot unbalanced as shown in Figure 5-29(B) and 5s in Figure 5-31 From 5s to 7s, the robot moved to the front until it reached 3 degrees. After that, the robot reacted to keep its balance based on the sensor values. Hence, the minimum angle that can be detected is 3 degrees for this case. From 8s in Figure 5-31, the robot began turning its body against the internal movement by utilizing the analyses of the distributed pressure patterns. In this case, the outputs of the sensor elements are constrained as follows;

$$SL_1 > SL_3 \geq SL_2 \qquad (5\text{-}24)$$

where the SL_i represents the sensor output from the ith sensor on the left foot. Based on the sensor values, to make its foot normal to the ground surface, the robot needs to move its body back until the robot turned to the balance position again at 10 seconds in Figure 5-31. However, the robot is still moving to reach at 20 degrees. Thus the humanoid robot repeatedly turned its body to be balance again at 13, 17 and 20 seconds in Figure 5-31.

Finally, the robot turned to the balance position again where the receiving forces on sensor 1 and 2 are equal as shown in Figure 5-29(C). The robot keeps the balance from this point. The next experiment aims to show that the proposed system enables us to realize human-machine interaction in case that human pushes the robot from the back side. A human then applied the pushing force from the back side of robot body by using his finger as shown in Figure 5-30(A) and at 25s in Fig. 5-31. Pushing force from human makes the robot unbalanced. At this state, the robot body began turning by utilizing the analyses of the distributed pressure patterns as described in Equation (5-24). Based on the sensor values, to make the force on sensor 1 and 2 equal, the robot move back against human as shown in Figure 5-30(B) and at 26s in Figure 5-31. Then human leaves their figure out of the robot and the robot still maintains the balance position without falling down as shown in Figure 5-30(C) and at 27s in Figure 5-31. As result, the robot could keep its body based on the balance control in spite of internal and external disturbances.

B) Robot balancing actions (Weight on back side)

B-1) Uncontrolled case

This experiment aims to show the failed example of the robot when the robot turn its body to the back side without using the proposed method. In this procedure, first I set the robot to balance with only the left leg. Then the robot turns its body into the back side by 1 degree/s until 20 degrees to make the robot unbalanced. As a result, after the robot turns to the back without the balance control, the robot fell down to the back direction as shown in Figures 5-32(A), (B) and (C) respectively.

(A)   (B)   (C)

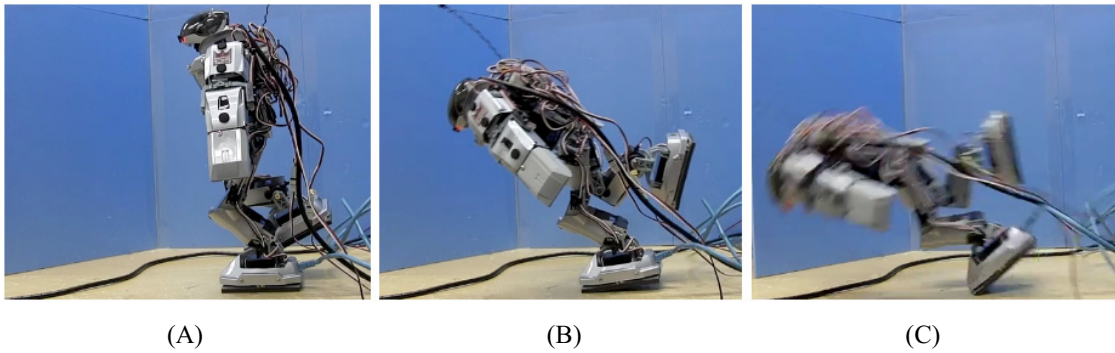**Figure 5-32.** Actual robot motion when the robot turns back (Without balance control)

(A)   (B)   (C)

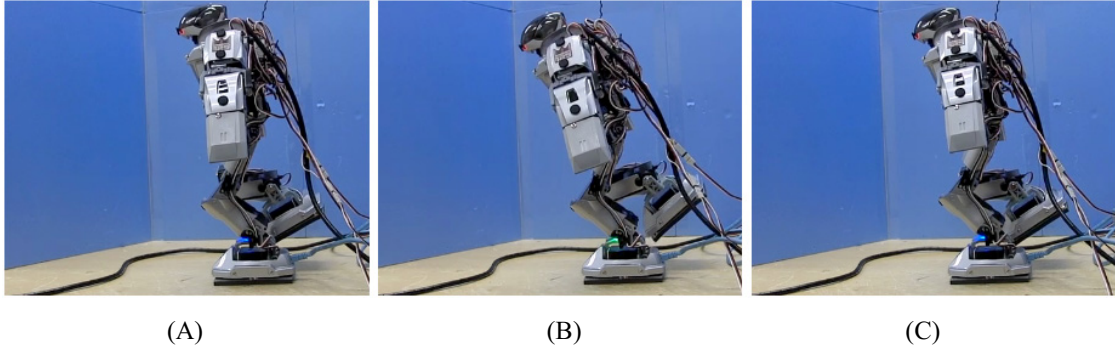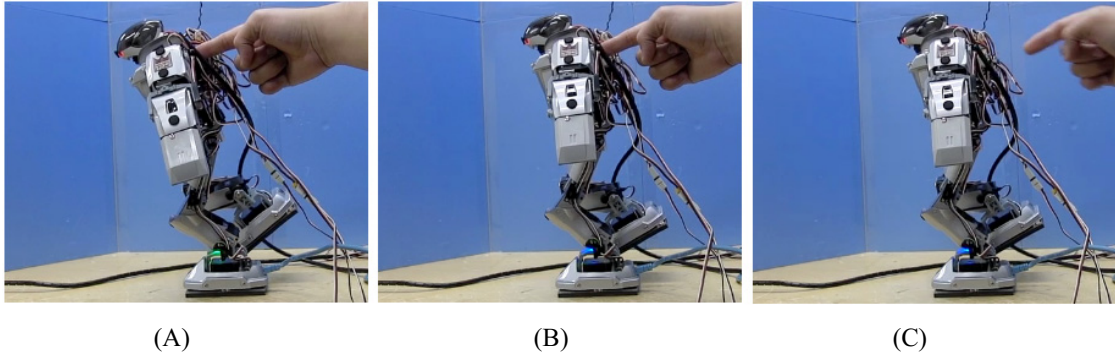**Figure 5-33.** Actual robot motion when the robot turns back (With balance control)

(A)   (B)   (C)

Figure 5-34. Actual robot keeps the balance when human pushing front side

B-2) Controlled case

The experiment aims to show two successful examples of the balance control of the robot. One is the same unbalanced situation as the failure case. In this case, although the robot turned its body to the back side by itself the same as the previous experiment, the robot could keep its balance. The other is the unbalanced situation caused by the
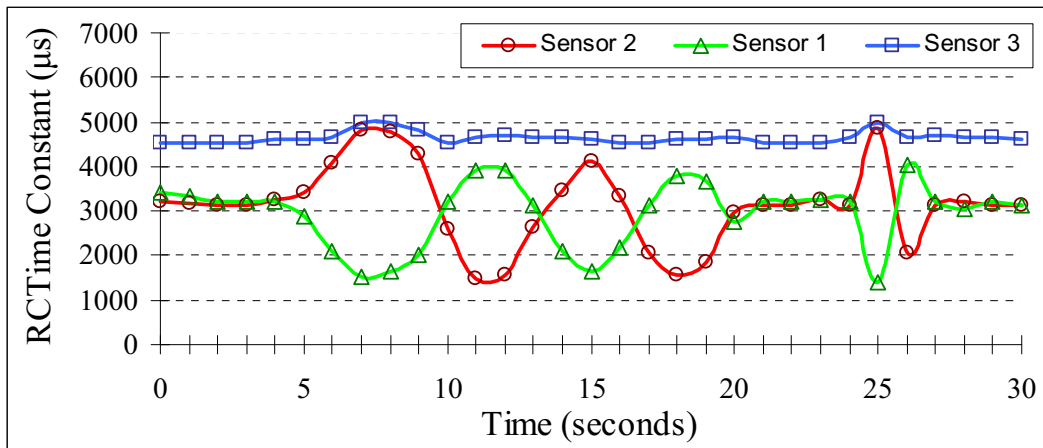
Figure 5-35. Sensor data of robot foot when the robot has one leg balance control {Robot turns back itself (5-20s) and Push front-side by human (25s)}

human. In this experiment, human pushed the robot from the front side to realize human-machine interaction. The robot also could balance its body despite the disturbance from the human. Figure 5-33 shows the actual movement when the robot turns to the back side by itself. Figure 5-34 shows actual movement when the robot interacts with human when human pushes the robot from the front side. Figure 5-35 shows the sensing data of this experiment. In this procedure, I first set the robot to stand with only left leg as shown in Figure 5-33(A) and at the beginning (0 second) in Figure 5-35. Then the robot starts to turns its body into the back side like the previous experiment to make the robot unbalanced as shown in Figure 5-33(B) and 5s in Figure 5-35. From 5s to 7s, the robot moved to the back until it reached 3 degrees. After that, the robot reacted to keep its balance based on the sensor values. Hence, the minimum angle that can be detected is 3 degrees for this case. From 8s in Figure 5-35, the robot began turning its body against the internal movement by utilizing the analyses of the distributed pressure patterns. In this case, the outputs of the sensor elements are constrained as follows;

$$SL_2 > SL_3 \geq SL_1 \qquad\qquad (5\text{-}25)$$

Based on the sensor values, to make the foot normal to the ground surface, the robot needs to move its body front until the robot turned to the balance position again at 10 seconds in Figure 5-35. However, the robot is still moving to reach 20 degrees. Thus

the humanoid robot repeated turns its body to keep balance as shown at 13, 17 and 20 seconds in Figure 5-35. Finally, the robot turned to the balance position again where the receiving forces on sensor 1 and 2 are equal as shown in Figure 5-33(C). The robot keeps the balance from this point. The next experiment aims to show that the proposed system enables us to realize human-machine interaction in case that human pushes the robot from the front side. A human then applied the pushing force from the front of robot body by using his finger as shown in Figure 5-34(A) and at 25s in Figure 5-35. The force from the human makes the robot unbalanced. At this state, the robot body began turning by utilizing the analyses of the distributed pressure patterns as described in equation (5-25). Based on the sensor values, to make the force on sensor 1 and 2 equal, the robot move to the front against human as shown in Figure 5-34(B) and at 26s in Figure 5-35. Then human leaves their figure out of the robot and the robot still maintains the balance position without falling down as shown in Figure 5-34(C) and at 27s in Figure 5-35. As the results, the robot also could keep its body based on the balance control in spite of the disturbance from the internal and external forces.

C) Robot balancing actions (Weight on right side)

C-1) Uncontrolled case

This experiment aims to show the failed example of the robot when the robot turn its body to the right side without proposed method. In this procedure, first I set the robot to balance with only the left leg. Then the robot turns its body into the right side by 1 degree/s until 20 degrees to make the robot unbalanced. As a result, after the robot turns to the right without balance control, the robot fell down to this direction as shown in Figure 5-36 (A), (B) and (C) respectively.
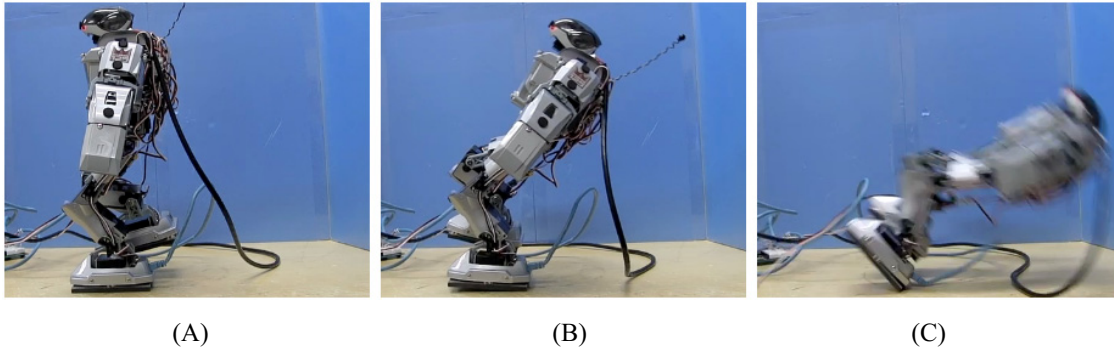
C-2) Controlled case

The experiment aims to show two successful example of the balance control of the robot. One is the same unbalanced situation as the failure case. In this case, although the robot turned its body to the right side by itself the same as the previous experiment, the robot could keep its balance. The other is the unbalanced situation caused by the human. In this experiment, human pushed the robot from the left side to realize human-

Figure 5-36. Actual robot motion when the robot turns left (Without balance control)
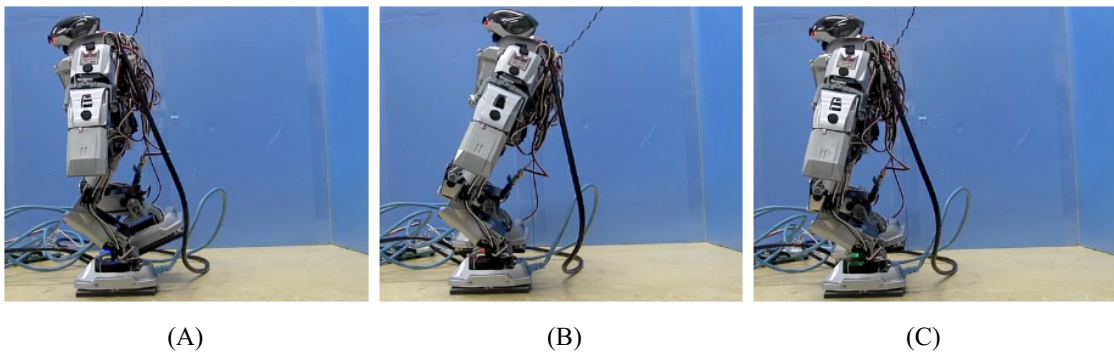

Figure 5-37. Actual robot motion when the robot turns left (With balance control)
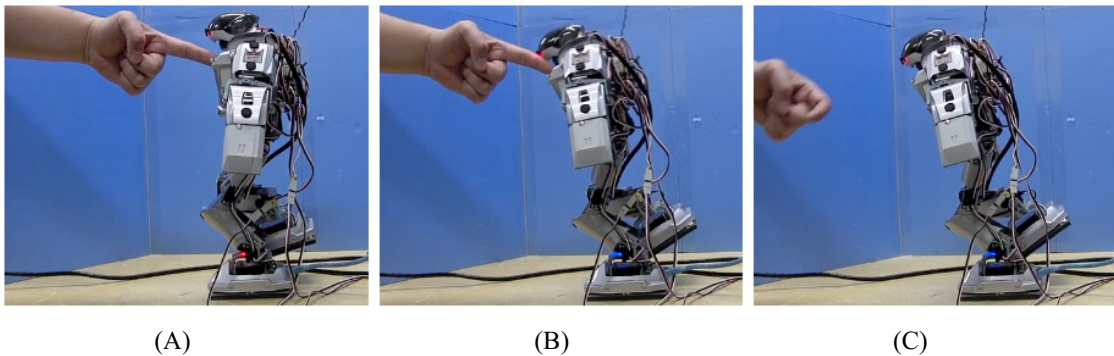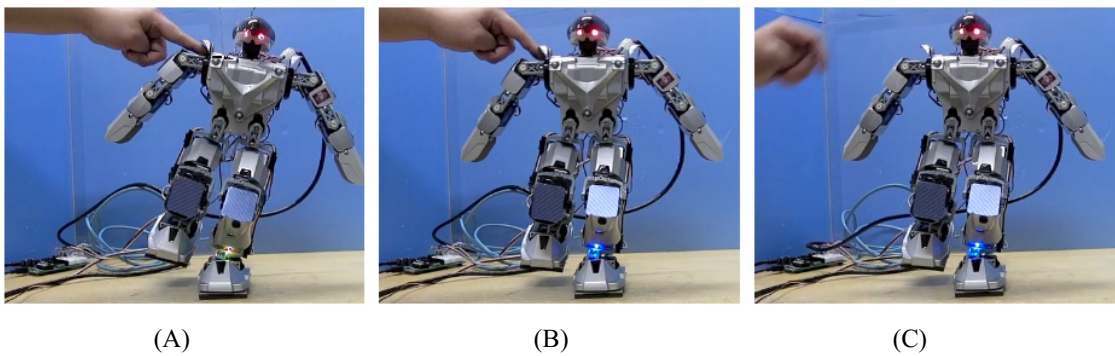

Figure 5-38. Actual robot keeps the balance when human pushing right side

machine interaction. The robot also could balance its body despite the disturbance from the human. Figure 5-37 shows the actual movement when the robot turns to the right side by itself. Figure 5-38 shows actual movement when the robot interacts with human when human pushes the robot from the left side. Figure 5-39 shows the sensing data of this experiment. In this procedure, I first set the robot to stand with only left leg as shown in Figure 5-37(A) and at the beginning (0 second) in Figure 5-39. Then the robot starts to
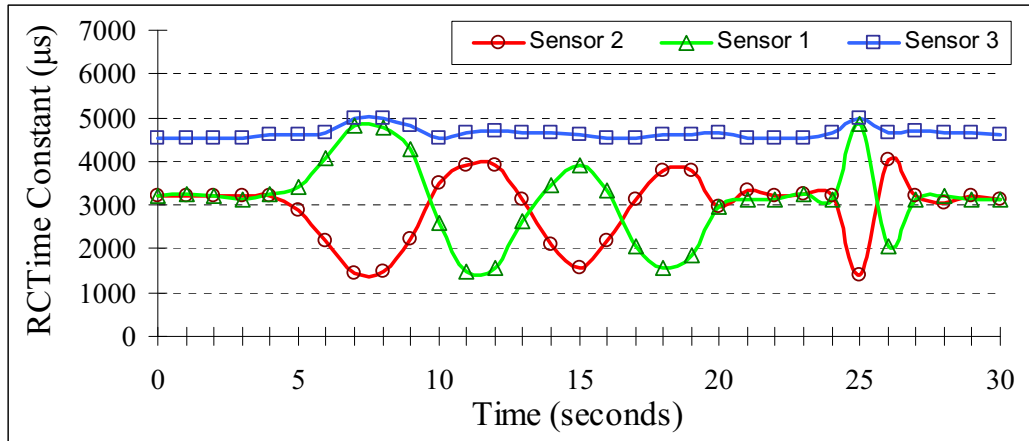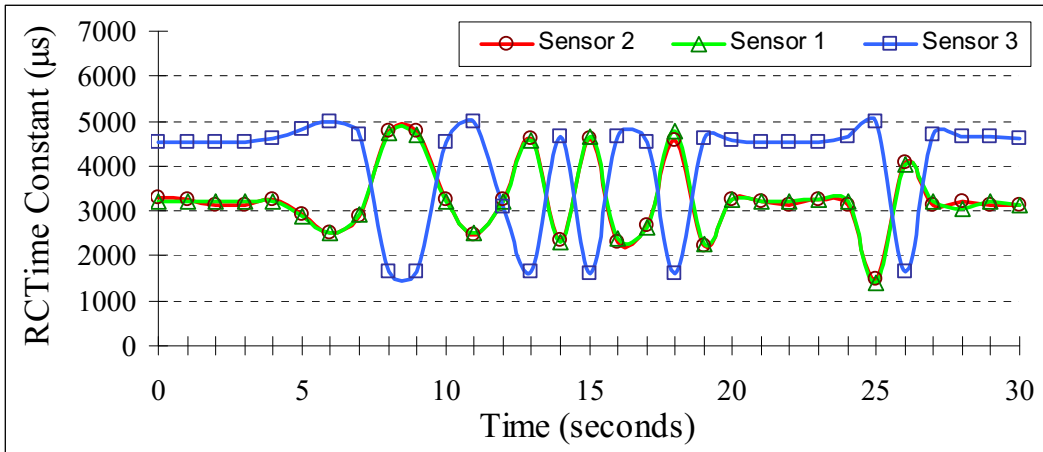
Figure 5-39. Sensor data of robot foot when the robot has one leg balance control {Robot turns left itself (5-20s) and Push right-side by human (25s)}

turn its body into the right side same as previous experiment to make the robot unbalanced as shown in Figure 5-37(B) and 5s in Figure 5-39. From 5s to 6s, the robot moved to the right until it reached 2 degrees. After that, the robot reacted to keep its balance based on the sensor values.

Hence, the minimum angle that can be detected is 2 degrees for this case. From 6s in Figure 5-39, the robot began turning its body against the internal movement based on the analyses of the distributed pressure patterns. In this case, the outputs of the sensor elements are constrained as follows;

$$(SL_1 \approx SL_2) > SL_3 \tag{5-26}$$

Based on the sensor values, to make the foot normal to the ground surface, the robot needs to move its body left until the robot turned to the balance position again at 8s in Figure 5-39. However, the robot is still moving to reach 20 degrees. Thus the humanoid robot repeatedly turns its body to keep its balance as shown at 10, 12, 14, 15, 16, 18, 19 and 20 seconds in Figure 5-39. Finally, the robot turned to the balance position again as shown in Figure 5-37(C). The robot keeps the balance from this point. The next experiment aims to show that the proposed system enables us to realize human-machine interaction in case that human pushes the robot from the left side. A human then applied

116

the pushing force from the left of robot body by using his finger as shown in Figure 5-38(A) and at 25s in Figure 5-39. The force from the human makes the robot unbalanced. At this state, the robot body began turning by utilizing the analyses of the distributed pressure patterns as described in equation (5-26). Based on the sensor values, to make the robot balance, the robot move left against human as shown in Figure 5-38(B) and at 26s in Figure 5-39. Then human leaves their figure out of the robot and the robot still maintains the balance position without falling down as shown in Figure 5-38(C) and at 27s in Figure 5-39. As results, the robot could also keep its body based on the balance control in spite of the disturbance from the internal and external forces.

D) Robot balancing actions (Weight on left side)

D-1) Uncontrolled case

This experiment aims to show the failed example of the robot when the robot turns its body to the left side without the proposed method. In this procedure, I first set the robot to balance with only the left leg. Then the robot turns its body into the left side by 1 degree/s until 20 degrees to make the robot unbalanced. As a result, after the robot turn to the left without balance control, the robot fell down to this direction as shown in Figures 5-40(A), (B) and (C) respectively.

D-2) Controlled case

The experiment aims to show two successful example of the balance control of the robot. One is the same unbalanced situation as the failure case. In this case, although the robot turned its body to the left side by itself the same as the previous experiment; the robot could keep its balance. The other is the unbalanced situation caused by the human. In this experiment, human pushed the r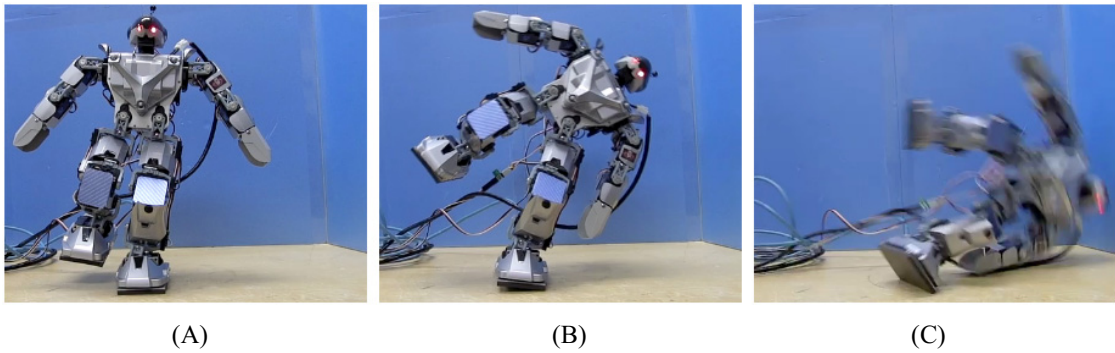obot from the right side to realize human-machine interaction. The robot also could balance its body despite the disturbance from the human. Figure 5-41 shows the actual movement when the robot turns to the right side by itself. Figure 5-42 shows actual movement when the robot interacts with human when human pushes the robot from the left side. Figure 5-43 shows the sensing data of this experiment. In this procedure, I first set the robot to stand with only left leg as shown in Figure 5-41(A) and beginning (0 second) in Figure 5-43. Then the robot starts to turn its

(A)   (B)   (C)
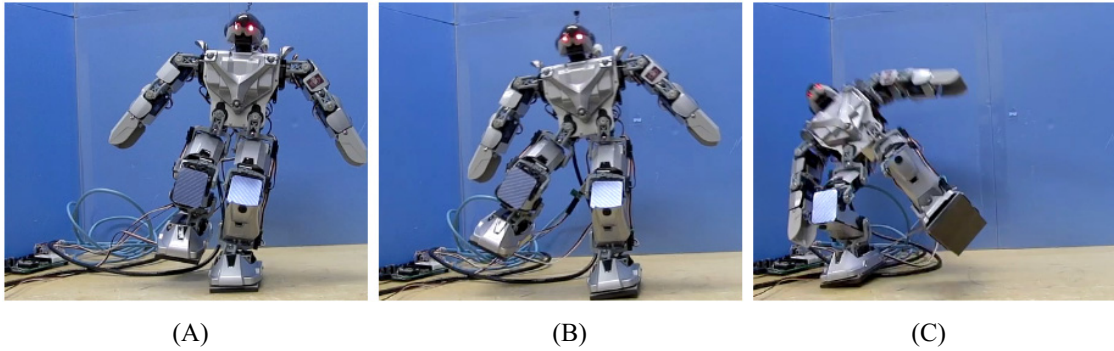
Figure 5-40. Actual robot motion when the robot turns right (Without balance control)

(A)   (B)   (C)
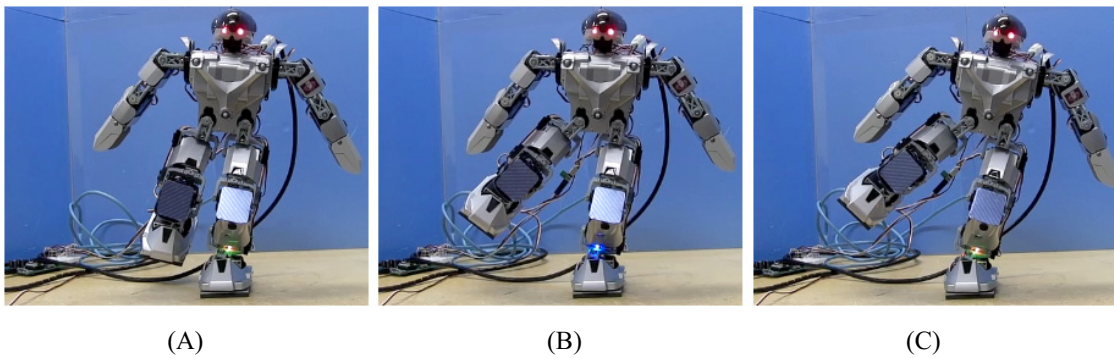
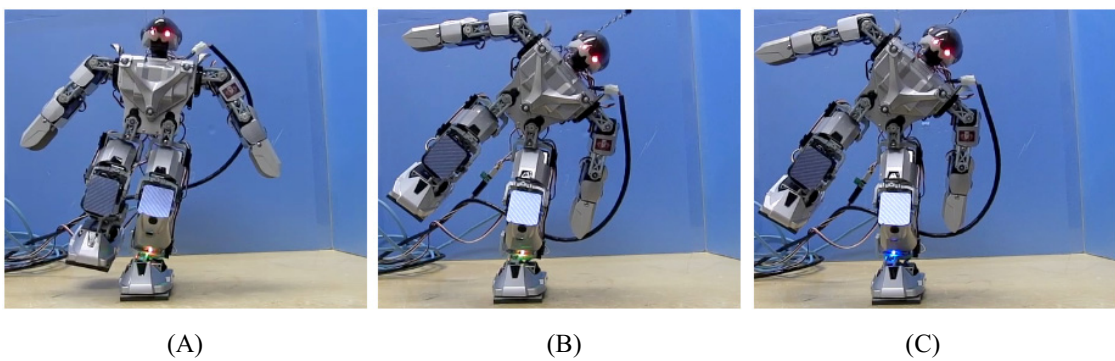**Figure 5-41.** Actual robot motion when the robot turns right (With balance control)


(A)   (B)   (C)
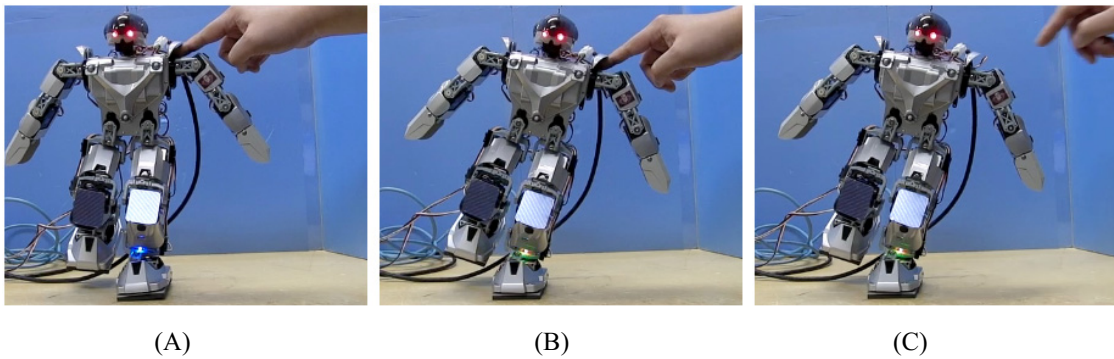
Figure 5-42. Actual robot keeps the balance when human pushing left side

body into the left side like the previous experiment to make the robot unbalanced as shown in Figure 5-41(B) and 5s in Figure 5-43. From 5s to 6s, the robot moved to the front until it reached 2 degrees. After that, the robot reacted to keep its balance based on the sensor values. Hence, the minimum angle that can be detected is 2 degrees for this case. From 6s in Figure 5-43, the robot began turning its body against the internal
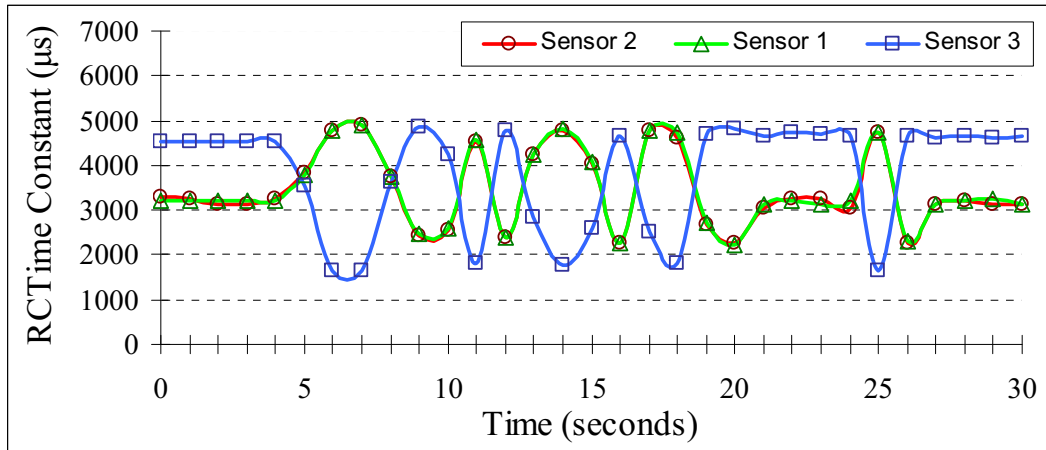
Figure 5-43. Sensor data of robot foot when the robot has one leg balance control
{Robot turns right itself (5-20s) and Push left-side by human (25s)}

movement by utilizing the analyses of the distributed pressure patterns. In this case, the outputs of the sensor elements are constrained as follows;

$$(SL_1 \approx SL_2) < SL_3 \tag{5-27}$$

Based on the sensor values, to make the foot normal to the ground surface, the robot needs to move its body right until the robot turned to the balance position again at 8s in Figure 5-43. However, the robot is still moving to reach 20 degrees. Thus the humanoid robot repeatedly turns its body to keep its balance as shown at 8, 10, 11, 13, 15, 16, 19 and 21 seconds in Figure 5-43. Finally, the robot turned to the balance position again as shown in Figure 5-41(C). The robot keeps the balance from this point. The next experiment aims to show that the proposed system enables us to realize human-machine interaction in case that human pushes the robot from the right side. A human then applied the pushing force from the right of robot body by using his finger as shown in Figure 5-42(A) and at 25s in Figure 5-43. The force from the human makes the robot unbalanced. At this state, the robot body began turning by utilizing the analyses of the distributed pressure patterns as described in equation (5-27). Based on the sensor values, to make the robot balance, the robot move left against human as shown in Figure 5-42(B) and at 26s in Figure 5-43. Then human leaves their figure out of the robot and the robot still maintains the balance position without falling down as shown in Figure 5-42(C) and at

27s in Figure 5-43. As the results, the robot also could keep its body based on the balance control in spite of the disturbance from the internal and external forces.

5.2.2.3. Continuous motion balancing task

A) Robot balancing actions (Swing the left leg)
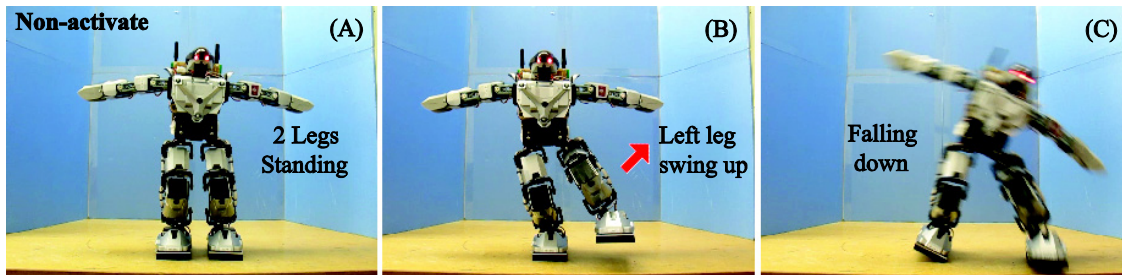
Figure 5-44. Actual robot motion when the robot swings its leg
(Without balance control)
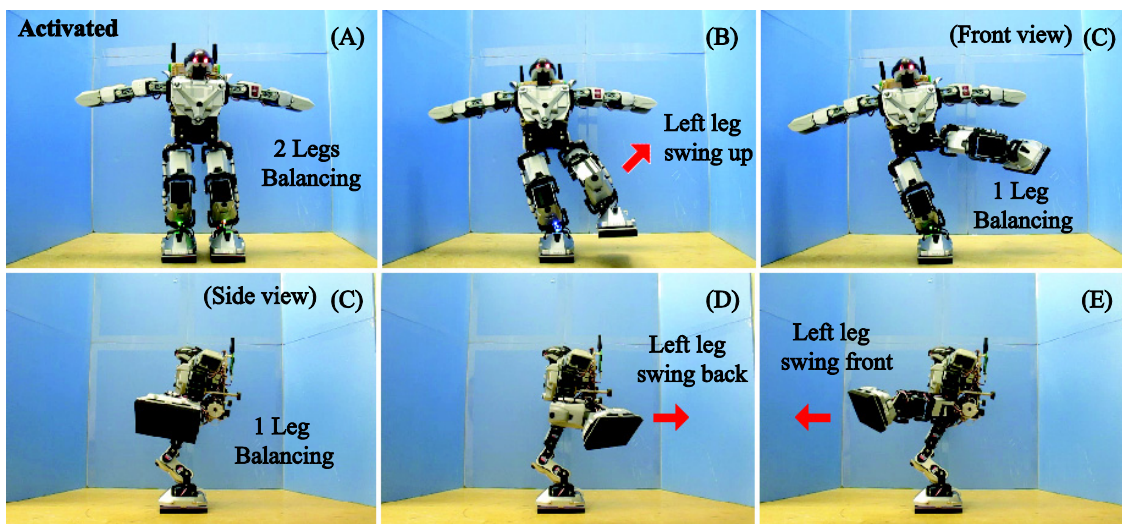
Figure 5-45. Actual robot motion when the robot swings its leg (With balance control)

A-1) Uncontrolled case

This experiment aims to show the failed example, when the robot moves and fall without using the proposed method. In this experiment, firstly I set the robot to stand with two legs. Secondly, the robot moves up the left leg for standing one leg. Thirdly, the robot swings up the left leg by increasing 1 degree step until reached 90 degree to make the robot unbalanced on left side body. As a result, the robot fell down to this direction until it reached 20 degrees as shown in Figures. 5-44(A), (B) and (C) respectively.

120

A-2) Controlled case

The experiment aims to show the successful example when the robot move its weight unbalance by using of proposed method. In this experiment procedure, first three steps are the same situation as the failure case. As a result, the robot can swings up the left leg over than 20 degrees without falling down. Then the robot continues to swing up the left leg until reached 90 degrees. The robot is able to keep its balance as shown in Figures 5-45(A), (B) and (C) respectively. Then, the robot swings back and front the left leg by 1 degree step until reached ±90 degree to make the robot unbalanced on the back and front side body. As a result the robot can keep its balance during these all movements as shown in Figures 5-45(C), (D) and (E) respectively.

5.3. Walking Applications

I conducted some experiments to confirm the ability of the proposed tactile sensing system for humanoid robot. I attempted to realize effective walking tasks of the humanoid robot on the various slopes, such as flat ground floor, upward slope and downward slope. In these applications, the robots no need any information about the contacted ground slope or orientation in advance.

5.3.1. Walking on the flat ground task

In this experiment, I aim to show the successful walking example on the flat ground. In this case, humanoid robot is controlled by the proposed method (Sensing function is activated). The experimenting procedure is start with, set the humanoid robot stand on the flat ground floor 0° as shown in Figure 5-46(A). Then, the robot begins the walking task by bending the knee, and then moves the left leg forward as shown in Figure 5-46(B), (C) and (D) respectively. As robot has activated the balance control function, the robot can maintain it balance during step forward motion of the left leg as shown in Figure 5-46(E). The robot continue the walking task by moves the right leg forward as shown in Figure 5-46(F), (G) and (H) respectively. The robot can maintain it balance during step forward motion of the right leg as well. As the result, the robot can maintain it balance during the walking forward by utilizing the proposed balancing controls.
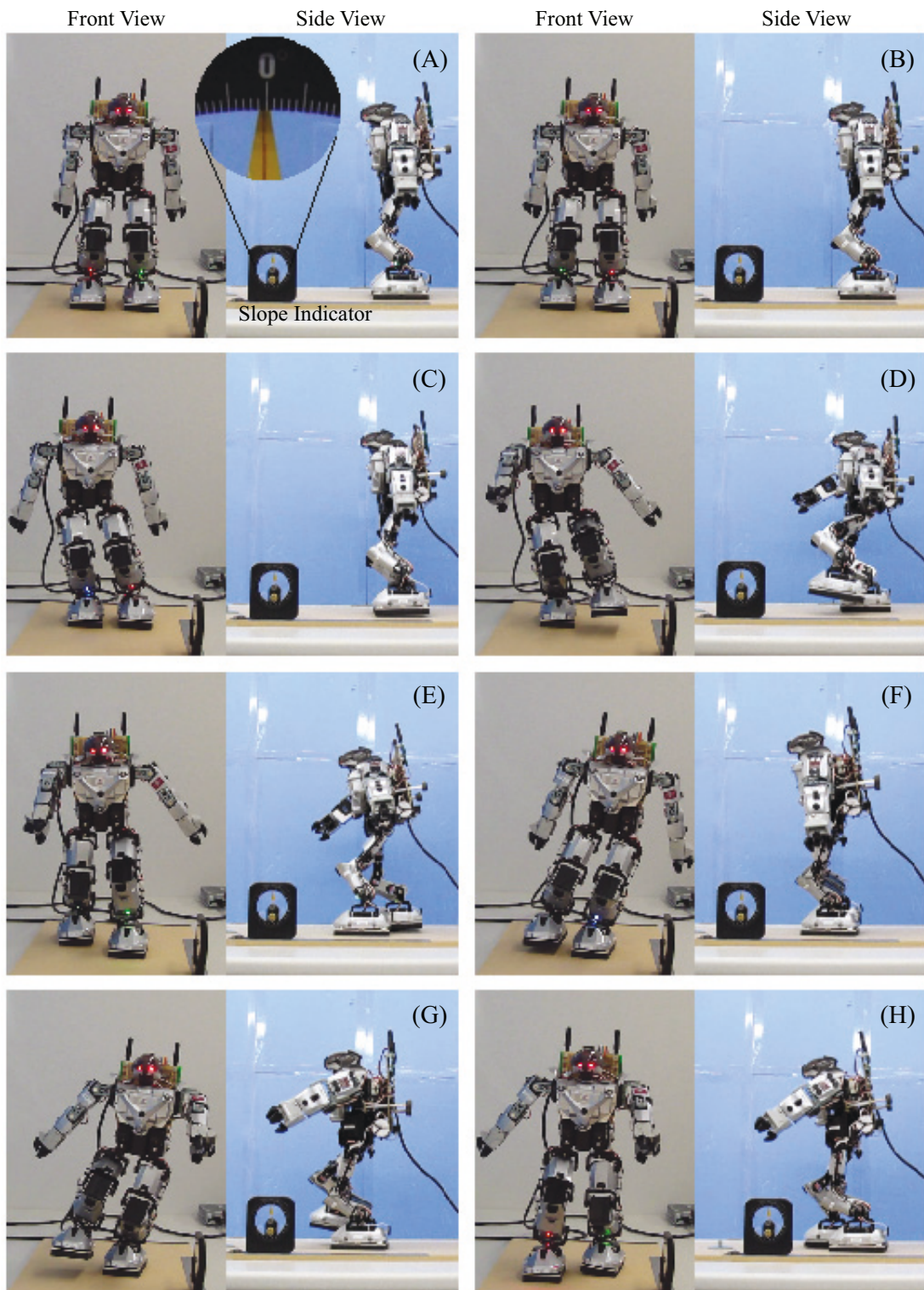
Figure 5-46. Actual robot motion when the robot walking on flat (With balance control)

122

5.3.2. Walking on the slopes task

5.3.2.1. Walking on upward slope

A) Uncontrolled case

Figure 5-47. Actual robot motion when the robot walking on upward slope
(Without balance control)

This experiment aims to show the failed balancing example. In this case, humanoid robot is not controlled by the proposed method. I first set the humanoid robot stand on the upward slope 5° as shown in Figure 5-47(A). Then, the robot begins the walking task by bending the knee, and then moves the left leg forward as shown in Figures 5-47(B) and (C) respectively. As robot has not activated the balance control function, the robot loss its balance and fall to backward. As a result, the humanoid robot fell down from the slope in to the back side as shown in Figure 5-47(D).

B) Controlled case

This experiment aims to show the successful balancing example. In this case, humanoid robot was controlled by the proposed method. The experimental procedure is

the same as the previous experiment as shown in Figure 5-48(A). However, due to the activated the balance control function, the robot began turning its body forward based on the analyses of the distributed pressure patterns. In this case, the outputs of the sensor elements are constrained as Equation (5-23). Based on the sensor values, the robot needs to move its weight into the front side until the forces on both legs satisfy the sensing relation as Equation (5-22). The robot turned forward to the balance position as shown in Figure 5-48(B). As shown in these figures, the robot could keep its body balanced by using the proposed method and it is ready for the next walking step. The robot keeps the angle between the supporting leg and ground floor during the next motion. Then the robot moves its weight into the right side until the forces on both legs satisfy the sensing relation as

$$(SR_1 = SR_2) < SR_3, (SL_{1, 2 \text{ and } 3} = 0) \tag{5-28}$$

At this state the robot is standing on one right leg as shown in Figure 84(C). Then the robot swings the right leg to the front and puts it down on the ground slope again as shown in Figure 5-48(D) and (E), respectively. At this point, the right foot poses must be normal to the ground surface as the preliminary sensing method which is described on section 5.1(Ground slope recognizing applications). After the robot keeps its foot position fixed, its foot position is then fixed and only the body pose are controlled by moving to the left side until the forces on both legs satisfy the sensing relation as

$$(SL_1 = SL_2) < SL_3, (SR_{1, 2 \text{ and } 3} = 0) \tag{5-29}$$

At this state the robot is standing with one left leg as shown in Figure 5-48(F). The robot then keeps the angle between the supporting leg and ground floor during the next motion. Then the robot swings the left leg to the front and puts it down to the ground slope again as shown in Figures 5-48(G) and (H), respectively. Throughout the experiments, I succeeded to keep the dynamic balance during the walking motion for biped walking on the upward slope the environment.
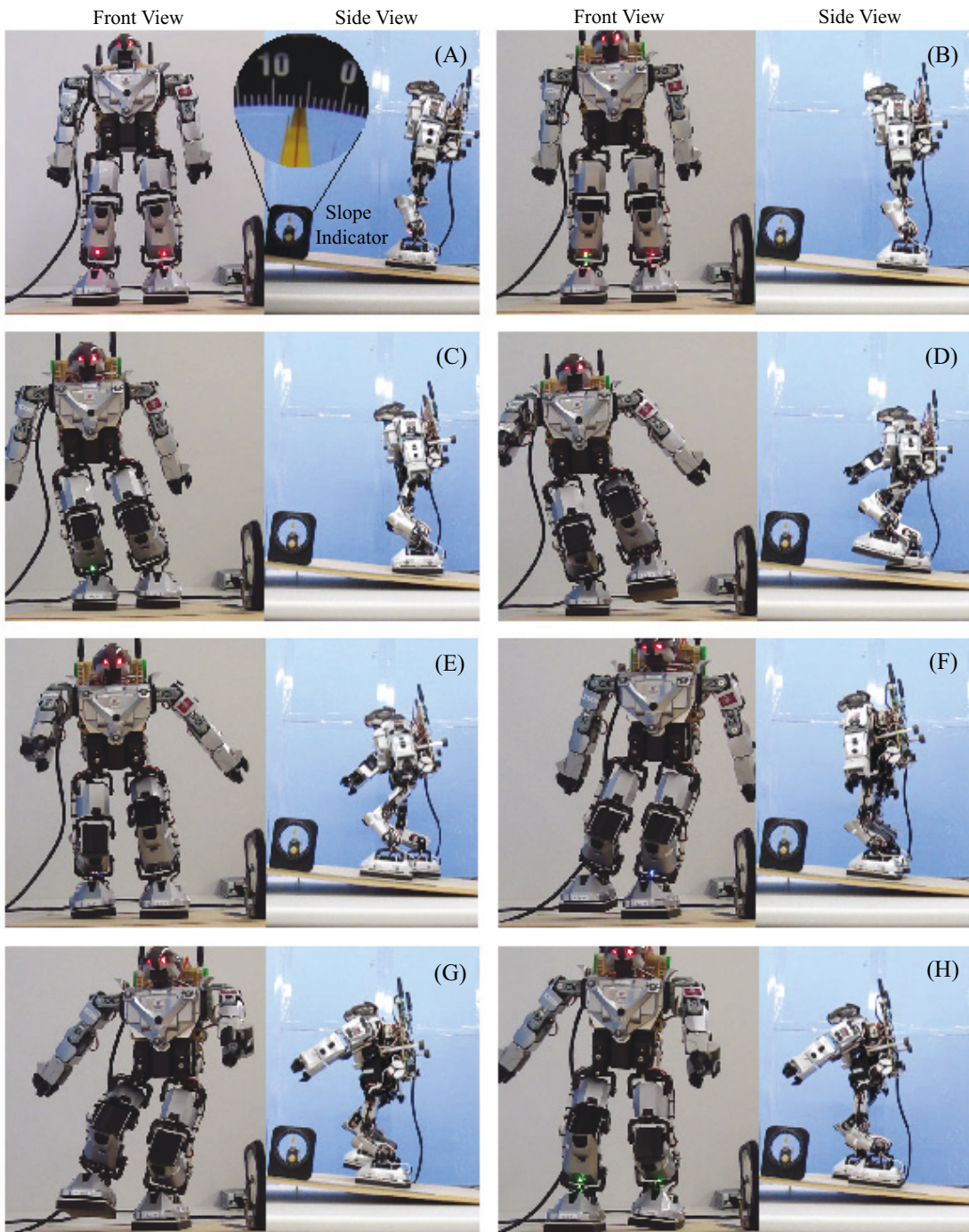
Figure 5-48. Actual robot motion when the robot walking on upward slope (With balance control)

5.3.2.2. Walking on downward slope
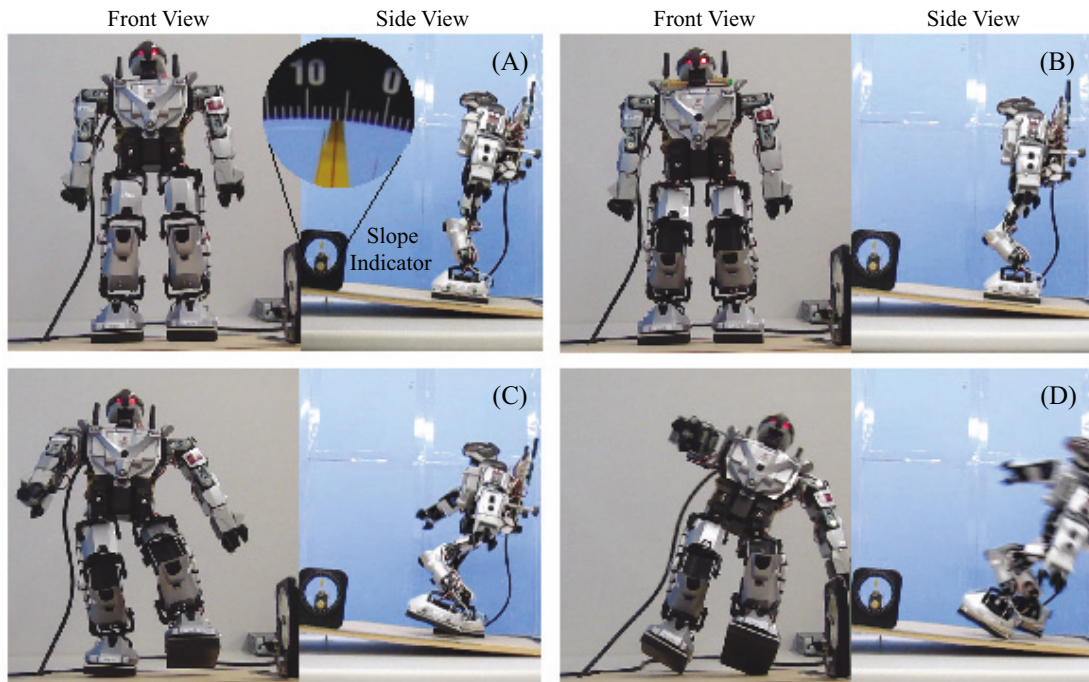
A) Uncontrolled case
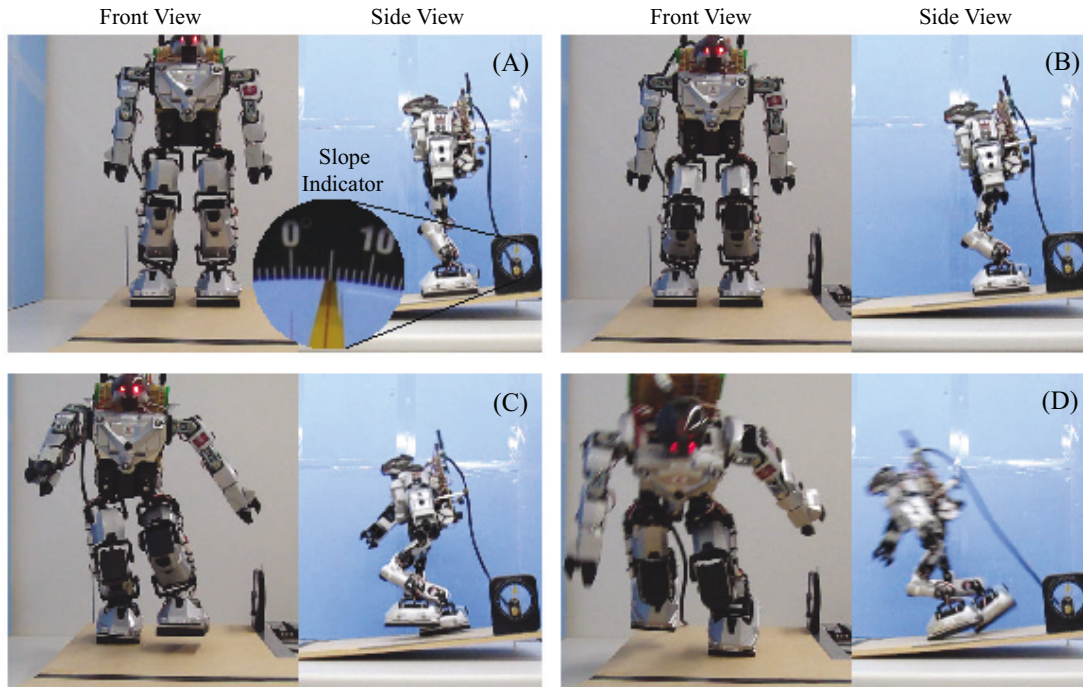
Figure 5-49. Actual robot motion when the robot walking on downward slope
(Without balance control)

This experiment aims to show the failed balancing example. In this case, humanoid robot is not controlled by the proposed method. I first set the humanoid robot stand on the downward slope 5° as shown in Figure 5-49(A). Then, the robot begin the walking task by bending the knee, and then move the left leg forward as shown in Figures 5-49(B) and (C), respectively. As the balancing control function has not activated the robot has lost its balance into the front side. As a result, the humanoid robot fell down from the slope to the front side as shown in Figure 5-49(D).

B) Controlled case

This experiment aims to show the successful balancing example. In this case, humanoid robot was controlled by the proposed method. The experimental procedure is the same as the previous experiment as shown in Figure 5-50(A). However, as the robot has activated the balance control function, the robot began turning its body backward
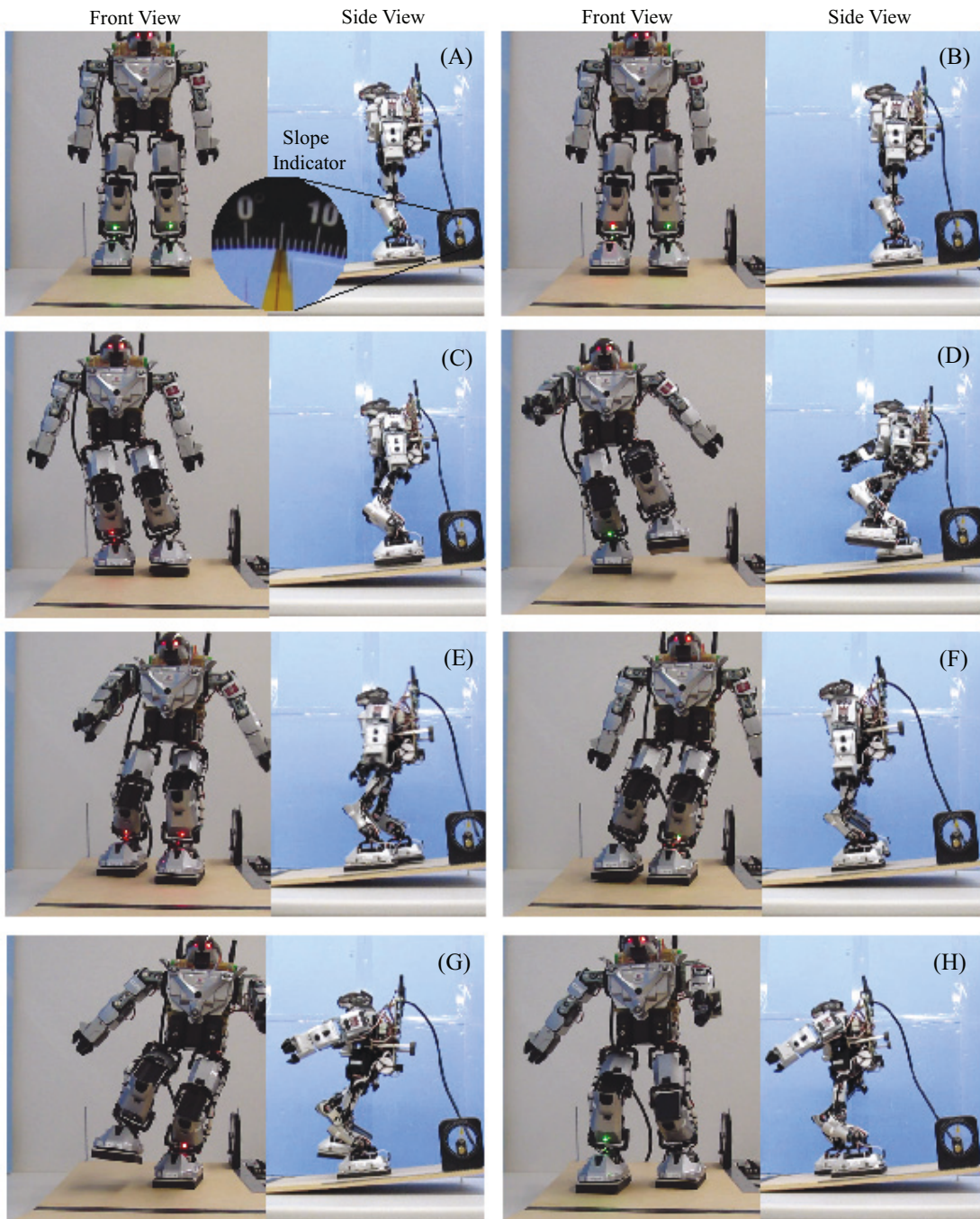
Figure 5-50. Actual robot motion when the robot walking on downward slope
(With balance control)

based on the analyses of the distributed pressure patterns. In this case, the outputs of the sensor elements are constrained as Equation (5-21). Based on the sensor values, the robot

needs to move its weight to the back side until the forces on both legs satisfy the sensing relation as Equation (5-22). The robot turned backward to the balance position as shown in Figure 5-50(B). As shown in these figures, the robot could keep its body balanced by the proposed method and it is ready for the next walking step. The robot then keeps the angle between the supporting leg and ground floor during the next motion. Then the robot moves its weight to the right side until the forces on both legs satisfy the sensing relation as Equation (5-28). At this state the robot is standing with one right leg as shown in Figure 5-50(C). Then the robot swings the right leg to the front and puts down to the ground slope again as shown in Figures 5-50(D) and (E) respectively. At this point, the right foot poses must be normal to the ground surface as the preliminary sensing method which is described on section 5.1(Ground slope recognizing applications). The foot position is then fixed and only the body pose are controlled by moving to the left side until the forces on both legs satisfy the sensing relation as Equation (5-29). At this state the robot is standing with one left leg as shown in Figure 5-50(F). The robot then keeps the angle between the supporting leg and ground floor during the next motion. Then the robot swings the left leg to the front and put down to the ground slope again as shown in Figures 5-50(G) and (H) respectively. Throughout the experiments, I succeed to keep the dynamic balance during the walking motion for biped walking on the downward slope the environment.

5.4. Summary

This chapter introduced the applications of proposed tactile sensing system for autonomous humanoid robot with experimental results. First I introduced the ground slopes recognition by conducted some experiments to confirm the ability of proposed method to move its feet normal to the ground surface in 3-D space. Then I introduced the balancing applications by utilizing the developed tactile sensor feet. The humanoid robot kinematics for balancing controls also was described here. Next, the experiments to confirm the two legs and one leg balancing tasks on the various environments such as different ground slopes, internal and external disturbances are introduced. I have also attempted to realize walking tasks of the humanoid robot on the various slopes.

CHAPTER VI

6. HUMAN- ROBOT INTERACTING APPLICATIONS

6.1. Cooperating Applications
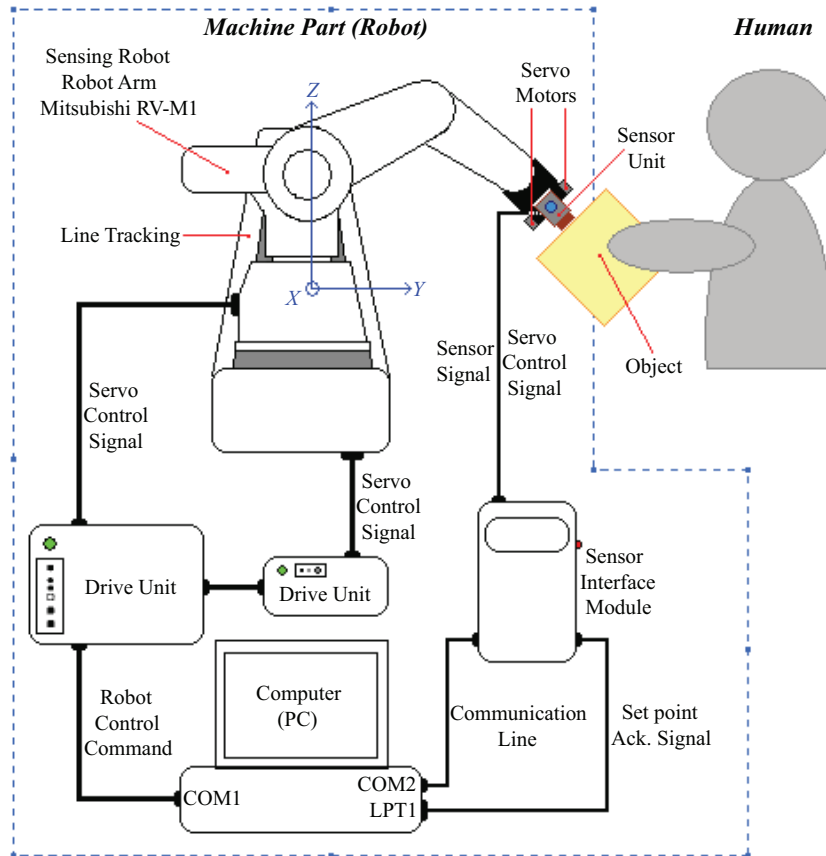
Figure 6-1. Diagram of tactile sensing system for cooperative tasks

In this application, I attempt to realize effective human–robot interaction, especially for human–robot cooperation via the object and proposed sensing device. A person utilized just one hand or finger to push the object towards the sensor, and the person and robot had to interact to hold the object. The experimental setup is shown in Figure 6-1. A robot arm was equipped with the proposed sensor to perform active surface recognition. The technique to estimate the contact angle between the sensor and a touched object plane was utilized. Hand pose control was used to keep the direction of movement normal to the 3-D plane object, which is often required to push an object for

positioning. This technique can, therefore be used for a cooperative task between a person and a robot to move a large object. The person might not be able to maintain object orientation during the movement due to the object weight. Therefore, to assist the person, the robot should support the person in different positions. In order to enable the robot to do this kind of task, the robot must move its hand normal to the object to support the object at different angles and levels. I have conducted the two main experiments to confirm the ability of proposed tactile sensing system. The first experiment to confirm the effectiveness of the robot hand pose action. The second experiment is to show some examples of human-robot cooperation to move an object together. In these applications, there is no need information about the object shape or orientation in advance.

6.1.1. Robot hand poses actions

6.1.1.1. Uncontrolled case
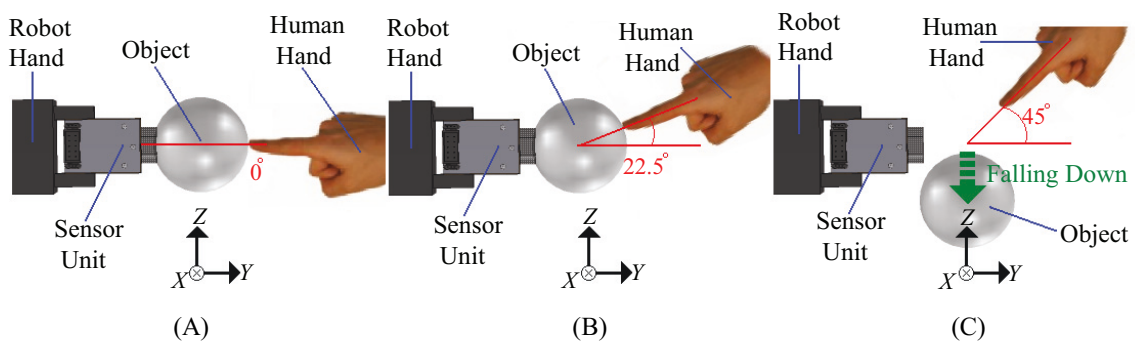
Figure 6-2. Human robot interaction for object holding (Without balance control)
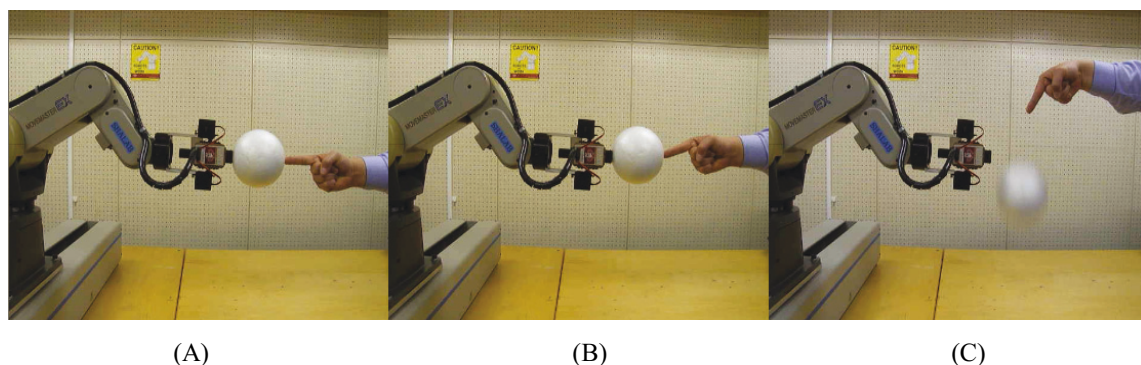
Figure 6-3. Actual interacting motion for object holding (Without balance control)

130

This experiment aimed to show the failed example of the human-robot interaction without the follow-up control of the robot. Figure 6-2 depicts the procedure of the failed example when the robot is not controlled and does not keep the robot hand direction normal to the object surface. Figure 6-3 shows the actual movement when the robot was not controlled and did not keep the robot hand direction normal to the object surface. In this procedure, the sensing robot firstly set its hand at zero degrees and then moved to the (0, 1, 0) direction into the waiting area. Then the sensing robot waited for a person to place an object plane on the sensing area. After the first touch, the person began turning the object freely from 0 to 45 degrees as Figures 6-2(A) and 6-3(A) to Figures 6-2(C) and 6-3(C), respectively. As a result, when the person moved the touched object, the robot did not follow the movement, and therefore the object fell down as shown in Figure 6-2(C) and 6-3(C) respectively.

6.1.1.2. Controlled case

(A)   (B)   (C)
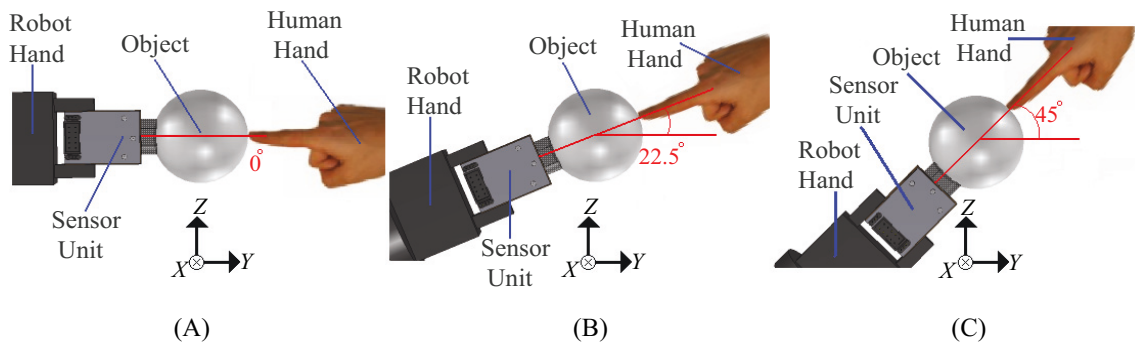
Figure 6-4. Human robot interaction for object holding (With balance control)

(A)   (B)   (C)
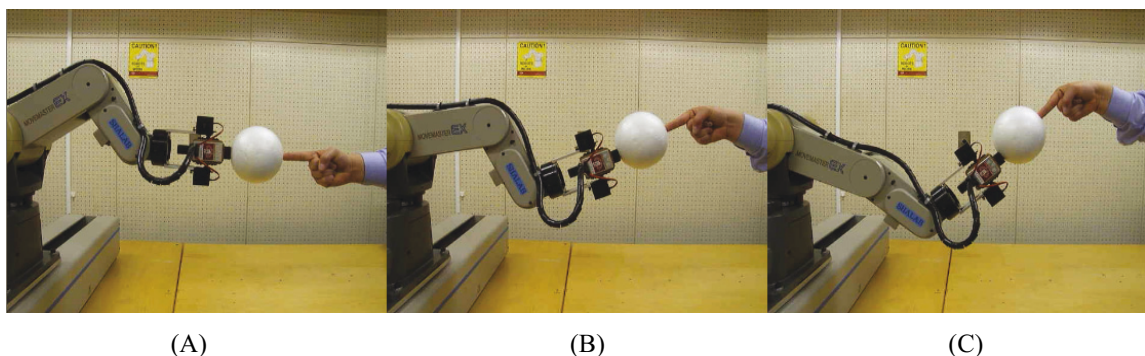
Figure 6-5. Actual interacting motion for object holding (With balance control)

131

This experiment aimed to show the successful example of the human-robot interaction with the follow-up control of the robot. Figure 6-4 depicts the procedure of the successful example when the robot is controlled and keeps the robot hand direction normal to the object surface. Figure 6-5 shows the actual movement when the robot was controlled and kept the robot hand direction normal to the object surface. The robot moved its hand direction to the waiting area and waited for a person to place an object plane on the sensing area. After the first touch, the person began turning the object freely from 0 to 45 degrees as Figures 6-4(A) and 6-5(A) to Figures 6-4(C) and 6-5(C), respectively. As a result, when the person moved the touched object, the robot followed the movement to help the person hold the object, the object was held by both human and robot as shown in Figures 6-4(C) and 6-5(C).

**6.1.2. Human and robot interaction through the objects**

In this application, I attempted to realize an effective human-robot interaction task. Especially, the human and robot cooperation task such as to move an object together by utilizing the proposed tactile sensor unit. A person utilizes just one hand or finger to push the object towards the sensor, and the person and robot had to interact to hold the object. The technique to estimate the contact angle between the sensor and a touched object plane was utilized. Hand pose control was used to keep the direction of movement normal to the 3-D plane object. I conducted the two example experiments to confirm the ability of the proposed tactile sensing system. The first experiment is to confirm the effectiveness of the robot hand pose action for human-robot cooperation to move an object together in 3-D. Another is I attempted to realize the technique for move various kind s of object. In these applications, the information about the object shape or orientation is not required in advance.

6.1.2.1 Cooperate to move an object in 3-D

This experiment aims to show that the proposed system enables us to realize human-machine interaction in 3-D. The sensing robot moved its hand direction to the waiting area and waited for a person to place an object plane on the sensing area. After
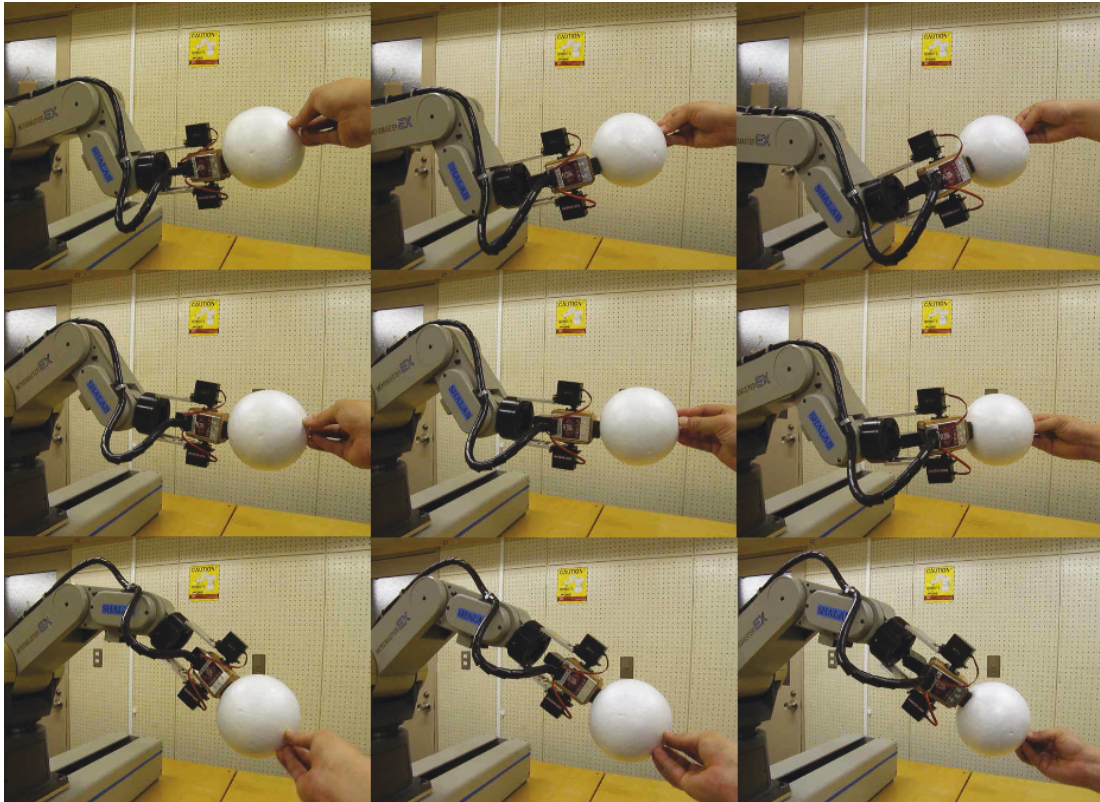
Figure 6-6. Actual motion of Human-Robot cooperation to move an object together

the first touch the person began turning the object freely in 3-D space. When the person moved the touched object, the robot followed the movement to help the person hold the object as shown in Figure 6-6. The experiment results indicate that the robot arm can move all their joint angles to follow the human movement. The photos showed that I could realize human-robot interaction not only in one direction but also in 3-D space.

6.1.2.2 Cooperate to move various kinds of objects

I also tried and succeeded in human-robot cooperation with various object shapes. The sensing robot first sets its hand at 0∘ and then moves to the (0, 1, 0) direction into the waiting area. Then the sensing robot waits for a person to place an object plane on the sensing area. After the first touch the person begins turning the object freely. When the person moves the touched object, the robot follows the movement to help the person hold the object. If the robot does not follow the person's motion, the object will fall. I tried and
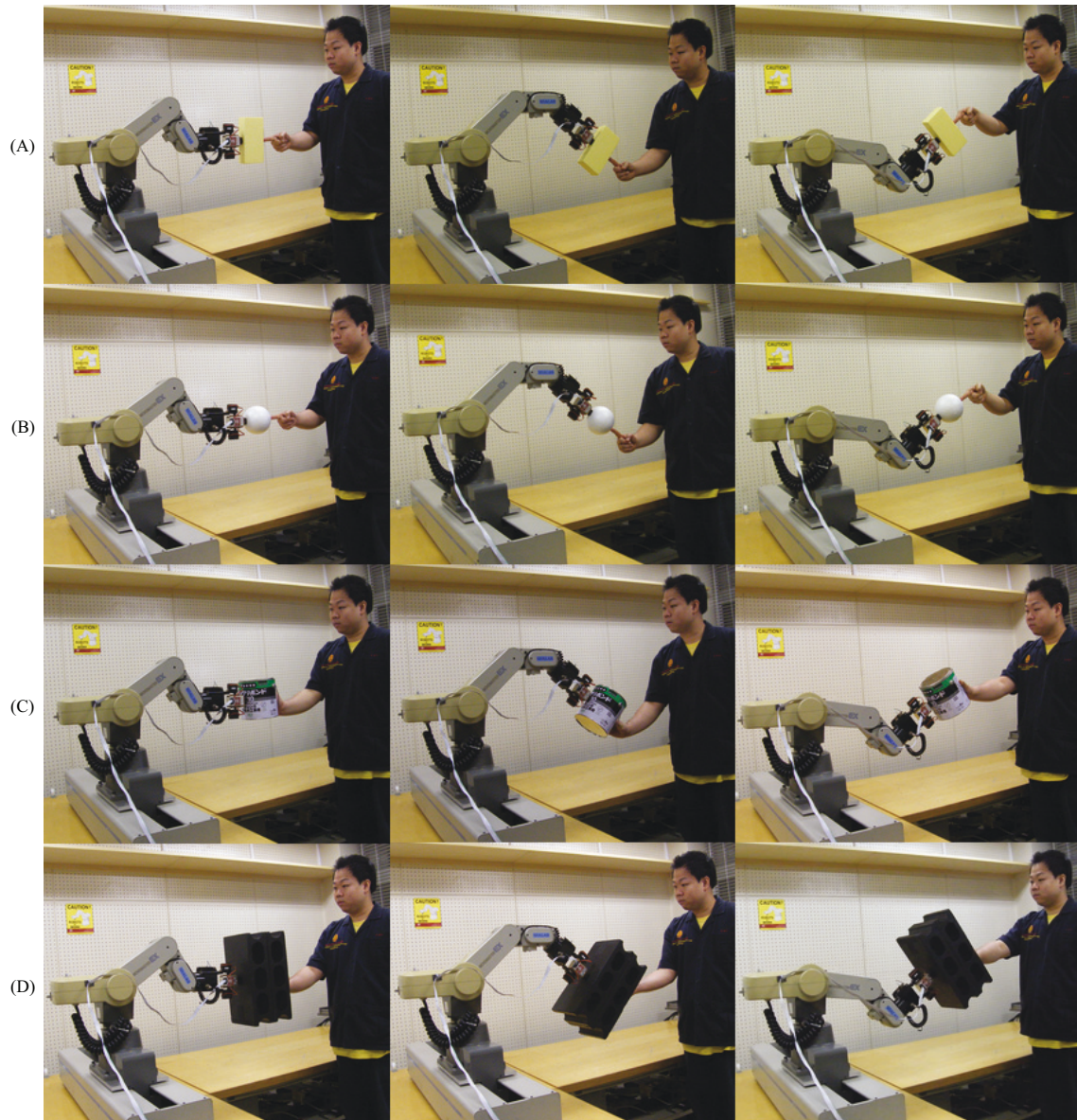
Figure 6-7. Actual motion of Human-Robot cooperation to move various objects together

succeeded in human–robot cooperation with various object shapes, such as a box, a sphere and a cylinder. Figure 6-7 is a photograph of human–machine cooperation to move an object as an example of human–machine interaction. As shown in the results, a robot can interact with a person *via* the object surface and the proposed tactile sensor. Throughout this experiment, the person moved the touched object plane freely in the 3-D plane and the robot was able to follow the person. Of course, such interactions are not

possible if there is no friction between the robot and the object. I also confirmed human–robot cooperation with various objects. I tested a 30g box, an 18g sphere, a 536g cylinder and a 264g block. Figure 6-7(A) to (D), respectively, shows photographs of human–machine cooperation to move the aforementioned objects.

6.2. Contact States Interacting Between Human and Robot

In this section, I attempted to realize an effective human and robot interaction, especially in case of contact states interacting between human and robot to avoid the robot damages which cause the falling down due to the unpredicted external force from the human. In the first experiment, I have conducted the experiments to confirm the ability of the autonomous humanoid robot that can maintain balance with their sensing feet from the disturbance by against the human pushing force. Second experiment, as the robot could not maintain the two leg balance if the pushing force is too large. In order to maintain its balance, the robot should move its leg on an opposite side to support its body against the various pushing force direction even human pushing harder. Throughout these experiments, the humanoid robot can keep its balance not only against human pushing but also to avoid the damages caused by the falling down and the robot do not need any information about the contacted ground slope or orientation in advance.

6.2.1. Maintain the two legs balance from a pushing force

| (A) | (B) | (C) | (D) |
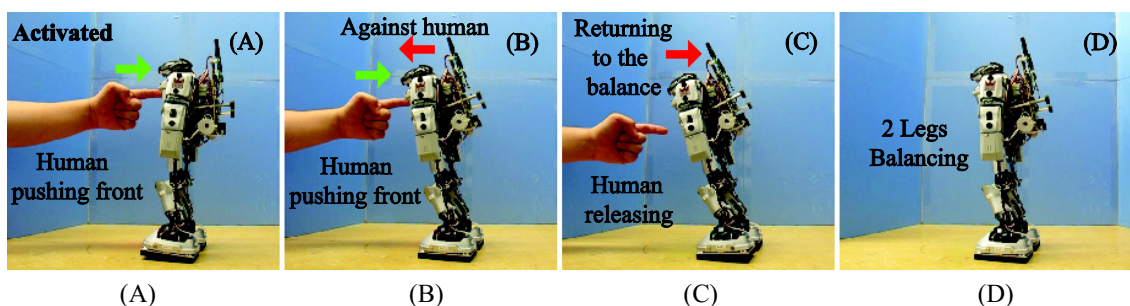
Figure 6-8. Actual motion when the robot maintains two legs balance from pushing force

In this experiment, I aim to show a successful balance example for realize human-robot interaction. This experiment was conducted to confirm the ability of an autonomous

humanoid robot that can maintain balance with their sensing feet from the disturbance by against the human pushing force. Firstly I set the robot standing with two legs balancing. Secondly, a human applied the pushing force from the front of robot body by using a human finger as shown in Figure 6-8(A). The pushing force from human makes the robot unbalanced. Thus, the robot move forward to against the human as shown in Figure 6-8(B). Then human leaves their finger out from the robot body. Finally, the robot can maintains the balance position without falling down as shown in Figures 6-8(C) and (D) respectively.

6.2.2. Maintain the balance with step motions

Although the previous experiment result shows that autonomous humanoid robot with proposed tactile sensing technique can maintain balance from the disturbance by against the human pushing force. However, the robot cannot maintain the two legs balance if the pushing force is too large or the human pushing harder.

To solve this problem, the robot should recognize the maximum force for standing two legs and should able to determine the direction of the pushing forces. The maximum force is utilized as the set point value for balancing control. For example, when the pushing force reaches the set point value, the robot will moves an opposite leg side of the pushing side to support its body against the pushing force even human pushing harder. Four experiments were conducted to provide the example of different pushing force directions to the robot as the following sections.

6.2.2.1. Human pushes the robot front on the right side

This first experiment aims to show that the proposed system enables us to realize human-robot interaction. In this experiment, a human pushes the robot front on the right side. In this procedure, I first set the robot stand balanced with two legs. A human then applied the pushing force to the front direction on the right side of the robot shoulder by using the finger as shown in Figure 6-9(A). At this state, the analyses of the distributed pressure patterns are the same as shown in Figure 3-11(A) for both legs. However, as the
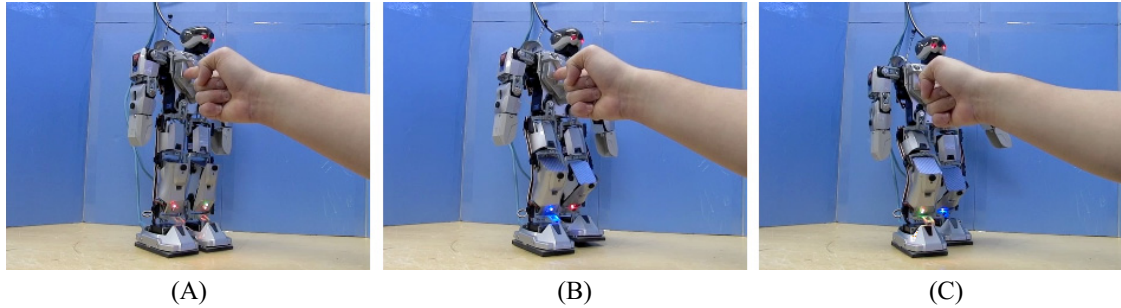
Figure 6-9. Actual motion when the robot maintains step leg balance from the human pushing force (on the front at the right side of robot body)

human pushes the robot into the right side, thus the sensor of right foot will receive the applied force faster than the sensor on left foot. Then the microcontrollers on the sensor interfacing unit send the data to the controlling board to move an opposite leg side (left leg) of the pushing side backward to support its body as shown in Figure 6-9(B). This figure shows beginning of step back motion. Finally, the robot completely moves the left leg step backward to support its body against the pushing force from human as shown in Figure 6-9(C). At this state the robot can keep its balance even human pushing harder.

6.2.2.2. Human pushes the robot front on the left side

Figure 6-10. Actual motion when the robot maintains step leg balance from the human pushing force (on the front at the left side of robot body)

In this experiment, the human applied the pushing force to the front direction on the left side of the robot shoulder as shown in Figure 6-10(A). At this state, the analyses of the distributed pressure patterns are the same both legs as shown in Figure 3-11(A). However, in this case, the sensor of left foot will receive the applied force faster than the sensor on right foot. Thus the control unit moves an opposite leg side (right leg) of the

pushing side backward to support its body as shown in Figure 6-10(B). Finally, the robot completely moves the right leg step backward to support its body against the pushing force from human as shown in Figure 6-10(C). At this state, robot can keep its balance even human pushing harder.

6.2.2.3. Human pushes the robot back on the right side

| (A) | (B) | (C) |

Figure 6-11. Actual motion when the robot maintains step leg balance from the human pushing force (on the back at the right side of robot body)

In this experiment, the human applied the pushing force to the back direction on the right side of the robot shoulder as shown in Figure 6-11(A). At this state, the analyses of the distributed pressure patterns are the same as shown in Figure 3-11(C) for both legs. However, in this case, the sensor of right foot will receive the applied force faster than the sensor on left foot. Thus the control unit moves an opposite leg side (left leg) of the pushing side forward to support its body as shown in Figure 6-11(B). Finally, robot has completely moves left leg step forward to support its body against the pushing force from human as shown in Figure 6-11(C). At this state the robot can keep its balance even human pushing harder.

6.2.2.4. Human pushes the robot back on the left side

In this experiment, the human applied the pushing force to the back direction on the left side of the robot shoulder as shown in Figure 6-12(A). At this state, the analyses of the distributed pressure patterns are the same as shown in Figure 3-11(C) for both legs. However, in this case, the sensor of left foot will receive the applied force faster than the sensor on right foot. Thus the control unit moves an opposite leg side (right leg) of the

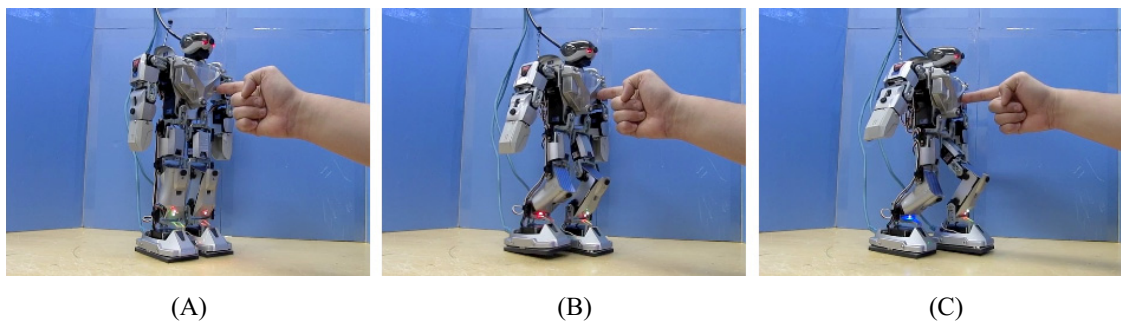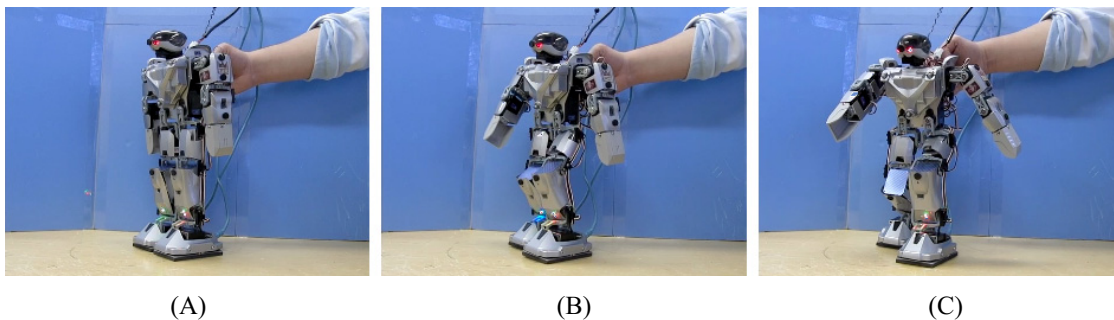|		
(A)	(B)	(C)
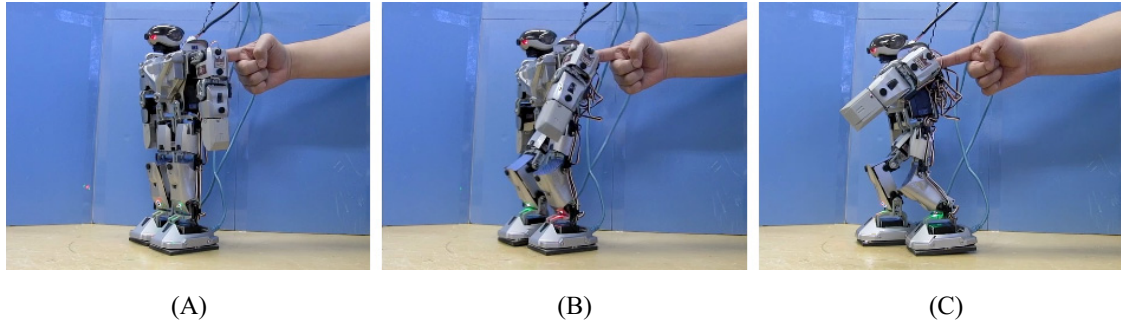
Figure 6-12. Actual motion when the robot maintains step leg balance from the human pushing force (on the back at the left side of robot body)

pushing side forward to support its body as shown in Figure 6-12(B). Finally, robot completely moves right leg step forward to support its body against the pushing force from human as shown in Figure 6-12(C). At this state the robot can keep its balance even human pushing harder.

6.3. Summary

This chapter introduced applications for human and robot interactions. Two main experiments were conducted to understand the human-robot interacting task.

First is the interaction with fixed position robot. In this case I employed the robotic arm with proposed tactile sensing hand to confirm the effectiveness of the robot hand pose action to move an object together with human. As the results, the robot with activated sensing hand can followed the human motion to help the person hold a various kind of objects in 3-D space. The successful tested objects are a 30g box, an 18g sphere, a 536g cylinder and a 264g block. In this application, the robot arm does not need any information about the object shape or orientation in advance.

Second is the interaction with mobile robot. In this case I employed the autonomous humanoid robot with proposed tactile sensing feet to confirm the effective human and robot interaction, especially in case of contact states interacting between human and robot to avoid the robot damages which cause the falling down due to the unpredicted external force from the human. As the result the autonomous humanoid robot can maintain balance with their sensing feet from the disturbance by against the human

pushing force. The robot also can move its leg on an opposite side to support its body against the various pushing force direction even human pushing harder. Throughout these experiments, the humanoid robot can keep its balance not only against human pushing but also to avoid the damages caused by the falling down and the humanoid robot does not need any information about the contacted ground slope or orientation in advance.

CHAPTER VII

7. CONCLUSIONS

This dissertation presented the tactile sensor system for robots and various active sensing techniques. The developed tactile sensing system is implemented on the industrial robot hand and humanoid robot feet.

The first main part of this thesis proposed a tactile sensing system and control method for industrial robot to realize object recognition. Tactile sensor has implemented on robot hand consists of three pieces of force sensitive resistors with peripheral circuits. The robot arm equipped with the sensor is controlled for active object recognition. The developed sensing device may not be enough for accurate force measurement. It is, however, useful for controlling robot arm to recognize the object shape and to maintain the hand orientation for human-robot cooperative tasks. The bandwidth of the sensor unit has not been examined yet. The total response of the sensor unit is slower than that of FSR, because the FSR is covered with the soft material whose mechanical reaction is slow. However, the proposed sensing unit works sufficiently well in all the applications shown in this thesis, as the each moving step motion of the robot arm has room enough to obtain the sensing time. Some applications and experimental results were introduced in this thesis such as, the object surface angle measurement, the object shape measurement, the surface normal detection, the surface normal following for human-robot interactions, the object edge recognition, the continue tracing an object edge, and the approach for welding application is also presented. The experimental results show that the proposed system can be used practically for obtaining the active object information and apply to many tasks. Accordingly, I suggest the future improvements of the sensing system for industrial robot should include the actual welding and interactive tasks. As I aim to develop a novel robot arm with a tactile sensor welding torch. The only simulated welding torch and a straight trajectory for tracing an object edge was examined. Hence, future works should include the other trajectories and reducing an error to realize the efficient automatic welding task in to the real working environment.

The second main part of this thesis proposed a novel tactile sensing system for autonomous humanoid robot. The developed sensors were implemented on the robotic feet. Each foot consists of three thin sheets of force sensitive resistors arranged triangularly with the peripheral circuits. I also showed various experiment results to confirm ability of proposed sensing system; first is an active tactile sensing technique to estimate the ground slope orientation at the specific contact point and then move the robot foot normal to the ground surface for active ground slope recognition. As the results, I first succeeded in automatic detection of the ground slope such as flat level surface, up, down, left and right slopes with 20 degrees each. The second is an active tactile sensing technique to estimate the strongest force position under the foot for balancing its body with one leg and two legs. As the results, I have succeeded in balancing the robot automatically with two legs on the various ground slopes such as flat level, front and back slopes. I also succeeded in the automatic balancing controls with two legs and one leg balance in spite of the robot moving itself (internal) and the external force such as the pushing force by human. The minimum angle that developed robot can be detected for balancing forward and backward is 3° degrees while the minimum angle that can be detected for balancing leftward and rightward is 2° degrees. Third, I also succeeded to realize the walking tasks on 5° upward and downward slopes. Throughout these all experiments, the robot could recognize the contact position, and balance its body on the ground slopes during the walking motions. For all applications, the information about the contacted ground slope or orientation is not required in advance. The proposed system can be independent from the control of robot body to make the distributed embedded control system. Thus the balancing problems in the robot motion planning and human-robot interacting forces are no need to be concern. Accordingly, I suggest the future improvements of the proposed system should include the development an internal body sensor network with similar embedded tactile sensing systems for other different parts of robot body such as fingers, hands and arms for increasing the capability of current system. I also would like to utilize the proposed sensor technique for effective dynamic walking task in the real unstructured environments and apply the proposed method to make human-robot interaction tasks more useful and flexible.

BIBLIOGRAPHY

[1]   Y. Motai and A. Kosaka, "Hand-Eye Calibration Applied to Viewpoint Selection for Robotic Vision", *IEEE Trans. on Industrial Electronics*, Vol. 55, No. 10, pp.3731-3741, 2008.

[2]   P.Vadakkepat, P. Lim, L.C. De Silva, L. Jing and L. Ling, "Multimodal Approach to Human-Face Detection and Tracking", *IEEE Trans. on Industrial Electronics*, Vol. 55,   No. 3, pp.1385-1393, 2008.

[3]   M. Rucci and P. Dario, "Active exploration procedures in robotic tactile perception", *Intelligent Robotic Systems*, pp.20-24, 1993.

[4]   E. Ishii, H. Nishi and K. Ohnishi, "Improvement of Performances in Bilateral Teleoperation by Using FPGA", *IEEE Trans. on Industrial Electronics*, Vol. 54, No. 4, pp.1876-1884, 2008.

[5]   H. Iwata, K. Tomita and S. Sugano, "Quantification of Human-Robot Physical Contact States based on Tactile Sensing," *in Proc. of IEEE Int'l. Conf. on Advanced Intelligent Mechatronics*, pp.610-615, 2003.

[6]   H. Iwata and S. Sugano, "Human-Robot-Contact-State Identification Based on Tactile Recognition", *IEEE Trans. on Industrial Electronics*, Vol. 52, No. 6, pp.1468-1477, 2005.

[7]   K. Suwanratchatamanee, M. Matsumoto and S. Hashimoto, "Balance Control of Robot and Human-Robot Interaction with Haptic Sensing Foots", *in Proc. of the 2nd IEEE Int'l. Conference on Human System Interaction*, pp. 68-74, 2009.

[8]   K. Suwanratchatamanee, M. Matsumoto and S. Hashimoto, "Haptic Sensing Foot System for Humanoid Robot and Ground Recognition with One Leg Balance", *IEEE Trans. on Industrial Electronics*, In Press, 2009.

[9]   J. Jockusch, J. Walter and H. Ritter, "A Tactile Sensor System for a Three-Fingered Robot Manipulator," *in Proc. of IEEE Int'l. Conf. on Robotics and Automation*, pp.3080-3086, 1997.

[10] M. E. Tremblay and M. R. Cutkosky, "Estimation friction using incipient slip sensing during a manipulation task", *in Proc. of IEEE Int'l Conf on Robotics and Automation*, pp.429-434, 1993.

[11] N. Chen, R. Rink and H. Zhang, "Local Object Shape from Tactile Sensing", *in Proc. of IEEE Int'l Conf. on Robotics and Automation*, pp. 3496-3501, 1996.

[12] N. Chen, H. Zhang and R. Rink, "Edge Tracking Using Tactile Serve", *in Proc. of IEEE/RSJ Int'l Conf. on Intelligent Robots and Systems*, pp.84-89, 1995.

[13] L. H. Sharif, S. Yamane, T. Sugimoto and K. Oshima, "Intelligent Cooperative Control System in Visual Welding Robot", *in Proc. of the 27th IEEE Annual Int'l. Conf. of Industrial Electronics Society*, pp.439-443, 2001.

[14] X. Liu and C. Xie, "Robotic Seam Tracking Utilizing Arc Light", *in Proc. of the 6th IEEE Int'l. Conf. on Intelligent Systems Design and Applications*, 2006.

[15] X. Liu and C. Xie, "Arc-Light Based Real-time Seam Tracking System in Welding Robot", *in Proc. of IEEE Int'l. Conf. on Control and Automation*, pp.2462-2467, 2007.

[16] C. Umeagukwu, B. Maqueira and R. Lambert, "Robotic Acoustic Seam Tracking: System Development and Application", *IEEE Trans. on Industrial Electronics*, Vol. 36, No. 3, pp.338-348, 1989.

[17] P. Koseeyaporn, "Continuous Surface Tracking for Welding Robot", *in Proc. of IEEE Int'l. Technical Conf*, pp.491-494, 2004.

[18] M. Shimojo and M. Ishikawa, "An Active Touch Sensing Method Using a Spatial Filtering Tactile Sensor", *in Trans. of the Institute of Electronics, Information and Communication Engineers* C-II, Vol.J74-C-II, No.5, pp.309-316, 1991.

[19] M. Tanaka, N. Li and S. Chonan, "Active Tactile Sensing Using A Two-Finger System", *in Proc of International Conference on Motion and Vibration Control*, pp.762-767, 2002.

[20] P. Vadakkepat, P. Lim, L. C. De Silva, L. Jing and L. L. Ling, "Multimodal Approach to Human-Face Detection and Tracking", *IEEE Trans. on Industrial Electronics*, Vol. 55, No. 3, pp.1385-1393, 2008.

[21] M. H. Lee and H. R. Nicholls, "Tactile sensing for mechatronics-a state of the art survey", *Mechatronics*, Vol. 9, pp.1-31, 1999.

[22] Y. Huang and X. Ming, "Two Type of Flexible Tactile Sensor Arrays of Robot for Three-dimension Force Based on Piezoresistive Effects", *in Proc. of IEEE In't. Conf. On Robotics and Biomimetics*, pp.1032-1037, 2009.

[23] G. M. Krishna and K. Rajanna, "Tactile Sensor Based on Piezoelectric Resonance", *IEEE Sensors Journal*, Vol. 4, pp. 691-697, 2004.

[24] T. Matsunaga, K. Totsu, M. Esashi and Y.Haga, "Tactile Display for 2-D and 3-D Shape Expression Using SMA Micro Actuators", *in Proc. of IEEE Annual Int'l. Conf. on Microtechnologies in Medicine and Biology*, pp.88-91, 2005

[25] A. Bicchi, J. K. Salisbury and D. L. Brock, "Contact Sensing from Force and Torque Measurements", *The Int'l Journal of Robotics Research*, Vol. 12, No. 3, pp. 249-262, 1993.

[26] T. Takeda, Y. Hirata and K. Kosuge, "Dance Step Estimation Method Based on HMM for Dance Partner Robot", *IEEE Trans. on Industrial Electronics*, Vol. 54, No. 2, pp.699-706, 2007.

[27] T. Tsuji, Y. Kaneko and S. Abe, "Whole-Body Force Sensation by Force Sensor with Shell-Shaped End-Effector", *IEEE Trans. on Industrial Electronics*, Vol. 56, No. 5, pp.1375-1382, 2009.

[28] K. Suwanratchatamanee, M. Matsumoto, R. Saegusa and S. Hashimoto, "A Simple Tactile Sensor System for Robot Manipulator and Object Edge Shape Recognition", *in Proc. of the 33rd IEEE Annual Int'l. Conf. of Industrial Electronics Society*, pp.245-250, 2007.

[29] K. Suwanratchatamanee, M. Matsumoto and S. Hashimoto, "A Simple Robotic Tactile Sensor for Object Surface Sensing", *The Int'l Journal of Robotics Society Japan, Advanced Robotic,* Vol.22, No.8, pp.867-892, 2008.

[30] K. Suwanratchatamanee, M. Matsumoto and S. Hashimoto, "A tactile sensor system for robot manipulator and continuous object edge tracking", *in Proc. of the 7th France-Japan and 5th Europe-Asia Congress on Mechatronics,* CD-ROM, 2008.

[31] K. Suwanratchatamanee, M. Matsumoto and S. Hashimoto, "Human -machine interaction through object using robot arm with tactile sensors", *the 17th IEEE Int'l. Symposium on Robot and Human Interactive Communication*, pp.683-688, 2008.

[32] F. Vecchi, C. Freschi, S. Micera, A. Sabatini and P. Dario, "Experimental evaluation of two commercial force sensors for applications in biomechanics and motor control", *International Functional Electrical Stimulation Society (IFESS)*, 2000.

[33] C. Lebosse, B.Bayle, M. de Mathelin and P. Renaud, "Nonlinear modeling of low cost force sensors", *in Proc. of IEEE Int'l. Conf. on Robotics and Automation*, pp.3437-3442, 2008.

[34] Tekscan, Inc., USA, "Flexi-Force user manual and technical data sheet (model A101)", *www. Tekscan.com.*

145

LIST OF PUBLICATIONS

[Journals/Transactions]

[論文]

1. ○Kitti Suwanratchatamanee, Mitsuharu Matsumoto, Shuji Hashimoto, "Robotic Tactile Sensor System and Applications", *IEEE Transactions on Industrial Electronics*, In-Press.

2. ○Kitti Suwanratchatamanee, Mitsuharu Matsumoto, Shuji Hashimoto, "Haptic Sensing Foot System for Humanoid Robot and Ground Recognition with One Leg Balance", *IEEE Transactions on Industrial Electronics*, In-Press.

3. ○Kitti Suwanratchatamanee, Mitsuharu Matsumoto, Shuji Hashimoto, "A simple robotic tactile sensor for object surface sensing", *The International Journal of RSJ (Robotics Society of Japan), Advanced Robotics*, Vol.22, No.8, pp.867-892, 2008.

[Proceeding of referred international conferences]

[査読付き国際会議]

1. ○Kitti Suwanratchatamanee, Mitsuharu Matsumoto, Shuji Hashimoto, "Tactile /Haptic Sensing System for Autonomous Humanoid Robots", *The IEEE 2009 International Student Experimental Hands-on Project Competition via Internet on Intelligent Mechatronics and Automation (HCIMA-2009)*, Internet conference, December 5, 2009. **"Selected Finalist 10 Teams"**

2. ○Kitti Suwanratchatamanee, Mitsuharu Matsumoto, Shuji Hashimoto, "Balance Control of Robot and Human-Robot Interaction with Haptic Sensing Foots", *The 2nd IEEE International Conference on Human System Interaction (HSI-2009)*, pp.68-74, Catania, Italy, May 21-23, 2009. **"Awarded the Best Paper (in the area of Intelligent systems)"**

3. ○Kitti Suwanratchatamanee, Mitsuharu Matsumoto, Shuji Hashimoto, "A Simple Tactile Sensing Foot for Humanoid Robot and Active Ground Slope Recognition", *The 5th IEEE International Conference on Mechatronics (ICM-2009)*, CD-Proc., ISBN:978-1-4244-4195-2, Malaga, Spain, April 14-17, 2009.

4. ○Kitti Suwanratchatamanee, Mitsuharu Matsumoto, Shuji Hashimoto, "Tactile /Haptic Sensor for Robots and Applications", *The IEEE 2008 International Student Experimental Hands-on Project Competition via Internet on Intelligent Mechatronics and Automation (HCIMA-2008)*, Internet conference, December 7, 2008. **"Won 3rd-Prize Award"**

5. ○Kitti Suwanratchatamanee, Mitsuharu Matsumoto, Shuji Hashimoto, "A novel tactile sensor torch system for robot manipulator and object edge tracking", *The 34th Annual International Conference of the IEEE Industrial Electronics Society 2008 (IECON-2008)*, pp.2617-2622, Orlando, Florida, USA, November 10-13, 2008.

6. ○Kitti Suwanratchatamanee, Mitsuharu Matsumoto, Shuji Hashimoto, "Human-machine interaction through object using robot arm with tactile sensors", *The 17th IEEE International Symposium on Robot and Human Interactive Communication (RO-MAN-2008)*, pp.683-688, Munich, Germany, August 1-3, 2008.

7. ○Kitti Suwanratchatamanee, Mitsuharu Matsumoto, Shuji Hashimoto, "A tactile sensor system for robot manipulator and continuous object edge tracking", *The 7th of France-Japan (5th Europe-Asia) Congress on Mechatronics (Mecatronics-2008)*, CD-Proc., Le Grand-Bornand, France, May 21-23, 2008.

8. ○Kitti Suwanratchatamanee, Mitsuharu Matsumoto, Ryo Saegusa, and Shuji Hashimoto, "A simple tactile sensor system for robot manipulator and object edge shape recognition", *The 33rd Annual International Conference of the IEEE Industrial Electronics Society 2007 (IECON-2007)*, pp.245-250, Taipei, Taiwan, November 5-8, 2007. **"Awarded Student scholarship"**

[Proceeding of referred domestic conferences]

[国内会議論文]

○Kitti Suwanratchatamanee, Mitsuharu Matsumoto, Shuji Hashimoto, "Balance Control Using Embedded Tactile Sensing Feet System for Humanoid Robot", (" 足底触覚システムによるヒューマノイドロボットのバランス制御"), *The 27th Annual Conference of the Robotics Society of Japan (RSJ-2009)*, CD-Proc., AC3H3-01, Yokohama, Japan, September 15-17, 2009.

[Master Thesis]

[修士論文]

○Kitti Suwanratchatamanee, "An Investigation of MODBUS and Development of MODBUS Master and Slaves", *Royal Melbourne Institute of Technology University (RMIT), Melbourne, Australia*, December, 2004.

[Bachelor Thesis]

[学士論文]

○Kitti Suwanratchatamanee, "Development of the CNC Wing Foam Cutting Machine", *Kingmongkut's University of Technology Thonburi (KMUT-T), Bangkok, Thailand*, March, 2002. **"Won 1st-Prize Award"**

LIST OF AWARDS

1. **The Best Paper** Award (in the area of Intelligent systems)

○Kitti Suwanratchatamanee, Mitsuharu Matsumoto, Shuji Hashimoto, "Balance Control of Robot and Human-Robot Interaction with Haptic Sensing Foots", *The 2ⁿᵈ IEEE International Conference on Human System Interaction (HSI-2009)*, pp.68-74, Catania, Italy, May 21-23, 2009.

2. **The 3rd-Prize Award**

○Kitti Suwanratchatamanee, Mitsuharu Matsumoto, Shuji Hashimoto, "Tactile /Haptic Sensor for Robots and Applications", *The IEEE 2008 International Student Experimental Hands-on Project Competition via Internet on Intelligent Mechatronics and Automation (HCIMA-2008)*, Internet conference, December 7, 2008.

3. **The Student Scholarship Award**

○Kitti Suwanratchatamanee, Mitsuharu Matsumoto, Ryo Saegusa, and Shuji Hashimoto, "A simple tactile sensor system for robot manipulator and object edge shape recognition", *The 33rd Annual International Conference of the IEEE Industrial Electronics Society 2007 (IECON-2007)*, pp.245-250, Taipei, Taiwan, November 5-8, 2007.
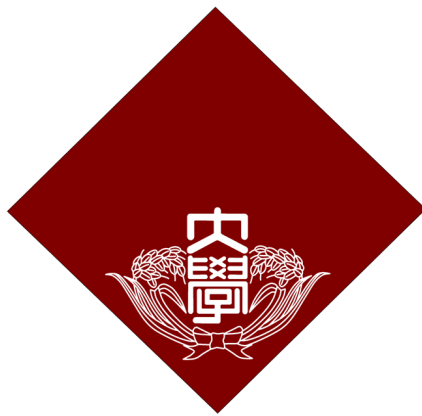
4. **The 1st-Prize Award**

○Kitti Suwanratchatamanee, "Development of the CNC Wing Foam Cutting Machine", *The 3rd Annual university project contest 2002*, Kingmongkut's University of Technology Thonburi (KMUT-T), Bangkok, Thailand, March, 2002.

LIST OF GRANTS AND SCHOLARSHIPS

1. 日本学術振興会特別研究院の英文名
   Research Fellow of the Japan Society for the Promotion of Science
   Position: Special researcher (DC2),　Reference number: 20-56621
   Research grant amount: 600,000 円 / year,　Period: 2009-04-01 ~ 2010-03-31
   Research grant amount: 600,000 円 / year,　Period: 2008-10-01 ~ 2009-03-31
   Salary: 200,000 円 / month,　Period: 2008-10-01 ~ 2010-03-31

2. 早稲田大学理工学術院グローバル COE 研究補助員
   Full time research assistance of Global Robot Academia
   Salary: 200,000 円 / month,　Period: 2008-07-01 - 2008-09-30

3. エプソン国際奨学財団
   Epson International Scholarship Foundation
   Amount: 100,000 円 / month,　Period: 2007-04-01 - 2008-09-30

4. 学術振興会特別研究員ＤＣ採用者支援奨学金
   Fellow of JSPS scholarship support DC adopter
   Amount: 300,000 円 / year,　Period: 2009-04-01 ~ 2010-03-31
   Amount: 300,000 円 / year,　Period: 2008-04-01 ~ 2009-03-31

5. 博士後期課程奨学金（工研）
   Doctoral Scholarship (Engineering Labs)
   Amount: 150,000 円 / year,　Period: 2007-04-01~ 2008-03-31
   Amount: 150,000 円 / year,　Period: 2006-04-01 ~ 2007-03-31

6. 私費外国人留学生授業料減免奨学金
   Tuition Reduction Scholarship Privately Financed International Students
   Amount: 117,400 円 / year,　Period: 2006-04-01 - 2007-03-31

7. RMIT University Special Financial Assistance Fund
   Amount: 3,000 $AUD / semester,　Period: 2004 Semester 2, 2004

早稲田大学

Tokyo, Japan
February 2010

Kitti Suwanratchatamanee
キティ・スワナラチャタマニイ